

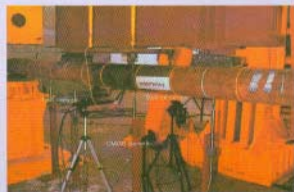
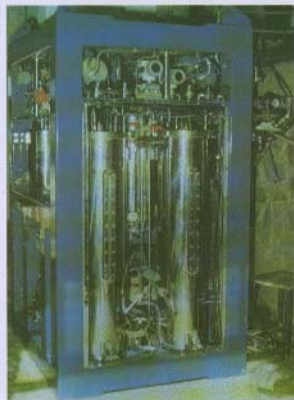
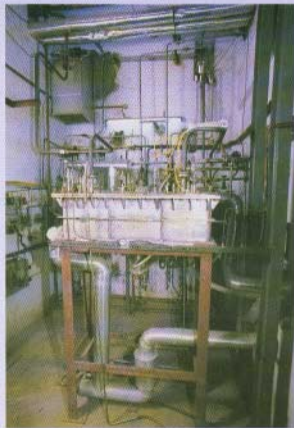
# BARC

NEWSLETTER

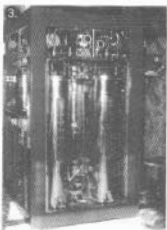
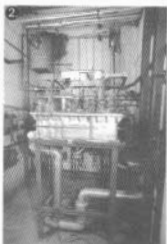
BARC FOUNDER'S DAY SPECIAL ISSUE

OCTOBER 2000

No. 201



**BHABHA ATOMIC RESEARCH CENTRE**

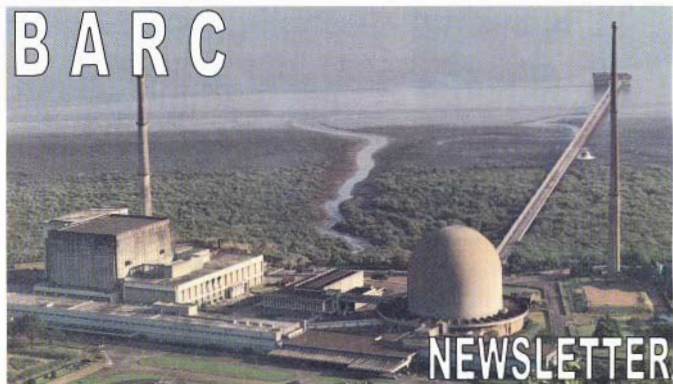


1. Experimental set-up to measure critical current of superconducting wires.
2. Sulphur Hexafluoride ( $\text{SF}_6$ ) Reactor.
3. Prototype of electrolyser plant (front view).
4. Vision system for fracture experiments.



Government of India

# BHABHA ATOMIC RESEARCH CENTRE



*BARC Founder's Day Special Issue*

October 2000  
Issue No. 201



## Homi Jehangir Bhabha (1909-1966)

### *A Tribute to the Founder & Architect of India's Atomic Energy Programme*

Homi J. Bhabha was born to Jehangir H. Bhabha and Meheren on October 30, 1909. He studied at the Cathedral and John Connon High School, the Elphinstone College and the Royal Institute of Science in Mumbai. He was brilliant in studies and won many prizes. At the age of eighteen, his parents sent him to Cambridge, where he passed the Mechanical Science Tripos and the Mathematics Tripos, both in first class. After pursuing research for a few years under the guidance of eminent scientists like Neils Bohr, Rutherford, Wolfgang Pauli and Enrico Fermi, Bhabha returned to India. He became a Special Reader in Theoretical Physics at the Indian Institute of Science, Bangalore.

On the recommendation of the Nobel laureate Dr C.V. Raman, he was elected as a Fellow of the Royal Society (FRS) in 1941. Many honours followed and he was conferred the degree of Doctor of Science by many Indian and foreign universities.

In 1945, Bhabha founded the Tata Institute of Fundamental Research (TIFR) in Mumbai with a grant from Sir Dorab Tata Trust. Later on August 10, 1948, the Atomic Energy Commission was set up by the Government of India with Bhabha as its Chairman. In 1954, the Department of Atomic Energy (DAE) was created to develop facilities needed for the atomic energy programme.

With the full backing of the then Prime Minister Jawaharlal Nehru, Bhabha started building the nuclear energy establishment, and various buildings and facilities started coming up at Atomic Energy Establishment, Trombay (AEET). Soon the research reactors Apsara, Zerlina and CIRUS were inaugurated. On January 12, 1967, AEET was re-named as Bhabha Atomic Research Centre in memory of Homi Bhabha.

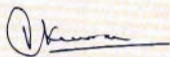
The seed sown by Bhabha for the atomic energy programme has grown and developed into a gigantic tree, comprising nuclear power stations, heavy water plants, radiopharmaceutical laboratories, etc., spread all over India, to cater to the diverse needs of the country in the areas of power production, agriculture, medicine and industry.

In the beginning of this new millennium, the Department of Atomic Energy aspires to fulfil the dream of the Indian masses to become self-reliant and self-sufficient in power production, and to provide supporting facilities in the agriculture and health sectors.

On this day, the birth anniversary of Homi Bhabha, the staff of Bhabha Atomic Research Centre and other units of DAE, remember with gratitude the founder of this great establishment. The nation owes a great debt to Bhabha for leading its people into an era of modern technology and making the nation at par with the developed nations in the field of nuclear energy development.

Bhabha's birthday is observed as the Founder's Day in BARC every year. This special issue of BARC Newsletter is being brought out on this occasion as a homage to this distinguished Son of India.

This volume could not have been brought out in time without the cooperative efforts of Mr T.C. Balan and Mr P.A.S. Warriyar of Library & Information Services Division, BARC.



(Dr Vijai Kumar)

Head, Library & Information Services Division  
Bhabha Atomic Research Centre

## CONTENTS

Towards ultimate control  
of atomic and molecular  
processes by lasers ..... 1

*B.N. Jagatap*

**Homi Bhabha Science & Technology  
Award for the year 1998**

Biomedical applications of lasers ..... 13

*P.K. Gupta*

**Homi Bhabha Science & Technology  
Award for the year 1998**

Scaling of the steady state and  
stability behaviour of  
single-phase natural circulation  
systems ..... 27

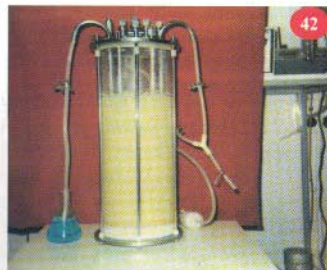
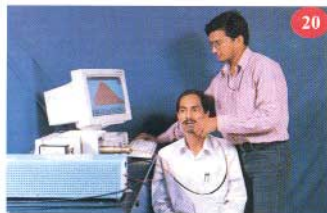
*P.K. Vijayan*

**BARC Technical Excellence Award for  
the year 1998**

Bioreactor technology for  
large scale cultivation of  
plant cell suspension cultures  
and production of bioactive  
compounds ..... 41

*D.P. Fulzele*

**BARC Technical Excellence Award for  
the year 1998**



### *Editorial Staff*

#### CHIEF EDITOR

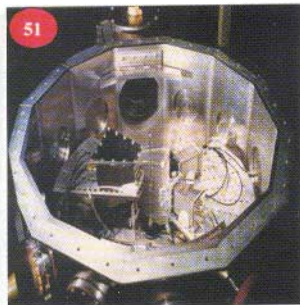
Dr Vijai Kumar

#### MANAGING EDITOR

T.C. Balan

#### COMPUTER GRAPHICS & LAYOUT

P.A.S. Warriyar



51

Gas detectors for heavy ion experimental nuclear physics research ..... 47  
*D.C. Biswas and R.K. Choudhury*  
**"S.N. Seshadri Memorial Instrumentation Award", 1997**

Simulation and experimental verification of hyperfine spectrum of U-233 ..... 57  
*B.N. Jagatap et al.*  
**Best Paper Award in the Annual Conference of Indian Nuclear Society (INSAC-2000), 2000**

Electron beam welding of copper to AISI-304 SS ..... 63  
*T.K. Saha et al.*  
**KCP Award 2000 at the International Welding Conference - IWC'99, 1999**



52

Phosphorus determination by derivative neutron activation analysis ..... 72  
*Y.M. Scindia et al.*  
**Best Paper Award at the 18<sup>th</sup> National Conference of Indian Council of Chemists, 1999**

Determination of H<sub>2</sub> content in zircaloy using hot vacuum extraction - quadrupole mass spectrometry (HVE-QMS) ..... 78  
*Y.S. Sayi et al.*  
**Best Paper Award at the Seventh National Symposium on Mass Spectrometry, 1996**



60

Uptake of metal ions by extraction chromatography using DMDBTDMA as the stationary phase ..... 81  
*S. Sriram et al.*  
**Best Paper Award at Nuclear & Radiochemistry Symposium, 1999**

Preparation and thermal studies on Pu(MoO<sub>4</sub>)<sub>2</sub> and Na<sub>2</sub>PO (MoO<sub>4</sub>)<sub>3</sub> ... 85  
*N.D. Dahale et al.*  
**Second Best Paper Award at the THERMANS 2000 Symposium**

A study of solid state reaction between strontium carbonate and ruthenium dioxide ..... 89

*R.K. Mishra et al.*

**Second Best Paper Award at the THERMANS-2000 Symposium**

Mass spectral studies for the determination and speciation of arsenic by Gas Chromatography-Mass Spectrometry (GC-MS) .....95

*S.K. Aggarwal et al.*

**Second Best Paper Prize in ISMAS Symposium on Mass Spectrometry, 1999**

Isotope ratio measurements for plutonium in isotopic reference materials by Thermal Ionisation Mass Spectrometry (TIMS) using total evaporation technique ..... 98

*S.K. Aggarwal et al.*

**Second Best Paper Prize in ISMAS Symposium on Mass Spectrometry, 1999**

Vacuum decomposition pattern of ferrous ammonium sulphate – a quadrupole mass spectrometric study ..... 103

*Y. Seshu Sai et al.*

**Second Best Paper Prize in ISMAS Symposium on Mass Spectrometry, 1999**

X-ray and thermal studies on Tl-Pu-Mo-O system ..... 106

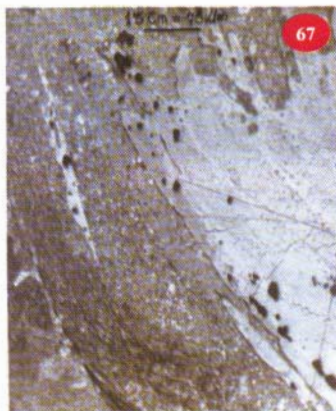
*N.D. Dahale et al.*

**Third Best Paper Award at the National Symposium and Conference on Solid State Chemistry and Allied Areas (ISCAS 99), 1999**

Normalized  $dZ/dT$  waveform for easy assessment of peripheral blood flow ..... 108

*Jagruti Chheda et al.*

**Consolation (UG) Prize in the Symposium on Biomedical Engineering and Nuclear Medicine (SBME-NM 2000)**





# TOWARDS ULTIMATE CONTROL OF ATOMIC AND MOLECULAR PROCESSES BY LASERS

**B.N. Jagatap**

Laser & Plasma Technology Division  
Bhabha Atomic Research Centre

**S**PECTROSCOPY HAS SHOWN amazing resilience and freshness ever since the development of quantum mechanics at the beginning of the 20th century. In the last two decades, thanks to the development of lasers, we have seen the return of spectroscopy to its former position of scientific prominence. In many respects the 1980s represented a period in which the spectroscopy with lasers underwent the difficult transition from being a purely academic subject to a discipline with important technological and commercial applications. This contemporary outlook of spectroscopy forms the basis of our work, both experimental as well as theoretical.

In the recent years, our work in lasers and spectroscopy focusses on the use of lasers to control and tailor atomic and molecular processes. This work encompasses three important issues in the contemporary physics. Firstly, it addresses the problem of isotope selective excitation and ionisation, which have important ramifications in the nuclear fuel cycle, specifically in the thorium utilisation programme of the department [1-9]. The systems we investigate in this domain are laser clean-up of U-233 and denaturing of zirconium. In the language of control theory the isotope specific excitation/ionisation using lasers is a "passive" control since it is realised by the use of intrinsic

isotope shifts exhibited by the atomic systems. In our work, we also seek "active" control wherein we devise strategies to change the atomic and molecular response in a fundamental manner to control excitation, ionisation and dissociation [10-15]. This forms the second important component of our work. Involved in this work are the ideas on coherent control which are expected to form the basis of the new generation of laser processing of materials. The third component of our work is to use lasers to control the external degrees of freedom such as positions and velocities of atoms to obtain cooled and trapped atoms for experiments on the foundations of physics [16-21]. The fascinating aspect of this entire endeavour is that while at the fundamental level it unravels new and important aspects of laser-atom and laser-molecule interactions, at the applied level it finds an importance in the configuration and realisation of laser selective processes for high value materials.

## Laser Clean-Up of U-233

The Indian nuclear power programme, in the long term, is based on energy from fission of U-233. The fissile U-233 is bred from fertile thorium of which our country has large deposits. In Indian nuclear fuel cycle (INFC), Th-232 will be converted to U-233 in advanced

heavy water reactors, fast breeder reactors and in the futuristic accelerator driven subcritical reactors. Production of U-233 is accompanied by the unavoidable formation of small quantities of U-232. The major cost of U-233 fuel is in the requirement of remote handling for fuel fabrication, transportation and fuelling operation, due to the hard  $\gamma$ -emitting daughter products of U-232. The economic gains of U-233 fuel will be boosted if U-232 impurity is removed or brought down to permissible level by employing a laser isotope separation (LIS) process. Such a process is referred to as "U-233 Clean-Up" process in INFC [1,4].

It must be emphasised here that the development of this process, from physics to technology, has to be done for the first time and independently in India, since no other country is as much dependent on thorium utilisation as India. Needless to say that the entire development has to be done without the benefit of published literature, data or report. This presents a truly a

challenging area of work and also provides the satisfaction of doing everything for the first time. The heart of the clean-up process is selective resonant three step photoionisation by tunable lasers. At the physics level, the process amounts to selective excitation and photoionisation of the impurity isotope, U-232, and subsequent removal of the ions by applying electrostatic field [3-6]. Building of the requisite separation physics for the Clean-up process, therefore, requires firstly a large amount of atomic data which has to be generated in house using various spectroscopic techniques. To ensure high selectivity and large photoionisation efficiency we need data on isotope shifts (IS), hyperfine structure (HFS) of U-233 due to non-zero nuclear spin, level lifetimes, absorption and photoionisation cross-sections etc. Furthermore to configure a process which minimises isotopic scrambling during the collection of ions, one needs to know various collision cross-sections involving atoms and ions; the information of which is also provided by spectroscopy.

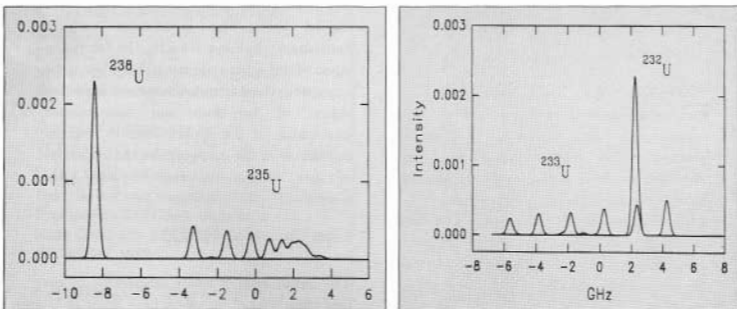


Fig.1. Spectra of (U-235, U-238) [experimental] and (U-232, U-233) [simulated] for a typical first step transition.

Our efforts have been to generate this crucial data base using a variety of theoretical and experimental techniques [6-8]. Our theoretical work resulted in the first ever data base for (U-232, U-233) system. An example of these efforts we show in Fig. 1 simulated spectra of (U-235, U-238) and (U-232, U-233) systems for a typical first step-transition. Note here that the U-233 has a broad hyperfine structure and that the odd-even staggering of U-233 results in a small isotope shift (U-232, U-233). It is also clear from Fig.1 that the separation task in the clean-up process is a demanding one, since overlapping of spectra of U-232 and U-233 will be more as a rule than an exception. Somewhat better situation is presented in Fig.2, which shows simulated spectrum for another first step transition exhibiting an adequate spectral separation. An extensive simulation work has helped us to identify the transition sequences such as this (cf. Fig.2) which form the foundations of the Clean-up process.

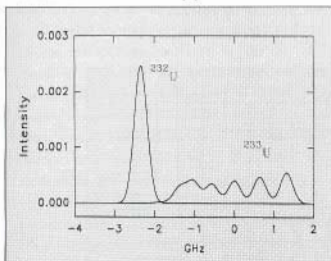


Fig. 2. Simulated spectrum of a transition of U-232 and U-233, which shows a clear spectral separation.

On the experimental side, conventional high resolution spectroscopic techniques together with laser spectroscopic techniques involving one or several lasers, operating under pulsed and continuous modes, have to be implemented for generating this data base for the clean-up process

[7,8]. High resolution spectroscopy of radioactive isotopes requires quite a different approach from the conventional spectroscopy. Only a few experiments would be possible with radioactive elements and to get the same amount of reliable data, new techniques have to be devised. New high resolution spectroscopic sources developed during the course of our work are shown in Fig. 3.



Fig.3. Spectroscopic sources developed for high resolution spectroscopy related to the clean-up programme. These sources work with milli to microgram quantities of isotopes of interest. Top: Hollow cathode discharge sources for emission spectroscopy and laser spectroscopy. Bottom: Atomic beam source for high resolution fluorescence spectroscopy.

These sources work with milligram to microgram quantities of samples thereby avoiding the

problems connected with radioactive nature (eg. U-232) of interest. In Fig.4, we show high resolution spectrum of U-238, U-235 and U-233 recorded on a recording Fabry Perot Optical Spectrometer. Capability such as this has been achieved through innovative approaches backed by the expertise developed over the years. This work has also thrown newer possibilities on high resolution spectroscopy of higher actinides and highly radioactive materials. The confidence 'in our approach is provided by close matching of the simulated and experimental atomic data; an example of which is presented explicitly in our award winning paper [7] included in this volume.

The spectroscopic data provides only the initial conditions for laser-atom interactions. The selectivity and stripping efficiency are determined by the kinetics of laser-atom interactions [5,6]. High selectivity is required in the clean-up process on two accounts; firstly to minimise the loss of the fissile isotope and secondly to minimise the photon cost. High accessibility is

of the sample or the rarity of the isotopes important for recovery of the LIS process and thereby minimising the number of stages required to obtain desired purity of the processed material. We have done detailed investigations of photoionisation physics to obtain the regions of operating parameters such as laser and vapour characteristics. Various issues studied here are second step selectivity, Boltzmann inaccessibility, spectral accessibility, criterion for selection of transitions etc. These results give the first cut analysis of the physics of the separation task involved in the clean-up process. In Fig. 5, we show the results of one such study, where the selectivity and accessibility is investigated as a function of laser bandwidth and axial temperature of the vapour. The operating conditions of the process are decided by the trade off between selectivity and accessibility. Our work on the selectivity physics provides guidelines, clarifies issues related to selectivity, throughput and recovery in the U-233 clean-up process.

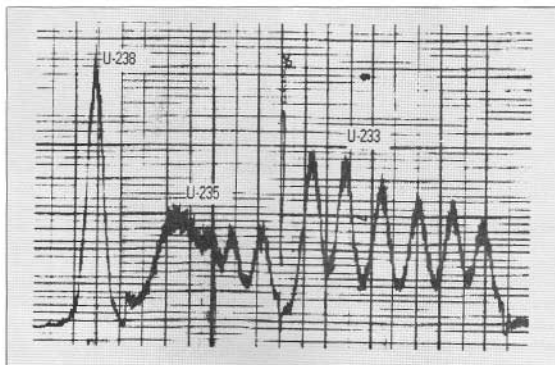


Fig.4. High resolution spectrum of 5915 Å transition in uranium isotopes recorded in our laboratory. Experiments such as this provide data on isotope shifts and hyperfine structures required for the clean-up programme.

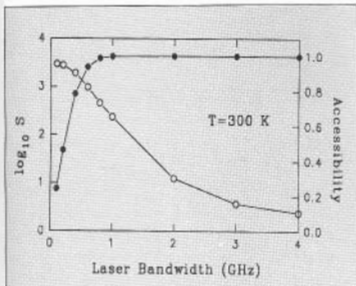


Fig. 5. Variation of selectivity (S, ●) [left scale] and accessibility (○) [right scale] as a function of laser band width.  $T$  is the axial temperature of the vapour and accessibility refers to the spectral overlap of the atomic transition with tunable laser. Simulations such as this help to arrive process parameters of the clean-up process.

Another example of our work on "passive" control is "denaturing" of zirconium which is intimately connected with INFC [9]. The thermal reactors utilising thorium fuel cycle use considerable tonnage of zirconium in the fixed in-core components as well as in the fuel cladding. Zirconium has five isotopes and the neutron absorption cross-section of 0.186 b is mainly contributed by Zr-91 which has an abundance of 11.2%. If the concentration of this isotope in zirconium is reduced to 3%, the absorption cross-section will reduce to 0.088 b. Use of such "denatured" zirconium for the pressure tubes, calandria and cladding would allow greater design flexibility and extended fuel cycles for nuclear reactors, both AHWRs as well as PHWRs.

Since the denaturing of zirconium involves removal of the middle isotope, the proposed method is LIS in atomic vapour. This method is particularly attractive in view of the development of LIS process for U-233 clean-up. Of course new spectroscopic and innovative photo-

ionisation schemes need to be adapted. This need stems from the fact that the isotope shifts in the spectrum of zirconium is in the range of 100-200 MHz. This, along with the broad hyperfine structure of Zr-91 (nuclear spin  $I=5/2$ ), results in the overlap of the spectrum of Zr-91 with the spectra of the even isotopes. The absence of spectral separation, therefore, makes selective photoionisation of Zr-91 difficult. It is, however, possible to introduce isotopic selectivity by invoking alternate photoionisation physics namely, selective photoionisation by laser polarisation induced population trapping. We have developed extensive simulation procedures which can be used for identifying the optimal transition sequences and laser polarisations for selective photoionisation of Zr-91. Our work points out to the special features of this separation task and provides the required physics base for the process of denaturing of zirconium.

## Coherent Control of Atomic & Molecular Processes

LIS is based on the concept of "passive" control since the isotope selectivity in photoionisation is achieved due to intrinsic atomic properties such as isotope shifts. When the photoreacting system is energetically degenerate, controlling the outcome of the atomic/molecular process requires a more fundamental approach. One such approach is "coherent control" which is based on the interference between optical transitions. This phenomenon arises when atomic/molecular system is driven coherently through two competing path-ways which exhibit interference analogous to a double slit experiment in optics. This interference in turn can be controlled by parameters of the driving fields enabling control of excitation, ionisation and dissociation of atomic/molecular systems. This methodology provides interesting solutions in many areas of chemical physics ranging from

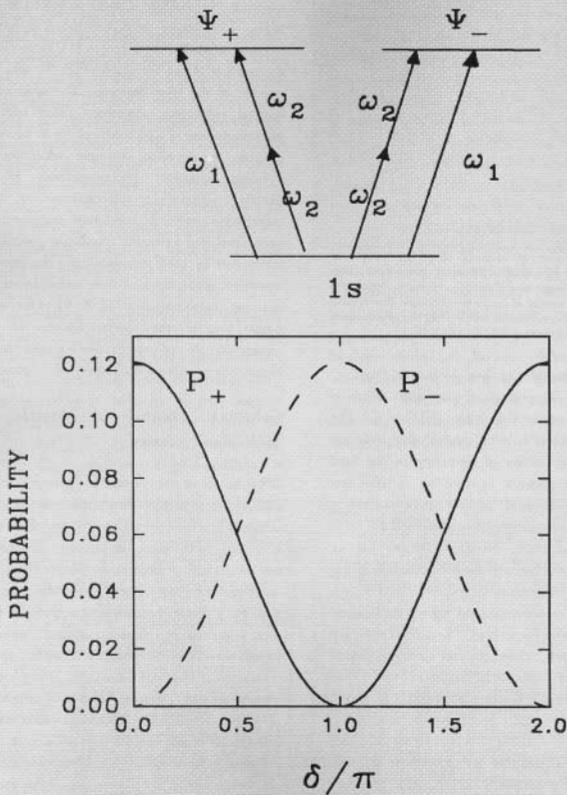


Fig.6. Coherent control of the populations in the hybrid states  $\Psi_{\pm}$ . Top: One- vs two- photon excitation competition set up using laser of frequency  $\omega_2$  and it's second harmonic  $\omega_1$ . Bottom: The populations of the hybrid states  $P_{\pm}$  as a function of the relative phase  $\delta = \delta_1 - 2\delta_2$  of the two pulsed lasers exciting  $n=1$  to  $n=2$  transition of the hydrogen atom. For details see Ref.[11].

lasers without population inversion to control of chemical reactions [10].

An interesting example of the coherent control is provided by our theoretical work on the production of dipolar hydrogen atom  $2s$ - $2p$  resonance hybrid,  $\Psi_{\pm} = (|2s\rangle \pm |2p\rangle) / \sqrt{2}$ , through the use of competitive one- and two-photon transitions from the ground state [11]. Note here that the hybrid states are energetically near degenerate and a usual excitation process will be nonselective in the sense that it will populate both these states equally. By providing two competing paths, we can control the excitation to a specific hybrid state. In Fig. 6, we show this control scenario as a function of the phase difference between the lasers inducing the one- and two-photon transitions. Here complete control over the production of specific hybrid state is achieved by changing relative phase of two monochromatic laser beams which alters the degree of destructive interference between two paths of excitation. This aspect of controlling transitions without changing the radiation intensity is interesting from both basic and applied point of view. In molecular systems, we have shown that similar control can be established by competition between two-photon optical excitation pathways [12].

To study such intricate control phenomenon, we require the state of the art theoretical models and experiments. Our investigations on spectroscopy and dynamics of femtosecond, two colour, pump-probe experiments involving simultaneous and sequential two-photon excitation illustrate how theory and experiments go hand in hand [13]. One of the consequences of our theory is to predict  $\cos^4\theta$  dependence of the excited state fluorescence for  $\alpha$ -NPO molecule in contradistinction to  $\cos^2\theta$  dependence in azulene

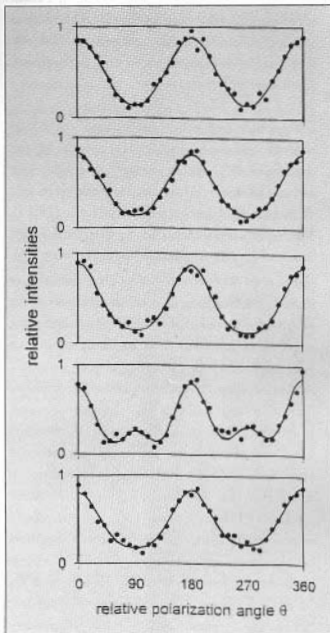


Fig. 7. Experimental and theoretical results on the fluorescence intensity for  $\alpha$ -NPO molecule undergoing a "direct" two-photon transition as a function of the angle between the polarisation vectors of two lasers. From top to bottom, the average pump power per dye laser (400 fs FWHM) are 470, 500, 540, 560 and 580 mW respectively. The  $\cos^4\theta$  component varies as 20%, 50%, 70%, 60% and 75%. For details see Ref. [13].

molecule. Here  $\theta$  is the angle between the polarisation vectors of pump and probe lasers. Further, this dependence can be controlled by controlling the laser intensities. These theoretical predictions were verified in totality in a series of

controlled experiments. In Fig.7, we show these experimental and theoretical results. This work is of importance also in the measurement of dipole moments of molecular states and femtosecond actinometry.

Development of very sophisticated theoretical methods is a pre-requisite for much of the contemporary spectroscopic research. An example of this is our theoretical work in the area of intense field laser-atom interactions [14,15]. The rapid developments in the laser technology have now made it possible to realise very high intensity ( $>10^{12}$  W/cm<sup>2</sup>) ultra short pulsed laser sources. Such unprecedented intensities are at the origin of a considerable interest in studying the response of an atom or a molecule to intense laser fields which include above threshold ionization, high harmonic generation, multiple ionization and stabilization in atomic systems. Intense field laser-atom interaction is inherently non-perturbative since the atom experience a laser electric field which is comparable to or more than the Coulomb field of the atomic electron. Understanding of the nonlinear response of atom to such fields, therefore, requires an explicit non-perturbative time-dependent approach. What we look here is the "direct" solution of the time dependent Shrodinger equation with time dependent sinusoidal potential; a daunting task even for a simplest atomic system such as one electron atom and a challenging problem in computational physics.

We have developed a methodology based on split operator fast Fourier transform (SOFFT) technique and implimented it sucessfully on Anupam parallel computing machine, which can be used conveniently for studying intense field phenomena in hydrogen-like atoms and diatomic molecules. Such theoretical studies serve as a direct test for comparison between experiments

and theory. In Fig.8 we show the probability of ionisation of hydrogen atom by a 10 fs pulse of  $10^{12}$  W/cm<sup>2</sup> intensity. Such calculations are possible to be done only in a few laboratories in the world. We have used this computational scheme to study the problems of phase dependent excitation, ionization and harmonic generation. These provide many interesting control phenomenon hetherto unknown in low intensity regime.

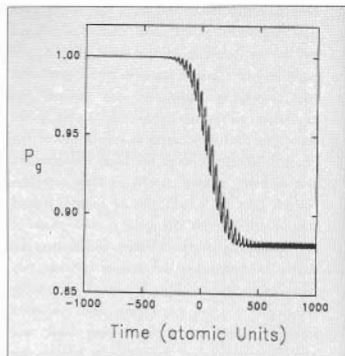


Fig. 8. An example of "exact" calculation of intense field laser-atom interaction. Shown is the ground state probability ( $P_g$ ) of hydrogen atom exposed to an intense short duration (10 fs FWHM) laser pulse. The calculations were performed using split operator fast Fourier transform technique on Anupam.

## Laser Cooling of Atoms

So far we have seen the role of laser in controlling the internal degrees of freedom. Laser cooling is an area which looks to control and manipulate the external degrees of freedom, the positions and velocities, of atoms using electromagnetic fields [16-18]. Last two decades have seen an enormous progress in development of techniques to cool and trap neutral atoms and ions. These techniques have made it possible to



reach entirely new regimes of low temperature such as nano kelvin and to perform ultra high precision experiments to test the elementary laws of nature. The techniques of laser cooling and trapping have matured to a point that they are finding applications in other areas of science, e.g. high resolution spectroscopy, metrology, nonlinear optics, collision physics, condensed matter physics etc. Atomic cooling techniques have been used to cool dilute alkali vapours to sub-micro kelvin temperatures to achieve Bose-Einstein condensation; a phenomenon which had eluded physicists for over seventy years. Very recently, the atom laser, coherent beam of massive bosons, has become a reality [18].

India has remained isolated from all these excitements for a long time. BARC has taken up lead in this field and planned an extensive programme on laser cooling and trapping of atoms and ions in the IX FYP. This programme aims at setting up a facility for laser cooling and trapping of atoms and perform a variety of experiments at the foundations of physics. We are developing this programme with local expertise and local technology. In that regard BARC, with its inherent multidisciplinary character, is an ideal place where such an activity can flourish. In the IX FYP, the objectives of the programme are two fold: ultra-high resolution spectroscopy for fundamental physics experiments and experiments leading to Bose-Einstein condensation. We expect to get involved, in due course, in atom optics which refers to a fresh outlook in which atomic beams are thought of and manipulated like photons in light beams and a collection of techniques for doing such manipulations.

Development of laser cooling techniques, namely various types of traps, is central to all these programmes. One of the most efficient traps for neutral atoms is the magneto-optical trap

(MOT) which is based on the scattering force in an inhomogenous magnetic field [16]. MOT provides an elegant way of obtaining large sample of cold and trapped atoms. It has a comparatively large trap depth and is capable of achieving densities as high as  $10^{12}$  atoms/cc at a temperature down to a few micro Kelvin. We have successfully developed and installed a MOT in BARC for cooling of Cs atoms. This has been made possible through a number of developments in the areas such as spherical quadrupole magnetic field, ultra high vacuum optical chamber, saturated absorption spectroscopy using diode lasers, wavelength locking of diode lasers and optics. Some of these issues have been tackled for the first time in this country.

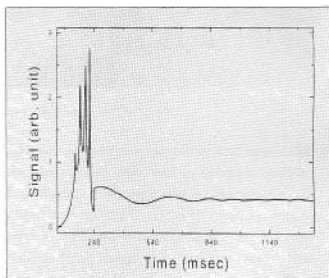


Fig.9. An example of locking of the tunable diode laser frequency on the red side of the cooling transition. The high resolution saturated absorption spectrum of D2 transition of Cs is clearly seen. The laser is locked on the red side (~ 10 MHz) of the cooling transition  $F=4 \rightarrow F=5$  of atomic Cs.

An example of these efforts is shown in Fig. 9 where we show locking of the diode laser wavelength about 10 MHz on the red side of the cooling transition of Cs. In Fig.10, we show a view of the magneto-optical trap installed as a part of the laser cooling facility in BARC. This trap is a major workhorse in our planned experiments on the cold and trapped atoms.



*Fig.10. A view of the magneto-optical trap designed and developed in BARC.*

These experiments also include verifications of a number of aspects of laser-atom interaction such as non-classical effects, quantum jumps and photon statistics [19-21]. We have also begun work on the next generation of traps, i.e. "Clover leaf" traps required for tighter and lossless confinement of neutral atoms as in the experiments for obtaining Bose condensates [17].

## Conclusions

The control of atoms, molecules and the processes involving them is a central issue in the contemporary spectroscopy. The classical perception of spectroscopy is to study the way the quantum systems behave, that is to understand the atomic/molecular processes; the outcome of which always decided by the laws of probability and statistics. In the new scenario of

"ultimate" control, we think in terms of setting the rules of the game, pre-determining the winner and modifying the spectroscopic properties in such a way that the winner is always the chosen one. The impact of this "new wave" in spectroscopy has been so overwhelming that it now encompasses a wide spectrum of areas from very basic to very applied. This has also a tremendous impact on many technologies including nuclear technology, as shown by our work on U-233 clean-up. The programmes undertaken by us hold promise for many such areas of interest to our research centre.

## Acknowledgement

The author thanks Dr. S.K. Sikka, Director SS&SG and Dr. N. Venkatramani, Head L&PTD for their keen interest in this work and

continued encouragement. Many helpful discussions with Dr. A.P. Roy, formerly Head, Spectroscopy Division are gratefully acknowledged. Thanks are due to the colleagues and collaborators, Mr L.M. Gantayet, Dr. S.A. Ahmad, Dr K.G. Manohar, Dr. A. Venugopalan, Ms A.P. Marathe, Shri. S. Pradhan, Dr S.V. Lawande and Prof. W.J. Meath.

## References

- (1) Kakodkar, BARC News Letter, No.182, March 1999.
- (2) R. Chidambaram, XI Prof. Brahm Prakash Memorial Lecture, Indian Institute of Metals, Bangalore, August, 1995.
- (3) B.N. Jagatap, L.M. Gantayet and U.K. Chatterjee, Proceedings of INSAT-97 (Kottayam, 1997), p.4.
- (4) B.N. Jagatap, ISRAP Bull. 10, 23 (1999).
- (5) L.M. Gantayet, B.N. Jagatap, K.G. Manohar and K.C. Sahoo, Proceedings of INSAC-2000, "Power from Thorium: Status, Strategies and Directions", (BARC, 2000), p.123.
- (6) B.N. Jagatap, Proceedings of INSAC-2000, "Power from Thorium: Status, Strategies and Directions", (BARC, 2000), p.241.
- (7) B.N. Jagatap, L.M. Gantayet, S.A. Ahmad, A. Venugopalan, A. Ramanujam, A.P. Marathe and B.K. Ankush, Proceedings of INSAC-2000, "Power from Thorium: Status, Strategies and Directions", (BARC, 2000), p.235.
- (8) A.P. Marathe, S. Pradhan, A. Venugopalan, K.G. Manohar and B.N. Jagatap, Proceedings of INSAC-2000, "Power from Thorium: Status, Strategies and Directions", (BARC, 2000), p.238.
- (9) B.N. Jagatap and L.M. Gantayet, Proceedings of INSAC-2000, "Power from Thorium: Status, Strategies and Directions", (BARC, 2000), p.243
- (10) B.N. Jagatap, ISRAP Bull. 8, 2 (1997).
- (11) B.N. Jagatap and W.J. Meath, J. Chem. Phys. 113, 1501 (2000).
- (12) B.N. Jagatap and W.J. Meath, Chem. Phys. Lett. 258, 193 (1996).
- (13) B.N. Jagatap, W.J. Meath, D. Tittlebach Helmrich and R.P. Steer, J. Chem. Phys. +103, 121 (1995).
- (14) B.N. Jagatap in "Spectroscopy: Perspectives and Frontiers", ed. A.P. Roy, (Narosa, 1997), p.106.
- (15) B.N. Jagatap, in "Nonlinear optics and Laser Spectroscopy", Ed. S.C. Abbi and S.A. Ahmad. (Narosa, 2000) p.134.
- (16) .N. Jagatap, K.G. Manohar, S.G. Nakhate, A.P. Marathe and S.A. Ahmad, Curr. Sc. 76, 207 (1999).
- (17) See for example, B.N. Jagatap, A.P. Marathe, K.G. Manohar, R.C. Sethi and S.A. Ahmad, in "Current Trends in Atomic and Molecular Physics", Ed. K.K. Sud, (Kluwer-Plenum, NY, 2000) p.299.
- (18) See for example, K.G. Manohar and B.N. Jagatap, Curr. Sc. 76, 1420 (1999).
- (19) S.V. Lawande and B.N. Jagatap, Phys. Rev. A39, 683 (1989); Phys. Lett. A126, 335 (1988).

(20) B.N. Jagatap and S.V. Lawande, Phys. Rev. A44, 6030 (1991); Opt. Comm. 82, 17 (1991).

(21) Q.V. Lawande, B.N. Jagatap and S.V. Lawande, Phys. Rev. A42, 4343 (1990).

*In the recent years, our work in lasers and spectroscopy focusses on the use of lasers to control and tailor atomic and molecular processes. This work encompasses three important issues in the contemporary physics. Firstly, it addresses the problem of isotope selective excitation and ionisation, which have important ramifications in the nuclear fuel cycle, specifically in the thorium utilisation programme of the Department of Atomic Energy. The second important component of our work pertains to the strategies we have devised to change the atomic and molecular response in a fundamental manner to control excitation, ionisation and dissociation. The third component of our work is to use lasers to control the external degrees of freedom such as positions and velocities of atoms to obtain cooled and trapped atoms for experiments on the foundations of physics.*

*Dr B.N. Jagatap is the recipient of the Homi Bhabha Science & Technology Award for the year 1998.*



*Dr B.N. Jagatap graduated from the 20<sup>th</sup> batch of BARC Training School and obtained his Ph.D (Physics) from University of Mumbai in 1988. He has been associated with the Interdisciplinary Centre for Chemical Physics, University of Western Ontario, Canada, as Post Doctoral Fellow (1993-94) and Visiting Scientist (1999 and 2000-2001).*



# BIOMEDICAL APPLICATIONS OF LASERS

P.K. Gupta

Biomedical Applications Section, Centre for Advanced Technology  
Indore, 452 013, India

## Abstract

*The use of lasers for medical diagnosis, and for therapy initiated by photo-excitation of natural chromophores or exogenous photosensitisers, is receiving considerable current attention. Developments in these areas are expected to have profound influence on the quality of health care. Therefore, an activity in these areas was started at CAT in 1992-93. The initial efforts have been to explore the use of laser induced fluorescence spectroscopy for cancer diagnosis, and investigate the photo-biological effects of laser irradiation on living organisms. The article provides an overview of the work carried out at CAT in both these areas. Some of the new activities taken up at CAT on development of techniques for optical imaging and laser micromanipulation of microscopic objects are also briefly discussed.*

## Introduction

LASERS DUE TO THEIR SEVERAL remarkable properties are finding widespread applications in medicine<sup>1</sup>. The use of lasers in surgery, which started within a year of the invention of laser, is now well established. Lasers have made possible minimally invasive ultra-precise surgery with reduced patient trauma and hospitalization time. The use of lasers for medical diagnosis is also attracting considerable interest and significant advancements are being made<sup>2,3</sup>. This work is motivated by the fact that the onset and the progression of a disease are often accompanied by biochemical/morphological changes, which can be sensitively monitored by laser spectroscopic techniques. These techniques can therefore lead to disease diagnosis at an early stage before the disease becomes difficult to manage. The other important advantages offered by laser spectroscopic techniques are their potential for

in-situ, near real time diagnosis and the use of non-ionizing radiation which makes them particularly suited for mass screening and repeated use without any adverse effects.

Another area of growing interest is the use of lasers for non-surgical therapeutic applications<sup>4,5</sup>. It exploits light induced activation of naturally occurring or administered photosensitisers. A good example is the fast developing photodynamic therapy of cancer<sup>6,7</sup> where photoexcitation of a tumor localized drug leads to selective destruction of tumor with minimal effect on healthy tissue. There are also indications that selective photoexcitation of native chromophore in the tissue may lead to therapeutic effects. Clinical reports available in literature<sup>8,9</sup> as well as results from Choithram Hospital and Research Center (CHRC)<sup>10,11</sup>, Indore have shown that irradiation with lasers or other narrow bandwidth light sources can lead to several therapeutic effects like accelerated wound

healing, treatment of pulmonary tuberculosis and treatment of pain of various etiologies. The mechanisms for these therapeutic effects are not very well understood. The clinical potential of this rather simple and inexpensive therapeutic modality is motivating considerable work in this direction and substantial progress is being made<sup>12</sup>.

Realizing the profound influence optical diagnosis and phototherapy can have on the quality of health care, work in these areas was initiated at CAT in 1992-93. Several studies have been made to investigate the photo-biological effects of laser irradiation on living organisms and to explore the use of laser induced fluorescence spectroscopy for cancer diagnosis. Following studies on samples resected at surgery or biopsy from patients with cancer of different organs, systems suitable for clinical use have been developed at CAT. One unit has been installed at a cancer screening center for screening patients with neoplasm of uterine cervix. The other unit has been used to carry out a pilot study on 25 patients with histopathologically confirmed cancer of oral cavity and encouraging results obtained.

Work has also been initiated at CAT in some other promising areas. One of these is the development of techniques for optical imaging through turbid media. These have the potential to provide sub-millimeter resolution imaging without the need for ionizing radiation and associated risks<sup>13</sup>. The other activity taken up is development of laser trap and microbeam set up. These set ups are finding widespread applications in biomedicine for non-contact micromanipulation of microscopic objects and are expected to have an impact far beyond than just being a new physical tool for biological research<sup>14</sup>.

In this article we first provide an overview of the work carried out at CAT on the use of laser

induced fluorescence spectroscopy for cancer diagnosis. The results of the studies carried out to investigate photo-biological effects of laser irradiation on living organisms are presented next. This is followed by a brief discussion of some of the new activities taken up at CAT.

## Laser Induced Fluorescence (LIF) Spectroscopy for Diagnosis of Cancer

LIF has been used for diagnosing cancer in two ways. One approach involves systemic administration of a drug like haematoxylin derivative (HpD) which is selectively retained by the tumor. When photoexcited with light of appropriate wavelength, the drug localized in the tumor fluoresces. This fluorescence is used for detection and imaging of the tumor. Photoexcitation also leads to populating the triplet state via intersystem crossing. The molecule in excited triplet state can directly react with biomolecules or lead to generation of singlet oxygen, which is toxic to the host tissue. The resulting destruction of the host tissue is exploited for photodynamic therapy of tumor. From the point of view of use in diagnosis this approach has two drawbacks; a possible dark toxicity of the drug and the possibility of drug induced photosensitization. For example a major drawback with the use of HpD has been drug-induced photosensitization of the skin necessitating the patient to avoid light for a few weeks. There is therefore interest in developing tumor markers where the triplet state is rapidly quenched and thereby photosensitization is avoided. The other approach, the one that has received more attention in recent years, does not use any exogenous tumor markers. Instead it exploits for diagnosis the subtle changes in the spectrum as well as the decay time of fluorescence from native tissues as it transforms from normal to the malignant state. The studies carried out over the last few years have shown

considerable promise of this approach for diagnosis of the cancer of various organs like uterine cervix, esophagus, lung, breast, and oral cavity<sup>2,4</sup>

#### *In-vitro studies at CAT*

A schematic of the experimental arrangement used at CAT for in-vitro studies on autofluorescence spectroscopy of human tissues is shown in Fig. 1. It uses a home-built pulsed N<sub>2</sub> laser the output of which is coupled to an optical fiber (core diameter 400μm) via dichroic mirror that reflects N<sub>2</sub> laser radiation (337nm) and transmits longer wavelength fluorescence output. The power of the laser pulse is monitored by a

beam splitter-photodiode combination. The fluorescence from the tissue, kept in contact with the fiber, is collected by the same fiber and imaged on the entrance slit of a scanning monochromator. The wavelength-dispersed light at the exit slit of the monochromator is detected by a photomultiplier tube detector. A microprocessor-based system developed at CAT is being used for on-line acquisition of N<sub>2</sub> laser power and fluorescence spectral data. For excitation/emission spectroscopic studies at other wavelengths a commercial spectrofluorometer (SPEX, Fluorolog II) was used. In the following, we briefly summarize the results of the studies carried out at CAT on autofluorescence from tissues from different organs.

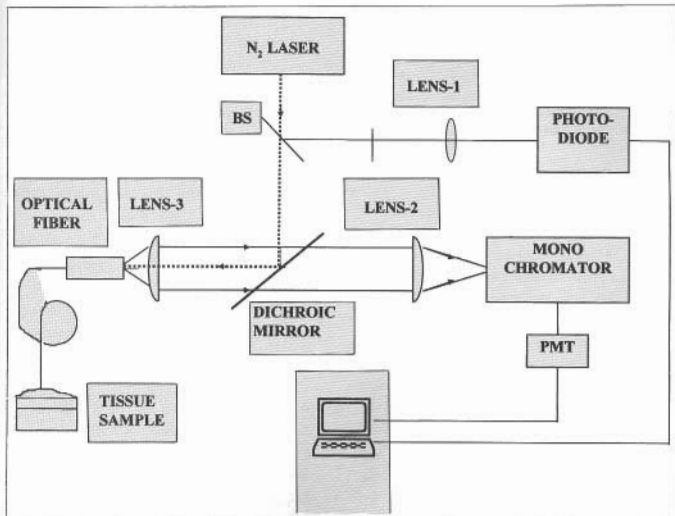


Fig. 1. Schematic diagram of the experimental set-up for autofluorescence spectroscopy of tissues.

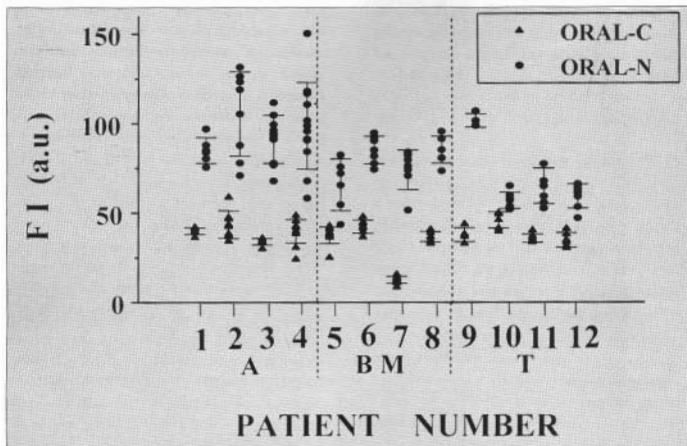


Fig. 2. Scatter plot for the integrated fluorescence intensity for  $N_2$  laser excited spectra of paired cancerous and normal oral tissue sites from 12 patients selected at random. Patients number 1 to 4 had cancer of alveolus (A); 5 to 8 had cancer of buccal mucosa (BM) and 9 to 12 had cancer of tongue (T).

### Cancer of oral cavity

Oral cancer is one of the most common cancers in India and several other South Asian countries. Laser induced fluorescence technique is particularly well suited for early detection of oral cancers due to the easy accessibility of this organ. Studies on 337 nm excited autofluorescence spectra from oral tissues (alveolus, buccal mucosa and the tongue tissue samples obtained from patients with the cancer of oral cavity) revealed significant differences in the total, spectrally integrated fluorescence intensity ( $\sum_{\lambda} I_r(\lambda)$ ;  $360 \leq \lambda \leq 600$  nm) from cancerous and normal oral tissue sites. In Fig. 2 we show a plot for the spectrally integrated fluorescence intensity for paired cancerous and adjoining normal tissue sites of 12 patients (4 alveolus, 4 buccal mucosa

and 4 tongue) selected at random from the patients investigated. The considerably higher values of  $\sum_{\lambda} I_r(\lambda)$  for normal tissue sites is apparent. The mean value of  $\sum_{\lambda} I_r(\lambda)$  from normal tissue sites was larger by a factor of 2 compared to that from cancerous tissue sites. At the other excitation wavelengths ( $\lambda_{ex} = 300$  nm and 460 nm), no significant difference in fluorescence yield between cancerous and normal oral tissue sites was observed.

With 337 nm excitation use of  $\sum_{\lambda} I_r(\lambda)$  alone as a discrimination parameter provided excellent discrimination between cancerous and normal oral tissue sites. The scatter plots for the values  $\sum_{\lambda} I_r(\lambda)$  from all cancerous and the normal tissue sites of the oral cavity are shown in Fig. 3. The sensitivity and specificity values for



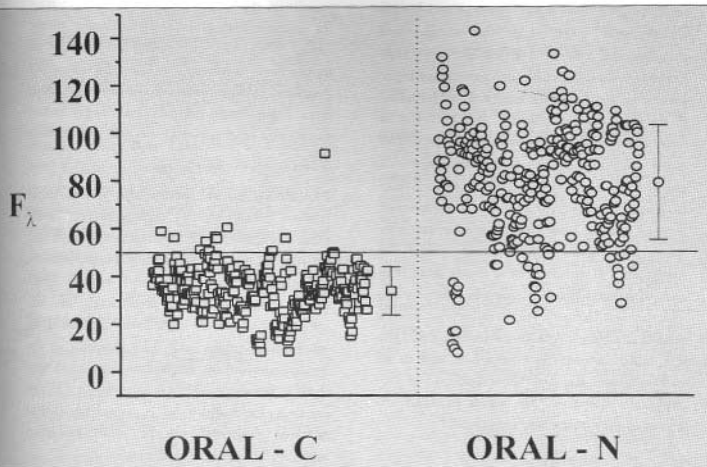


Fig. 3. Scatter plot for the spectrally integrated fluorescence intensities from cancerous (ORAL-C) and normal (ORAL-N) sites of the oral cavity over the total sample size investigated. The bars show mean value  $\pm$  standard deviation.

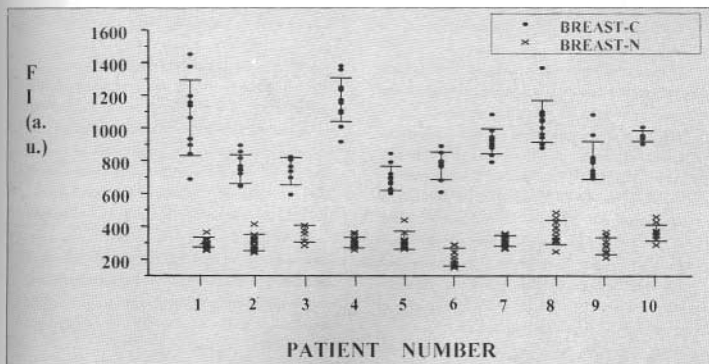


Fig. 4. Scatter plot for the spectrally integrated fluorescence intensity of paired cancerous and adjoining normal breast tissue samples from ten patients.

discriminating cancerous from normal oral tissues were ~90% over the sample size investigated<sup>15</sup>. Use of a stepwise multi-variate linear regression (MVLRL) analysis with ten input parameters led to only a marginal improvement in the discrimination results<sup>16</sup>. It is pertinent to note that having a discrimination parameter based only on  $\sum_{\lambda} I_{\lambda}(\lambda)$  has the advantage of a much simpler experimental arrangement, since no spectral resolution is required. It can however be used as a good discrimination parameter only when the difference in intensity values for malignant and normal sites is much more than the variations possible due to the various experimental factors. Applicability to in-vivo studies therefore needs to be investigated. The LIF based approach is expected to lead to an early diagnosis and may allow detection of pre-malignant alterations for which presently no effective non-invasive method exists.

#### *Breast cancer*

Autofluorescence spectroscopy of breast tissue with  $N_2$  laser excitation showed that the cancerous tissue was considerably more fluorescent compared to the normal and the benign tumor tissue<sup>17,18</sup>. A scatter plot for the integrated fluorescence intensity from paired cancerous sites and adjoining normal breast tissue sites from 10 patients is shown in Fig. 4. The ratio of the mean fluorescence intensity for cancerous sites to that from normal and benign tumor sites were -2.82 and 3.23 respectively in the study involving 63 patients, 28 with ductal carcinoma and 35 with fibroadenoma<sup>18</sup>. With 300 nm and 488 nm excitation the cancerous sites were more fluorescent than the normal. However, no statistically significant difference was observed in the fluorescence intensity of cancerous and benign tumor sites. Therefore, while cancerous tissue could be discriminated from normal with good sensitivity and

specificity, the discrimination results were poor for discriminating cancerous from benign tumor tissue. With 337 nm excitation, the use of fluorescence intensity as a discrimination parameter could however, discriminate cancerous tissue from, both normal and benign tumor tissue, with sensitivity and specificity values of > 99%<sup>19</sup>.

Excitation-emission spectroscopy<sup>19</sup> and time-resolved measurements<sup>20</sup> carried out on breast tissue autofluorescence have revealed a significant variation in the concentration of fluorophores in malignant, benign tumor and normal tissue types. Some of the predictions of the spectroscopic analysis have been confirmed by biochemical estimation<sup>21</sup>. This variation in the concentration of the fluorophores explained why the discrimination results obtained with 337 nm excitation were much better compared to that obtained with the use of other excitation wavelengths by other researchers<sup>22</sup>.

Although breast cancer is not a superficial disease, the LIF based diagnosis of breast cancer can be conveniently done during needle biopsy. This is of interest because X-ray mammography, the best available means of detecting breast cancer at present, has two important drawbacks. First it leads to a very large number of false positives, i.e., a very large proportion (60-90%) of mammographically abnormal detection turn out to be benign upon invasive breast biopsy, leading to avoidable trauma and psychological stress to patients<sup>23</sup>. Secondly, frequent exposure to ionizing x-ray radiation during mammography has potential hazards, howsoever remote. Laser screening can be used without the adverse effects associated with the use of ionizing radiation. Further, the results of the in-vitro studies suggest that the LIF technique may offer much improved specificity.

### *Uterine cancer*

The  $N_2$  laser excited autofluorescence spectra from uterine tissue also showed significant differences between normal and cancerous tissue. The differences in the spectra were quantified using a stepwise MVLR analysis. The discrimination score based on a 4 variable MVLR analysis could discriminate cancerous sites from normal with sensitivity and specificity values of greater than 85% in general and up to 100% when the cancerous site showed red fluorescence characteristic of endogenous porphyrins<sup>24</sup>.

### *Reasons for the spectral differences*

An understanding of the factors responsible for the significant differences between the autofluorescence spectra of cancerous, benign tumor and normal tissue sites is clearly very important. This may not only help in optimization of the diagnostic system but may also provide valuable biochemical information on the tissue. Comprehension of the spectral

differences requires that the fluorophores present in the different tissue types are identified and their relative concentrations estimated.

The results of excitation/ emission<sup>15,19</sup>, synchronous luminescences<sup>25,26</sup> and time-resolved studies<sup>20</sup> carried out at CAT on breast and oral cavity tissues suggest a significant variation in the concentration of the fluorophores in the different tissue types. In particular, the studies reveal that while concentration of NADH is higher in malignant breast tissues compared to benign tumor and normal breast tissues<sup>19</sup>, the reverse is true for tissues from oral cavity where NADH concentration is higher in normal oral tissues<sup>15</sup>. These results have also been confirmed by enzymatic measurements of NADH concentration in malignant and normal tissues from breast and oral cavity<sup>21</sup>. The differences in fluorophore concentration inferred from spectroscopic studies qualitatively explain the observed spectral differences in the autofluorescence spectra of the oral and breast tissues.

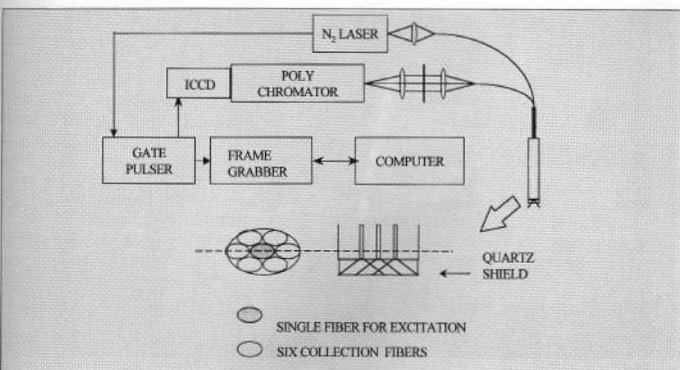


Fig. 5. A schematic of the prototype LIF based system developed at CAT for in-vivo studies on cancer diagnosis.

### *In-vivo studies*

A schematic of the LIF based system developed at CAT for in-vivo clinical studies is shown in Fig. 5. It consists of a sealed-off  $N_2$  laser (7 ns, 100  $\mu$ J, 10 Hz), an optical fiber probe, and a gateable intensified CCD detector. The diagnostic probe, developed in-house is a fiber bundle, which has two legs; one contains a single quartz fiber (NA 0.22, core diameter 400 $\mu$ m) and the other contains six quartz fibers (NA 0.22, core diameter 400 $\mu$ m). The central fiber delivers excitation light to the tissue surface and the six surrounding fibers collect tissue fluorescence from the surface area directly illuminated by the excitation light. The light coming from the distal ends of the six collection fibers is imaged at the entrance slit of a

polychromator coupled to the intensified CCD. The fiber bundle is enclosed in an SS tube (9 mm outer diameter). The tip of the probe is shielded by a quartz optical flat (2 mm thick). This is to provide a fixed distance between the tissue and the fibers for improved fluorescence collection and to protect contamination of the fiber tips with body fluids. A photograph of the assembled unit is shown in Fig. 6.

One unit has been installed at a cancer screening center at Indore and is being used to record autofluorescence spectra of different regions from uterine cervix of patients screened for neoplasm of uterine cervix. The other unit at CAT has been used to carry out a pilot study on 25 patients with histopathologically confirmed squamous cell carcinoma of oral cavity<sup>27</sup>. The

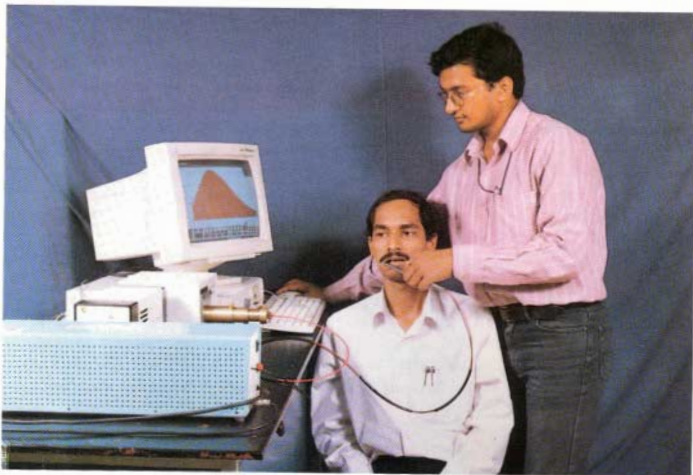


Fig. 6. A photograph of the LIF based system developed at CAT for cancer diagnosis.

discrimination algorithm developed could differentiate the squamous cell carcinoma of the oral cavity from normal squamous tissue with a sensitivity and specificity, towards cancer, of 86% and 63%, respectively. The results are shown in Fig. 7. The reason for the relatively lower specificity values appears to be the fact that most of the patients who participated in this study were at an advanced stage of malignancies. Some of the visually uninvolved sites assumed to be normal may therefore not be truly normal. This follows because the normal appearing

region surrounding the cancerous tumor may have biochemical changes due to the field-effect of the malignancy. Indeed, when the discrimination analysis was carried out on the basis of the spectra averaged over all cancerous sites and the spectra averaged over all normal sites from a patient, a sensitivity and specificity towards cancer of 100% were obtained. The remarkably good results obtained on site averaged spectra suggests that a few of the normal sites had signatures very different from the other sites of the group.

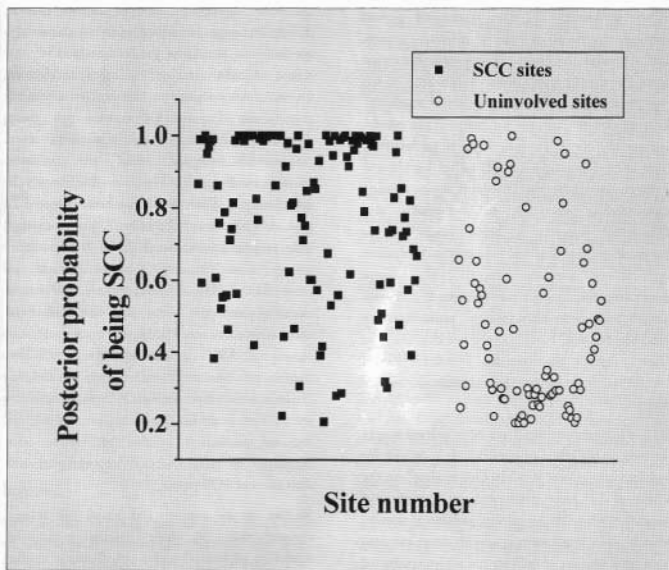


Fig. 7. The posterior probabilities of being classified as squamous cell carcinoma (SCC) for the tissue sites investigated.

## Studies on Photobioactivation

The use of light for non-surgical therapeutic applications exploits photochemical reactions initiated by photo-excitation of natural chromophores or exogenous drugs localized in the tissue. Some well-known examples of the therapeutic use of light<sup>28</sup> are its use in the treatment of psoriasis, neonatal jaundice, skin tuberculosis, photodynamic therapy of cancer, etc. Several researchers have also reported that irradiation with narrow bandwidth light (laser) can have profound effect on cellular cultures and animal models<sup>5</sup> and can also lead to therapeutic effects in humans<sup>6a,10</sup>, like, accelerated wound healing, treatment of pain of different origins, etc.. Although the usage of lasers for non-surgical laser therapeutic applications is growing it has not yet become an established clinical modality<sup>29</sup> because the mechanisms for many of the photo-therapeutic effects are not very well understood. The clinical potential of this rather simple and inexpensive therapeutic modality is motivating considerable work in this direction and substantial progress is being made<sup>11</sup>. It is pertinent to note that for these photo-therapeutic applications any conventional light source generating the appropriate wavelength and with the desired parameters (energy, pulse duration etc.) can be used. However, the better control on laser light characteristics often makes phototherapy more convenient with the use of lasers.

At CAT several studies have been carried out to investigate the effect of laser radiation on cellular cultures and animal models. Our studies<sup>30</sup> on the effect of  $N_2$  laser irradiation on the skin of animal models (albino rabbits and mice) showed that  $N_2$  laser irradiation at certain doses can lead to a proliferation of cells in the active epidermal layer of the rabbit/mice skin. Such proliferation of cells can contribute to faster healing of the wounds reported in several clinical studies.

Further, the fact that an inhibition of cell proliferation was observed at higher dose highlights the importance of a careful study of the parametric dependence in order to elicit the desired clinical response. Since macrophages play an important role in the process of wound healing, effect of light on macrophages has also been studied and stimulation of macrophages observed following He-Ne laser irradiation<sup>31</sup>.

The studies on narrow bandwidth light effects on *E-coli* bacterial systems carried out at CAT have provided two interesting results. First, it has been observed<sup>32</sup> that He-Ne laser irradiation can stimulate respiratory electron transfer process through change in redox state of respiratory components. Since the production of ATP, the source of cellular energy, is linked to electron transfer such stimulation can lead to enhanced metabolism. Experiments carried out using different inhibitors for the respiratory chain components suggest that the primary photoreceptor at He-Ne laser wavelength is cytochrome d. Secondly, it has been observed<sup>33,34</sup> that He-Ne laser (632.8nm) pre-irradiation induces protection towards UVC irradiation in several *E.coli* strains. The magnitude of protection was found to depend on He-Ne laser intensity, exposure time and the period of incubation between He-Ne laser exposure and subsequent UVC irradiation. The results also suggest involvement of singlet oxygen in the He-Ne laser induced protection. Recent experiments with *E-Coli* strain KY706/pPL-1 suggest that the induced protection is due to He-Ne laser irradiation induced induction of *phr* gene and activation of SOS repair.

Studies carried out on red blood cell lysate<sup>35</sup> showed that  $N_2$  laser irradiation induces oxidation of hemoproteins. Mechanistic studies and experiments with deoxygenated red blood cell lysate rule out involvement of any reactive oxygen species and suggests that the process is

photochemical and not intrinsic photosensitizer induced photodynamic reaction. A single cell gel electrophoresis set up was also developed and used to investigate UVA induced DNA damage in mice peritoneal macrophages<sup>36</sup>.

Studies on photodynamic effect of photosensitisers on cellular cultures and animal have also been initiated at CAT. Studies were carried out on the photodynamic inactivation of *Bacillus subtilis* cells by He-Ne laser irradiation in presence of methylene blue (MB) and toluidine blue (TB). Results show that outside the cell both MB and TB lead to photodynamic generation of singlet oxygen causing a decrease in cell membrane fluidity. However, whereas TB remains outside the cell and does not lead to generation of free radicals, in MB mediated photodynamic action, superoxide radical generated intracellularly is the major contributor to the cell damage<sup>17</sup>. Investigations have also been carried out photodynamic effect of MC540 and ALA on cell lines of epithelial neoplasm and on ALA induced accumulation of protoporphyrin (Pp) in tumor and skin of fibrosarcoma bearing mice. Effect of glucose pre-treatment and fractionated delivery of ALA on Pp accumulation in tumor and tumor to skin ratio of Pp was investigated. A pilot study on photodynamic therapy of animal tumors has also been carried out<sup>38</sup>. This was a collaborative work with a group at RMC to characterize a photosensitiser drug patented jointly by Radiation Medicine Centre (RMC), Mumbai, and IIT, Mumbai.

## Development of Techniques for Optical Imaging

Optical imaging has the potential to provide sub-millimeter resolution imaging without the need for ionizing radiation and associated risks. The fundamental problem with optical imaging is that in contrast to x-rays optical photons are strongly scattered in tissue, which leads to a

blurring of the image. Several approaches can be used to pick out the useful image bearing light from the background-scattered light<sup>13</sup>. One approach is to exploit the fact that the scattered light emerges from the tissue in all directions and also takes longer time to emerge as compared to the component of light which does not undergo any scattering or is predominantly forward scattered. Therefore, using spatial filters and by use of ultra-short temporal gates (of picosecond / sub-picosecond duration) image bearing components can be filtered out. Though the spatial resolution achievable in these techniques is very high (few tens of microns), these can not be used for imaging through large tissue thickness since the amount of image bearing light falls off exponentially with the increase in the thickness of the scattering medium. One approach to address this problem is to selectively amplify the image bearing light using non-linear optical techniques. Experiments on optical imaging through turbid media have been carried out at CAT using a Streak Camera with temporal resolution of ~ 10 ps and also by utilizing stimulated Raman scattering (SRS) approach for time gating. A spatial resolution of ~ 300  $\mu\text{m}$  has been observed in the present set-up.

## Development of Laser Optical Trap-Microbeam Set Up

Development of laser trap and microbeam set up has also been taken up at CAT because it is finding widespread applications in biomedicine for non-contact micromanipulation of microscopic objects<sup>14</sup>. Laser microbeam is essentially a pulsed laser beam coupled to a microscope. The large intensities (of up to  $10^{13}$   $\text{W}/\text{cm}^2$  with UV laser microbeam) generated at the focal point of the large numerical aperture microscope objective can be used to cut, perforate or fuse microscopic objects with sub-micrometer accuracy. As these intensities arise

only at the focal point, it is possible to work within the depth of a transparent object without opening it. Optical tweezer or laser optical trap uses the light of a CW infrared laser for transport of microscopic objects. Here, the gradient forces arising due to the large gradient of light intensity in the focussed laser beam and the resulting gradient in the light pressure and the electric field are used to trap microscopic objects at the focal point of the laser beam. Unlike mechanical microtools, the optical trap is gentle and absolutely sterile and can be used to capture, move and position single cells or subcellular particles without direct contact or significant damage. A laser trap set up has recently been made operational at CAT and used to trap polystyrene microspheres and motile bacteria (*Pseudomonas* and *E-Coli*).

## Conclusions

There exist considerable current interest in the development of laser-based techniques for *in-situ*, near real time diagnosis. Several studies have been carried out at CAT on laser induced fluorescence of tissues resected at surgery or biopsy from patients suffering from cancer of oral cavity, breast or uterus. These studies have provided very encouraging results on discrimination of cancerous tissue sites from benign tumor tissue or normal tissue sites. N<sub>2</sub> laser based systems have been developed for clinical studies and are being used for *in-vivo* studies on the diagnosis of cancer of oral cavity and uterine cervix. A pilot study on 25 patients with histopathologically confirmed squamous cell carcinoma of oral cavity has been completed and satisfactory discrimination results obtained.

Photobioactivation using endogenous and exogenous chromophores also holds considerable promise for a variety of therapeutic applications. However, realizations of this potential requires careful studies on the effects of narrow

bandwidth light on cellular cultures and animal models so that the mechanisms responsible for the various photo-therapeutic effects are better understood. Several studies in this direction have also been carried out at CAT.

## Acknowledgments

The author will like to thank his colleagues at Biomedical Applications Section and Laser Applications and Electronics Division, CAT who have contributed to the work described in the paper. It is also a pleasure to thank Dr. D. D. Bhawalkar, Director, CAT for his support and encouragement.

## References

1. See for example (i) Wolbarsht, M. L., ed., "Laser applications in medicine and biology", Vol. 1-5, Plenum Press, New York, 1971, 1974, 1977, 1989 and 1991; (ii) Caro, R. C. and Choy, D. S. J., (Guest eds.) Optics and Photonics News, Special issue on Optics and Light in Medicine, Oct. 92, pp. 9-44 and (iii) Gupta, P. K., in "Medical Physics for Human Health Care", (eds. Bhatnagar, P.K., Pradhan, A. S., and Reddy, A. R.), Scientific Publishers, Jodhpur, 1997, pp. 143-161 and references therein.
2. Servick-Muraca, E., and Benaron, D., (eds.), "OSA Trends in Optics and Photonics on Biomedical Optical Spectroscopy and Diagnostics", Optical Society of America, Washington, D.C., Vol. 3, 1996.
3. Wagnieres, G. A., Star, W. M., and Wilson, B. C., Photochem. Photobiol. 1998, 68, 603-632.
4. Special Section: Biomedical Applications of Lasers, Curr. Sci., 1999, 77, 885-941.



5. Karu, T. I., "Photobiology of low-power laser therapy", Harwood Academic Publishers, London, 1989.
6. Ohshirao, T, and Calderhead, R. G., "Low level laser therapy a practical introduction", John Wiley and Sons, Chichester, 1988; Ohshirao, T, "Low reactive level laser therapy: practical applications", John Wiley and Sons, Chichester, 1991.
7. Henderson, B. W., and Dougherty, T. J., (eds.), "Photodynamic Therapy Basic Principles and Applications", Marcel Dekker, New York, 1992.
8. Baxter, G. D., "Therapeutic lasers, Theory and Practice", Churchill Livingstone, Edinburgh, 1994.
9. Yamamoto, H., Okunaka, T., Furukawa, K., Hiyoshi, T., Konaka, C., and Kato, H., *Curr. Sci.*, 1999, 77, 894-903.
10. Bhagwanani, N. S., *Laser News*, 1995, 6(3), 8-12, and 6(4), 6-8.
11. Gupta, P. K., and Bhawalkar, D. D., *Curr. Sci.*, 1999, 77, 925-933.
12. Karu, T. I., *J. Photochem. Photobiol. B: Biol.*, 1999, 49, 1-17.
13. Rudolph, W., and Kempe, M., *J. Mod. Optics*, 1997, 44, 1617-1642.
14. Greulich, K. O., "Micromanipulation by light in biology and medicine", Birkhauser Verlag, Berlin, 1999.
15. Majumder, S. K., Gupta, P. K. and Uppal, A., *Lasers Life Sci*, 1999, 8, 211-227.
16. Majumder, S. K., Gupta, P. K. and Uppal, A., in "Optical Diagnostics of Biological Fluids III", (ed. Priezhev, A. V.), *Proc. Soc. Photo-Opt. Instrum. Eng.*, 1998, 3252, pp. 158-168.
17. Majumder, S. K., Uppal, A., and Gupta, P. K., in "Trends in Optics and Photonics Volume on Biomedical Spectroscopy and Diagnosis" Eds. Benavon, D., and Sevcik-Muraca, E., *Optical Society of America*, Vol. 3, 1996, pp. 142-146.
18. Gupta, P.K., Majumder, S. K., and Uppal, A., *Lasers Surg. Med.*, 1997, 21, 417-422.
19. Majumder, S. K., Gupta, P. K., Jain, B., and Uppal, A., *Lasers Life Sci*, 1999, 8, 249-264.
20. Jain, B., Majumder, S. K., Gupta, P. K., *Lasers Life Sci.*, 1998, 8, 163-173.
21. Uppal, A., Majumder, S. K. and Gupta, P. K., *Proc. National Laser Sympos.*, 1998, IIT Kanpur, pp. 219-220.
22. Katz, A, Alfano, R. R., in *Servick-Muraca, E., and Benaron, D., (eds.), "OSA Trends in Optics and Photonics on Biomedical Optical Spectroscopy and Diagnostics"*, *Optical Society of America*, Washington, D.C., 1996, Vol. 3. pp. 132-133, and references therein.
23. Maranto, G., *Scientific American*, 1996, 275, 113.
24. Majumder, S. K., Uppal, A., and Gupta, P.K., *Curr. Sci.*, 1996, 70, 833-836.
25. Majumder, S. K., and Gupta, P. K., in "Optical Diagnostics of Biological Fluids III", (ed. Priezhev, A. V.), *Proc. Soc. Photo-Opt. Instrum. Eng.*, 1998, 3252, pp. 169-178.
26. Majumder, S. K., and Gupta, P. K., *Lasers Life Sci.*, 2000, 9, 143-152
27. Majumder, S. K., Mohanty, S. K., Ghosh, N., Gupta, P. K, Jain, D. K., and Khan, F., *Curr. Sci.*, (in press).

28. Regan, J. D., and Parrish, J. A., (eds.), "The science of photomedicine", Plenum Press, New York, 1982.
29. Basford, J. R., *Lasers Surg. Med.*, 1995, 16, 331-342.
30. Agnihotri, S., Sachdeo, S., Sharma, A., Kcerti, V., and Gupta, P. K., *Lasers Life Sci*, 1997, 7, 227-235.
31. Bansal, H., Dubey, A., and Gupta, P. K., *Proc. National Laser Sympos.*, IIT Kanpur, 1998, pp. 227-228.
32. Dubey, A., Gupta, P. K., and Bharti, S., *Lasers Life Sci*, 1997, 7, 173-180.
33. Kohli, R., Gupta, P. K., and Dubey, A., in "Biologic effects of light 1995", (eds. Holick, M. F. and Jung, E.G.), Walter de Gruyter and Co. Berlin, 1996, pp., 243-245.
34. Kohli, R., Gupta, P. K., and Dubey, A., *Radiation Research*, 2000, 153, 181-185.
35. Murali Krishna, C., Bose, B., and Gupta, P. K., *Radiation Research*, 2000, 153, 411-415.
36. Bock, C., Dubey, A., Greulich, K. O., and Gupta, P. K., *Mutation Research*, 1999, 439, 171-181.
37. Dubey, A., Bansal, H., and Gupta, P. K., *Indian J Biochem. & Biophysics*, 2000, 37, 245-250.
38. Murugesan, S., Gupta, P. K., Sharma, M., Dube, A., Noronha, O. P. D., Samuel, A. M., Shetty, S. J., Srivastava, S., Khare, R., Bhatnagar, R., and Pathak, S., Presented at XV Asia Pacific Cancer Conference, 12-15 December, 1999, Cancer Institute, Chennai.

*Dr P.K. Gupta is the recipient of the Homi Bhabha Science and Technology Award for the year 1998.*

*About the author ....*



*Dr. P.K. Gupta (M.Sc., Lucknow University, 1973) joined the erstwhile Laser Section, BARC, in 1974 after graduating through the BARC Training School. His research interests, while at BARC, included non-linear optical frequency conversion, CO<sub>2</sub> lasers and CO<sub>2</sub> laser pumped molecular gas lasers. Dr. Gupta was at Heriot Watt University, U.K. from November 1979 to November 1981 on a Commonwealth Scholarship Award and later on a postdoctoral fellowship during 1988-89. He obtained his Ph.D. degree from Heriot Watt University in 1981 for his work on efficient mid-infrared generation by optical pumping of molecular gases and non-linear optical mixing. Dr. Gupta moved to Centre for Advanced Technology (CAT), Indore, in March 1990. At CAT,*

*he initiated work on CO<sub>2</sub> laser pumped far-infrared lasers and on biomedical applications of lasers. He presently heads the Biomedical Applications Section, at CAT. Dr. Gupta has earlier received the 1988 NS Satyamurthy Memorial award of the Indian Physics Association for his contributions on mid-infrared coherent sources.*



# SCALING OF THE STEADY STATE AND STABILITY BEHAVIOUR OF SINGLE-PHASE NATURAL CIRCULATION SYSTEMS

P.K. Vijayan

Reactor Engineering Division  
Bhabha Atomic Research Centre

## Abstract

*Scaling methods for both the steady state and stability behaviour of single-phase natural circulation systems have been presented. For single-phase systems, simulation of the steady state flow can be achieved by preserving just one nondimensional parameter. Simulation of the stability behaviour requires geometric similarity in addition to the similarity of the physical parameters appearing in the governing equations. The scaling laws proposed have been tested with experimental data on single-phase natural circulation.*

## Introduction

NATURAL CIRCULATION IS being increasingly employed in many innovative designs of nuclear reactor cooling systems. The basic advantage of natural circulation systems is the enhanced safety due to its passive nature. One of the basic requirements, which arise prior to the incorporation of such systems in nuclear reactors, is the assessment of their performance. Generally, in the nuclear field the assessment is carried out by validated computer codes. Code validation is usually done with data obtained from scaled test facilities. The topic of the present paper is the scaling laws used for constructing such scaled facilities for simulating single-phase natural circulation. Such a scaled facility in nuclear parlance is also known as an integral test facility (ITF).

Scaling laws make possible the comparison of the performance of different natural circulation

systems and to extrapolate the data from small scale to prototype systems. Scaling laws for nuclear reactor systems are arrived at using the governing conservation equations. Pioneering work in the field of scaling laws for nuclear reactor systems have been carried out by Nahavandi et al. (1979), Zuber (1980) and Heisler (1982). The scaling law proposed by Zuber is also known as the power-to-volume scaling philosophy and is widely used for the construction of scaled test facilities simulating nuclear reactor systems. Power to volume scaling can be applied to both forced and natural circulation systems. However, the power-to-volume scaling philosophy has certain inherent distortions (especially in downsized components), which can suppress certain natural circulation specific phenomena like the instability (Nayak et al. (1998)). Hence it is necessary to examine the scaling laws which are specific to natural circulation. In the present

paper, the reported scaling laws for single-phase natural circulation loops are reviewed with respect to their use for predicting the steady state and stability behaviour. Then scaling procedures for single and two-phase systems are presented and tested against the available data on the steady state and stability performance of natural circulation loops. This exercise has shown that the steady state behaviour of single-phase loops can be simulated by a single dimensionless parameter. The simulation of the stability behaviour requires simulation of at least three dimensionless parameters in addition to geometric scaling. For the stability behaviour, scaling of the characteristic equation (obtained by the linear stability analysis method) appears to be the appropriate method for achieving similarity.

## Review of Scaling Laws

Several scaling laws have already been proposed for the design of scaled loops simulating natural circulation phenomenon (Zuber (1980), Heisler (1982) and Ishii-Kataoka (1984)). All the three scaling laws are derived from the governing differential equations. One of the problems associated with these scaling laws is that the number of similarity groups are too many and they do not provide steady state or stability solutions in terms of the proposed similarity groups. Therefore, testing of these scaling laws with the available experimental data is rather difficult without the use of system codes. This arises due to the fact that more than one scaling parameter is a function of the flow rate, which for a natural circulation loop is not known a priori. To overcome this problem, Vijayan et al. (1992) proposed a scaling procedure by which the steady state flow rate can be obtained as a function of just one similarity group. This procedure has been extended recently to nonuniform diameter loops (Vijayan (1999), see

also section 3). They have also obtained the stability solution in terms of the similarity groups.

## Proposed Scaling Laws for Single-Phase Natural Circulation

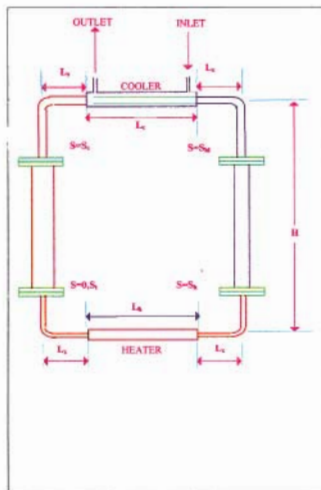


Fig. 1. Schematic of non-uniform diameter natural circulation loop

Consider a simple nonuniform diameter natural circulation loop as shown in Fig. 1 with a horizontal heat source at the bottom and a horizontal heat sink at the top. The heat sink is maintained by providing cooling water to the secondary side of the cooler at a specified inlet temperature of  $T_c$ . In this analysis, the secondary side temperature is assumed to remain constant. The heat flux at the heat source is maintained constant. Assuming the loop to be filled with an

incompressible fluid of constant properties except density (Boussinesq approximation where density is assumed to vary as  $\rho = \rho_0[1 - \beta(T - T_0)]$ ) with negligible heat losses, axial conduction and viscous heating effects, the governing differential equations can be written as

$$\frac{\partial W}{\partial s} = 0 \quad \dots\dots\dots(1)$$

$$\Gamma \frac{dW}{dt} = g \rho_0 \beta \int T dz - \frac{W^2}{2 \rho_0} \sum_{i=1}^N \left( \frac{f L_i}{D} + K_i \right) \frac{1}{A_i^2} \quad \dots\dots\dots(2)$$

where  $\Gamma = \Sigma L_i / A_i$ . It is also possible to absorb the local pressure loss coefficient,  $K_i$ , into an equivalent length,  $L_{e_i}$ , such that  $K_i = f L_{e_i} / D$ . With this correction, the momentum equation can be written as:

$$\Gamma \frac{dW}{dt} = g \rho_0 \beta \int T dz - \frac{W^2}{2 \rho_0} \sum_{i=1}^N \left( \frac{f L_{eff}}{D A_i^2} \right) \quad \dots\dots\dots(3)$$

Similarly, the energy equation for the different sections of the loop is given as:

$$\frac{\partial T}{\partial t} + \frac{W}{\rho_c A_c} \frac{\partial T}{\partial s} = \frac{q_h P_h}{A_c \rho_c C_p} \quad \text{Heater} \quad \dots\dots\dots(4a)$$

$$\frac{\partial T}{\partial t} + \frac{W}{\rho_c A_c} \frac{\partial T}{\partial s} = - \frac{U P_c (T - T_s)}{A_c \rho_c C_p} \quad \text{Cooler} \quad \dots\dots\dots(4b)$$

$$\frac{\partial T}{\partial t} + \frac{W}{\rho_p A_p} \frac{\partial T}{\partial s} = 0 \quad \text{Pipe} \quad \dots\dots\dots(4c)$$

The above equations can be non-dimensionalised using the following substitutions.

$$\omega = \frac{W}{W_{ss}}; \quad \theta = \frac{T - T_s}{(\Delta T_h)_{ss}}; \quad S = \frac{s}{H}; \quad Z = \frac{z}{H};$$

$$\tau = \frac{t}{t_r}; \quad a_i = \frac{A_i}{A_r} \quad \text{and} \quad d_i = \frac{D_i}{D_r} \quad \dots\dots\dots(5)$$

where  $t_r$ ,  $A_r$  and  $D_r$  are respectively the reference values of time, flow rate and hydraulic diameter defined as

$$t_r = \frac{V_t \rho_r}{W_{ss}}; \quad A_r = \frac{1}{L_t} \sum_{i=1}^N A_i L_i = \frac{V_t}{L_t} \quad \text{and}$$

$$D_r = \frac{1}{L_t} \sum_{i=1}^N D_i L_i \quad \dots\dots\dots(6)$$

It is easy to see that the reference time is nothing but the loop circulation time.  $D_r$  and  $A_r$  are respectively the length average hydraulic diameter and flow area of the loop and the total circulation length,  $L_t = \Sigma L_i$ . In case of negligible local pressure losses,  $\Sigma(L_{e_i})$ , becomes equal to the total circulation length,  $L_t$ , of the loop. The non-dimensional equations can be expressed as:

$$\gamma \frac{d\omega}{d\tau} = \frac{Gr_m}{Re_{ss}^3} \int \theta dz - \frac{L_t}{D_r} \frac{\omega^2}{2} \sum_{i=1}^N \left( \frac{f L_{eff}}{d a_i^2} \right) \quad \dots\dots\dots(7)$$

$$\frac{\partial \theta}{\partial \tau} + \frac{\omega}{a_h} \frac{\partial \theta}{\partial S} = \frac{V_t}{V_h} \quad \text{heater} \quad \dots\dots\dots(8a)$$

$$\frac{\partial \theta}{\partial \tau} + \frac{\omega}{a_c} \frac{\partial \theta}{\partial S} = - St \frac{P_c L_t}{A_c} \theta \quad \text{cooler} \quad \dots\dots\dots(8b)$$

$$\frac{\partial \theta}{\partial \tau} + \frac{\omega}{a_p} \frac{\partial \theta}{\partial S} = 0 \quad \text{pipes} \quad \dots\dots\dots(8c)$$

where  $\gamma = \Sigma L_i / a_i$ ,  $l_i = L_i / L_t$ ,  $(l_{e_i}) = (L_{e_i}) / L_t$ ,  $Gr_m = D_r^3 \rho_r^2 \beta g \Delta T / \mu^2$ , and  $St = Nu / Re_{ss} Pr$ . Assuming fully developed forced flow correlations are valid, the friction factor,  $f$ , can be expressed as

$$f_i = \frac{p}{Re_i^b} = \frac{p\omega^{-b}}{Re_{m,i}^b (d/a)_i^b} \dots\dots\dots(9)$$

where  $p=64$  and  $b=1$  for laminar flow and assuming Blasius correlation to be valid for turbulent flow  $p$  and  $b$  are respectively 0.316 and 0.25. In a non-uniform diameter loop, it is possible that some pipe sections are in turbulent flow ( $Re > 4000$ ) and some in laminar flow ( $Re < 2000$ ) and still others in transition flow ( $2000 < Re < 4000$ ). However, if we assume the entire length of the loop to be under either laminar or turbulent flow conditions, then equation (7) can be expressed as

$$\gamma \frac{d\omega}{d\tau} = \frac{Gr_m}{Re_m^b} \oint \theta dZ - \frac{L_r}{D_r} \frac{p\omega^{1-b}}{2 Re_m^b} \sum_{i=1}^N \left( \frac{l_{off}}{d^{1+b} a^{2-b}} \right) = \frac{Gr_m}{Re_m^b} \oint \theta dZ - \frac{pN_{G_i} \omega^{2-b}}{2 Re_m^b} \dots\dots\dots(10)$$

where  $N_G$  is a geometric parameter defined

$$as N_G = \frac{L_r}{D_r} \sum_{i=1}^N \left( \frac{l_{off}}{d^{1+b} a^{2-b}} \right) \dots\dots\dots(11)$$

**Steady state solution**

The governing equations for the steady state condition are obtained by dropping the time dependent terms. Also, by definition  $\omega$  (the non-dimensional flow rate) is unity at steady state. Therefore, the steady state momentum and energy equations can be written as:

$$\frac{Gr_m}{Re_m^b} \oint \theta dZ = \frac{pN_{G_i}}{2 Re_m^b} \dots\dots\dots(12)$$

$$\frac{1}{a_b} \frac{d\theta}{dS} = \frac{V_i}{V_h} \text{ for heater ; } \frac{1}{a_c} \frac{d\theta}{dS} = -St \frac{P_c L_{t1} \theta}{A_c}$$

$$\text{for cooler and } \frac{1}{a_p} \frac{d\theta}{dS} = 0 \text{ for pipes } \dots\dots\dots(13)$$

The steady state solutions for the temperature of the various segments of the loop can be obtained from Eq. (13) (see Vijayan (1999)). Using these

steady state solutions, the integral in equation (12) can be calculated as  $\oint \theta dZ = 1$ , for the loop shown in Fig. 1. Hence, the steady state flow rate can be expressed as

$$Re_{m,i} = \left[ \frac{2Gr_m}{pN_{G_i}} \right]^{1/(3-b)} = C \left( \frac{Gr_m}{N_{G_i}} \right)^r \dots\dots\dots(14)$$

where  $C=(2/p)^r$  and  $r = 1/(3-b)$ . Thus, knowing the value of  $p$  and  $b$  the constants  $C$  and  $r$  in equation (14) can be estimated. For laminar flow (where  $p=64$ , and  $b=1$ ) equation (14) can be rewritten as

$$Re_{m,i} = 0.1768 \left[ \frac{Gr_m}{N_{G_i}} \right]^{0.5} \dots\dots\dots(15)$$

Similarly, assuming Blasius friction factor correlation ( $p=0.316$  and  $b=0.25$ ) to be valid for turbulent flow we can obtain the following equation

$$Re_{m,i} = 1.96 \left[ \frac{Gr_m}{N_{G_i}} \right]^{0.364} \dots\dots\dots(16)$$

In the transition region, one can expect a continuous change in the exponent of equation (14) from 0.5 to 0.364 as well as for the constant from 0.1768 to 1.96. It may be noted that both equations (15) and (16) are the exact solutions of equation (12) assuming the same friction factor correlation to be applicable to the entire loop. For closed loops, often the same friction factor correlation may not be applicable for the entire loop even if the loop is fully laminar or fully turbulent. An example is a fully laminar loop with part of the loop having rectangular cross section and remaining part having circular cross section. Hence, one has to keep in mind the

assumptions made in deriving the relationship (14) while applying it.

The relationship expressed by Eq. (14) is derived for a rectangular loop with both the heater and cooler having the horizontal orientation. For other orientations also, it can be easily shown that the same relationship holds good if the loop height in the definition of the  $Gr_m$  is replaced with the centre-line elevation difference between the cooler and the heater,  $\Delta z$  (see Vijayan et al. (2000)). The same is true for other loop geometries like the figure-of-eight loop used in Pressurised Heavy Water Reactors (PHWRs). For the figure-of-eight loop, the heater power used in the  $Gr_m$  is the total power of both heaters. The equations are also applicable for identical parallel-channel or parallel-loops systems if the parallel channels/loops are replaced by an equivalent path having the same hydraulic diameter and total flow area.

#### Stability behaviour

Equation (14) has shown that simulation of the steady state behaviour is possible by simulating  $Gr_m/N_G$  for any natural circulation loop. The transient and stability behaviour, however, are described by equations (8) and (10). Substituting the steady state solution, the transient momentum equation can be rewritten as

$$\gamma \frac{d\omega}{d\tau} = \left( \int \partial \Delta z - \omega^{2-b} \right) (p/2)^{\frac{3}{3-b}} / \left( Gr_m^{\frac{b}{3-b}} / N_G^{\frac{3}{3-b}} \right) \dots \dots \dots (17)$$

From equations (17) and (8), it is obvious that the transient and stability behaviours are governed by the physical parameters  $Gr_m$ ,  $St$  and the geometric parameters of  $N_G$ ,  $\gamma$ ,  $V/V_h$ ,  $P L/A_c$  and the area ratio  $a$ . To reduce the number of independent parameters, it is customary to

combine  $St$  and  $P_c L_t / A_c$  into a single dimensionless parameter called  $St$ . Similarly,  $Gr_m$  and  $N_G$  can be combined as  $Gr_m^{b/3} / N_G^{3/3-b}$  so that the transient and stability behaviour can be expressed as

$$\omega(\tau) = f \left( \frac{Gr_m^{b/(3-b)}}{N_G^{3/(3-b)}}, St_m, \frac{V_t}{V_h}, \gamma \text{ and } a \right) \dots \dots (18)$$

Further reduction in the number of independent parameters is possible for special cases. For example, with a uniform diameter loop,  $(V_t/V_h) = (L_t/L_h)$ ,  $a=1$ ,  $\gamma=1$  and  $N_G = L_t/D$  so that

$$\omega(\tau) = f \left( \frac{Gr_m^{b/(3-b)}}{(L_t/D)^{3/(3-b)}}, St_m \text{ and } \frac{L_t}{L_h} \right) \dots \dots (19)$$

In addition to  $L_t/L_h$  other length scales also affect the stability behaviour. This can be established by carrying out a linear stability analysis. In this method, the loop flow rate and temperature are perturbed as

$$\omega = \omega_{ss} + \bar{\omega} \varepsilon e^{nt} \text{ and } \theta = \theta_{ss} + \bar{\theta} \varepsilon e^{nt} \dots \dots (20)$$

where  $\varepsilon$  is a small quantity,  $\bar{\omega}$  and  $\bar{\theta}$  are the amplitudes of the flow and temperature disturbances respectively, and  $n$  is the growth rate of the perturbations. Substituting Eq. (20) in equations (10) and (17), and using the continuity of temperature perturbation in various segments as the boundary condition, the characteristic equation for the stability behaviour can be derived. The characteristic equation for a uniform diameter loop with horizontal heat source and sink can be expressed as  $Y(n)=0$  (Vijayan and Austregesilo (1994)), where

$$Y(n) = n - \frac{(p/2)^{3/(3-b)}}{(Gr_m)^{b/(3-b)} (D/L_t)^{3/(3-b)}} \{ \psi(n, St_m) + 2 - b \} \dots \dots \dots (21)$$

where  $\psi(n, St_m) = \frac{L_t}{nH} \{1 - \exp(-nH/L_t)\} \exp(-nS_c H/L_t) \left( \frac{\bar{\theta}_h - \bar{\theta}_c}{\omega} \right)$  and

$$\left( \frac{\bar{\theta}_h - \bar{\theta}_c}{\omega} \right) = \frac{L_t}{nL_h} \{ \exp(-nL_h/L_t) - 1 \} + \{ \exp[-n(S_c - S_i - S_h)H/L_t] - 1 \} \frac{B+C}{D}$$

$$B = \frac{L_t}{nL_h} \exp(-nS_c H/L_t) \{1 - \exp(nL_h/L_t)\}; C = \frac{(\theta_{hi})_{St_m}}{n} [1 - \exp(-nL_c/L_t)]$$

and  $D = \exp\{St_m L_c/L_t\} - \exp(-n)$  where  $S_i = L_i/H$  and  $S_c = s_c/H$ .  $S_c$ ,  $S_i$  and  $S_h$  are the dimensionless distances from the origin (i.e.  $S=0$  in Fig. 1) in anti-clockwise direction. It is obvious from equation (21) that, apart from the parameters listed in (19), the ratios of the lengths are also required to be preserved to simulate the stability behaviour.

## Testing of Scaling Laws

The scaling laws presented in section 3 are tested against experimental data for both steady state and stability behaviour.

### Steady state behaviour

The steady state scaling laws were tested with data obtained from simple low pressure and high pressure loops. The data included both in-house experimental data and those compiled from literature.

### In-house data

For testing of the scaling laws, experiments were carried out in three uniform diameter rectangular loops with horizontal heater and horizontal cooler (Vijayan et al. (1992)). These loops (see Fig. 2) had the same length (both total and component lengths) and height but different internal diameters. These experiments helped to establish the adequacy of  $Gr_n/N_c$  as the scaling parameter for the steady state flow as the data from the three loops could be expressed in the

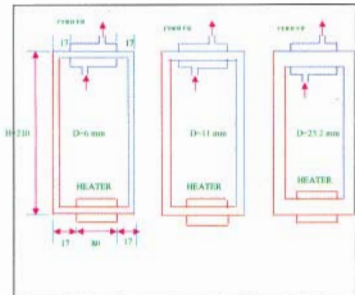


Fig.2 Uniform diameter loops with different external diameters and identical lengths (all dimensions in cm)

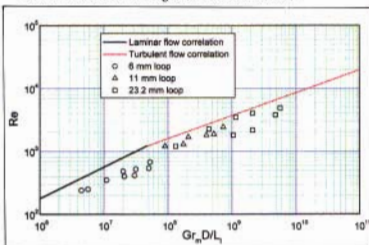


Fig.3 Steady state flow in uniform diameter loops

form of Eq. (14) with the same value of  $C$  and  $r$  (see Fig. 3). Subsequently, experiments were conducted to study the effect of the orientation of the heater and the cooler as different types of nuclear reactors have different orientations of the heat source (core) and the heat sink (steam



generator). For example, PHWRs have horizontal core and vertical steam generators, PWRs have vertical core and vertical steam generators and VVERs have vertical core and horizontal steam generators. In view of this, the heater and cooler orientations studied included the horizontal heater horizontal cooler (HHHC), horizontal heater vertical cooler (HHVC), Vertical heater horizontal cooler (VHHC) and vertical heater vertical cooler (VHVC). Further details of the experimental loop (see Fig.4) and data generated can be obtained from

Bade (2000) and Vijayan et al. (2000). The steady state data collected for different orientations of the heater and cooler are plotted without and with consideration of local pressure losses in Figs. 5a and b respectively. The experimental data is observed to be very close to the theoretical correlations for all orientations of the heater and cooler confirming the validity of the correlations (15) and (16). Considering the local pressure losses improves the agreement with the theoretical correlations (see Fig. 5b).

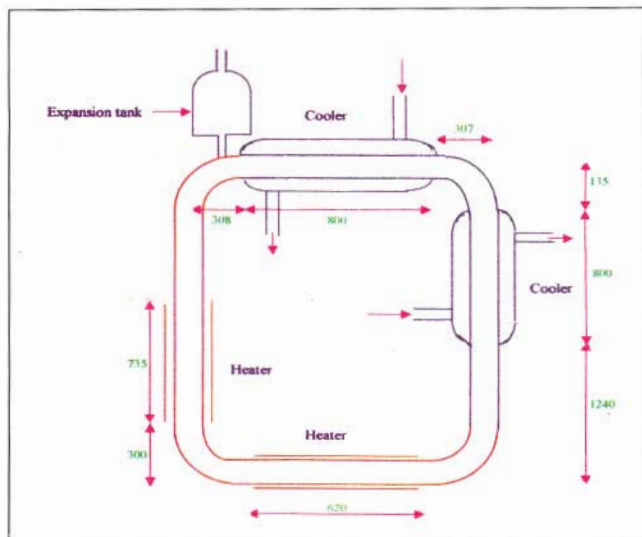


Fig. 4. Experimental loop to study the effect of orientation of the heat source and heat sink (all dimensions in mm)

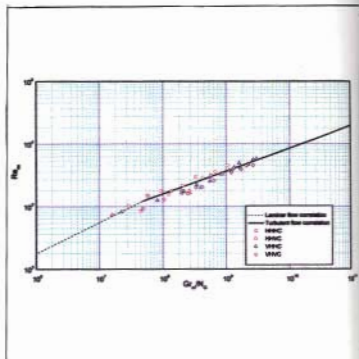
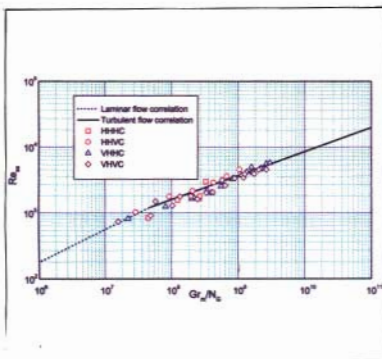


Fig. 5. Effect of heater and cooler orientations on steady state flow

Subsequent to this, experiments were carried out in the high pressure nonuniform diameter figure-of-eight loop FISBE (Facility for the Integral System Behaviour Experiments, see Fig.6), which simulates the Narora Atomic Power Station.

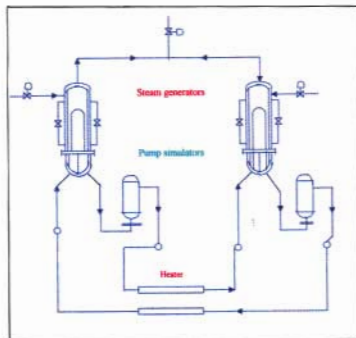


Fig. 6. Schematic diagram of FISBE

Steady state data from FISBE are compared with the present correlation in Fig. 7, which shows good agreement. It may be noted that for these

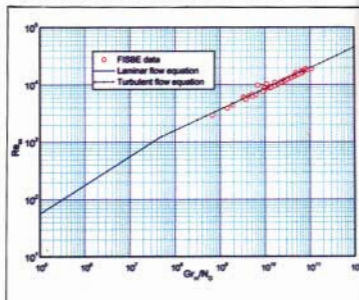


Fig. 7. Comparison of FISBE data with the theoretical correlation

tests the loop was an all pipe loop with a tubular heater section, a single U-tube steam generator and pumps replaced by pipe sections. Since the

SG used only one U-tube, more than 95% of the loop hydraulic resistance was due to this. Although the loop had several elbows, bends, Tees and other fittings, these were mainly concentrated in the large diameter pipe sections. Hence the contribution of the local pressure losses to the total hydraulic resistance became negligible giving good agreement with the turbulent flow correlation.

### Comparison with literature data

Several experiments on single-phase natural circulation loops are reported in the literature. The loops studied can be categorised as Uniform Diameter Loops (UDLs) and Nonuniform Diameter Loops (NDLs).

### Uniform Diameter Loops (UDLs)

The UDLs experimentally studied include both closed-loop and open-loop thermosyphons. Considering the shape of the loop, the closed loops can be further classified into rectangular, toroidal and figure-of-eight loops. Holman-Boggs (1960), Huang-Zelaya (1988), Misale et al. (1991), Bernier-Baliga (1992), Vijayan et al. (1992), Ho et al. (1997) and Nishihara (1997) obtained experimental natural circulation data in UDLs of rectangular shape. Uniform diameter open-loops were investigated by Bau-Torrance (1981, 1981a) and Haware et al. (1983).

Fig. 8 shows a comparison of the data with the theoretical correlations for laminar and turbulent flow for uniform diameter loops. The experimental data reported by Misale et al. (1991), Bernier-Baliga (1992) and Ho et al. (1997) are well predicted by the theoretical correlation. Most of these data points are from laminar flow region where the total local loss coefficient is negligible compared to  $L/D$  due to the large value of the friction factor. For the range  $2 \times 10^7 < Gr_m D/L_c < 3 \times 10^8$  significant deviation

is observed between the data and the correlation. Beyond  $Gr_m D/L_c$  of  $3 \times 10^8$ , the agreement is found to be better.

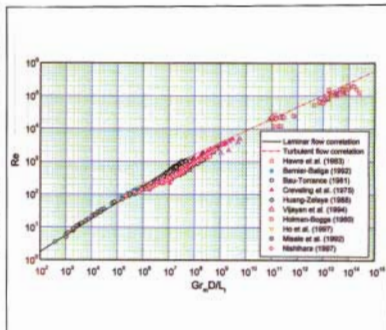


Fig. 8. Steady state natural circulation flow in UDLs without considering local losses

For all the steady state data reported in Fig. 8, it is assumed that  $\Sigma I_{\text{local}} = 1$ . But for all practical configurations of loops, local losses are present so that  $\Sigma I_{\text{local}} > 1$ . Hence, the observed deviations with the theoretical correlation may be attributed partly to the unaccounted local pressure losses in these loops. To study its effect, the local pressure loss coefficients due to elbows, bends, Tees, orifices, etc. given in Streeter and Wylie (1983) were used. The results are shown in Fig. 9. The turbulent flow data is now closer to the theoretical correlation indicating the significance of the local pressure losses at high Reynolds numbers where the friction factor is very low. The laminar region data is practically unaffected. The data for the transition region  $2 \times 10^7 < Gr_m/N_c < 3 \times 10^8$  is now closer to the theoretical correlation, but the deviation is still significant. This is the region where the correlation is not applicable as the loop is neither fully laminar nor fully turbulent. Instead the

loop is partly in the laminar region and partly in either transition or turbulent regions.

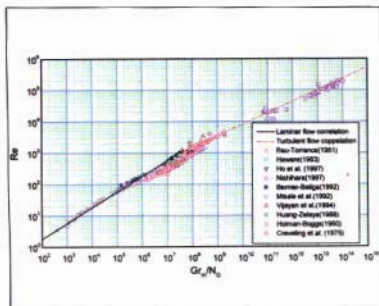


Fig. 9. Steady state natural circulation flow in UDLs without local losses

#### Nonuniform Diameter Loops (NDLs)

Most practical applications of natural circulation employ non-uniform diameter loops. Common examples are the nuclear reactor loop, solar water heater, etc. Most test facilities simulating nuclear reactor loops also use non-uniform diameter loops. Depending on the operating pressure, the non-uniform diameter loops can be categorised as High pressure loops and Low pressure loops. Most studies are conducted in the high-pressure test facilities simulating nuclear reactor loops. Typical examples are the SEMISCALE, LOBI, PKL, BETHSY, ROSA, RD-14, FISBE, etc. Some studies, however, are carried out in low-pressure facilities. Examples are the experiments carried out by Zvirin et al. (1981), Jeuck et al. (1981), Hallinan-Viskanta (1986), Vijayan (1988) and John et al. (1991). Most of the available experimental data in a usable form (i.e. full geometrical details are known) are from the low-pressure test facilities. High-pressure test data in a usable form was available only from FISBE. The data from NDLs are plotted in

Fig. 10, which shows reasonable agreement with theoretical correlation in the laminar and the turbulent flow regions. Significant deviation is observed for the intermediate values of  $Gr_n/N_G$  where the flow is neither fully laminar nor fully turbulent. Similar trend was observed in the case of UDLs. Interestingly, the parallel channel data of John et al. (1991) and parallel loop data of Jeuck et al. (1981) are also found to be in reasonable agreement with the theoretical correlation.

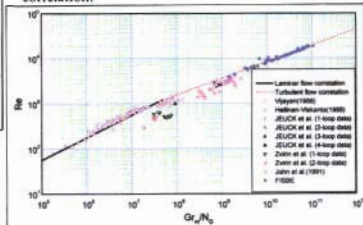


Fig. 10. Steady state flow in NDLs without considering local losses

#### Stability behaviour

Experimental data on stability behaviour are few. Even with the available data, it is often not possible to accurately estimate the parameters (see Eq. 21) affecting the stability behaviour. This is often caused by the fact that the heat transfer coefficient  $U$  used in the  $St_m$  is flow dependent, which makes it difficult to estimate it accurately. Due to this, the predicted stability behaviour is compared for different loops to test the validity of the scaling laws used. Figs. 11a and b show the predicted stability maps for laminar and turbulent flow respectively for different loops having the same length scale ratios, but with different diameters. As expected, the curves for all the loops merge giving a single curve for the stability behaviour. A prediction was also made for the different orientations of the heater and cooler for the loop shown in

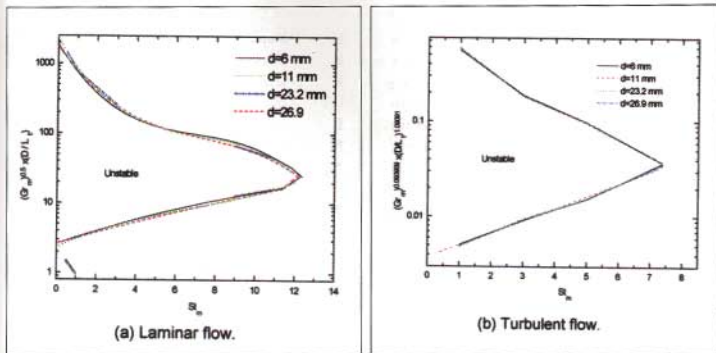


Fig. 11. Stability map for loops of different diameter

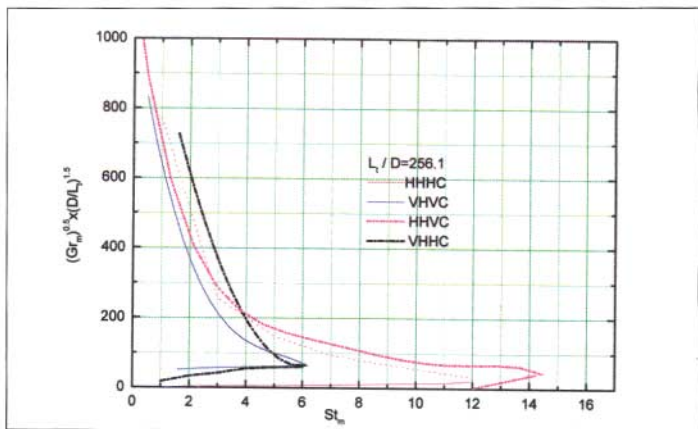


Fig. 12. Effect of heater and cooler orientations on the stability map

Fig. 4. The results are given in Fig. 12. As expected the results are found to be different for the different orientations, as the length scales are different even though the total circulation length and diameter are the same. This emphasizes the fact that simulation of the stability behaviour requires preservation of the length scales in addition to the physical parameters of  $St_m$ ,  $Gr_m$  and  $N_G$ . This is because the feedback effects are a strong function of the residence time, which depends on the length scale.

## Conclusions

Scaling laws for single-phase natural circulation systems have been presented. For single-phase systems, the steady state behaviour can be simulated by preserving  $Gr_m/N_G$  same in the model and prototype. For the stability behaviour, scaling of the characteristic equation (obtained by the linear stability analysis method) appears to be the appropriate method for achieving similarity. This requires simulation of at least three dimensionless parameters in addition to geometric scaling for single-phase loops. Simulation of the stability behaviour of uniform diameter loops requires preservation of the length scales in the model and prototype in addition to the similarity parameters appearing in the nondimensional governing equations.

## Nomenclature

A	- flow area, $m^2$
a	- dimensionless flow area, $A/A_0$
b	- constant in equation (9)
$C_p$	- specific heat, $J/kgK$
D	- hydraulic diameter, m
d	- dimensionless hydraulic diameter
f	- Darcy-Weisbach friction factor
g	- gravitational acceleration, $m/s^2$
$Gr_m$	- modified Grashof number,
	$D_0^3 \rho_0^2 \beta g \Delta T / \mu^2$

H	- loop height, m
k	- thermal conductivity, $W/mK$
K	- local pressure loss coefficient
l	- dimensionless length, $L/L_0$
L	- length, m
N	- total number of pipe segments
$N_G$	- dimensionless parameter defined by Eq. (11)
Nu	- Nusselt number, $UD/k$
p	- constant in Eq. (9)
P	- perimeter, m
Pr	- Prandtl number, $C_p \mu / k$
q	- heat flux, $W/m^2$
Q	- total heat input rate, W
Re	- Reynolds number, $DW/A\mu$
s	- co-ordinate around the loop, m
S	- dimensionless co-ordinate around the loop, $s/L_0$
$St_m$	- modified Stanton number
t	- time, s
T	- temperature, K
$\Delta T$	- reference temperature difference in $Gr_m$ defined as $(QH/A_0 \mu C_p)$
U	- heat transfer coefficient, $W/m^2K$
$V_0$	- total loop volume, $m^3$
W	- mass flow rate, $kg/s$
z	- elevation, m
Z	- dimensionless elevation ( $z/H$ ) or ( $z/\Delta z$ )
$\Delta z$	- centre line elevation difference between cooler and heater, m

## Greek Symbols

$\beta$	- thermal expansion coefficient, $K^{-1}$
$\mu$	- dynamic viscosity, $Ns/m^2$
$\theta$	- dimensionless temperature
$\rho_0$	- reference density, $kg/m^3$
$\tau$	- dimensionless time
$\omega$	- dimensionless mass flow rate

## Subscripts

c	- cooler
cl	- cold leg
e	- equivalent
eff	- effective
h	- heater
hl	- hot leg
i	- ith segment
p	- pipe
r	- reference value
s	- secondary

## References

1. Bade, M.H., Development of generalised correlation for steady state behaviour of single-phase natural circulation loops and investigations on the suppression of instability using helical wire inserts, M.E. Thesis, Shivaji University, Sangli, Maharashtra, India.
2. Bau, H.H. and Torrance, K.E, Int. J. Heat Mass Transfer 24 (1981) 597-609.
3. Bernier, M.A. and Baliga, B.R, Int. J. Heat Mass Transfer 35 (1992) 2969-2982.
4. Creveling, H.F. De Paz, J.Y. Baladi and R.J. Schoenhals, J. Fluid Mech. 67 (1975) 65-84.
5. Hallinan, K.P. and Viskanta, R. Heat Transfer from a rod bundle under natural circulation conditions, NUREG/CR-4556.
6. Haware, S.K. Grover, R.B. and Venkat Raj, V. HMT-D2-83, Proc. VIIth National Heat and Mass Transfer Conference, Indian Institute of Technology, Kharagpur, India, 1983.
7. Heisler, M.P, Nucl. Sci. Eng. 80 (1982) 347-359.
8. Ho, C.J, Chiou, S.P. and Hu, C.S, Int. J. Heat Mass Transfer, Vol. 40 (1997) 3553-3558.
9. Holman J.P and Boggs, J.H, J. Heat Transfer 82 (1960) 221-226.
10. Huang, B.J. and R. Zelaya, J. Heat Transfer 110 (1988) 487-493.
11. Ishii, M. and Kataoka, I. Nucl. Eng. Des. 81 (1984) 411-425.
12. John, B. and Kannan Iyer, Proceedings of 24<sup>th</sup> National Fluid Mechanics Conference, 1991.
13. Jeuck III, P., Lennert and Kiang, R.L, Rep. EPRI-NP-2006, 1981.
14. Misale, M. Tagliafico, L. and Tanda, G. Proceedings of the fourth International Symposium on Transport phenomena in heat and mass transfer, Sydney, 14-19 July (1991) p.203-211.
15. Nahavandi, A.N, Castellana, F.S and Moradkhanian, E.N, Nucl. Sci. Eng. 72(1979) 75-83.
16. Nayak A.K, Vijayan P.K, Saha D., Venkat Raj V, Aritomi M, J. Nuclear Science and Technology, 35, 712-722, 1998.
17. Nishihara, T., Proceedings of NURETH-8, Kyoto, Sept. 30-Oct. 4, (1997) 839-847.
18. Streeter, V.L and Wylie, E.B, 1983 Fluid Mechanics, p.243-45, McGraw-Hill Book Company, Singapore.
19. Vijayan, P.K. Investigations on the single-phase thermosyphon phenomenon in a figure-of-eight loop relevant to pressurised heavy water reactors, Ph. D. thesis, Indian Institute of Technology, Bombay, 1988.
20. Vijayan P.K, Bade, M.H, Saha, D, Sinha, R.K and Venkat Raj, V, A generalized correlation for the steady state flow in single-

phase natural circulation loops, BARC report, June 2000.

21. Vijayan, P.K, Nayak, A.K, Pilkhwal, D.S, Saha, D. and Venkat Raj, V, NURETH-5, Salt Lake City, UT, Vol.1, (1992) 261-267.
22. Vijayan, P.K. and Austregesilo, H, Nuclear Engineering and Design 152 (1994) 331-347.
23. Vijayan, P.K, Invited talk, M. Misale and F.Mayingner, (Eds.) 3-16, 1999, Proceedings of EURO THERM SEMINAR No. 63 on Single and Two-Phase Natural Circulation, 6-8 September 1999, Genoa, Italy.
24. Zvirin, Y. Jeuck III P, Sullivan, C.W, Duffey, R.B, J. Heat Transfer 103, (1981) 645-652.
25. Zuber, N, Problems in modelling of small break LOCA, Rep. NUREG-0724, October 1980.

*Natural circulation is being increasingly employed in many innovative designs of nuclear reactor cooling systems. The basic advantage of natural circulation systems is the enhanced safety due to its passive nature. One of the basic requirements, which arise prior to the incorporation of such systems in nuclear reactors, is the assessment of their performance. Generally, in the nuclear field the assessment is carried out by validated computer codes. Code validation is usually done with data obtained from scaled test facilities. The topic of the present paper is the scaling laws used for constructing such scaled facilities for simulating single-phase natural circulation. Such a scaled facility in nuclear parlance is also known as an integral test facility (ITF).*

*Dr P.K. Vijayan is the recipient of the BARC Technical Excellence Award for the year 1998.*

*About the author ....*



*Dr. P.K. Vijayan joined the 20<sup>th</sup> batch of BARC Training School after graduating in chemical engineering from the University of Calicut. Dr Vijayan obtained his Ph.D. from I.I.T. Bombay for his work on natural circulation in a figure-of-eight loop relevant to PHWRs. He has worked in GRS, Munich, for a year on the simulation of natural circulation systems. He has established himself as an expert in the area of nuclear reactor thermalhydraulics. Dr Vijayan's work on single-phase natural circulation loops is frequently cited by researchers as a significant contribution. His current research interests include stability of two-phase natural circulation, scaling of nuclear reactor systems and setting up of thermalhydraulic test facilities related to the Advanced Heavy Water Reactor and the Pressurised Heavy Water Reactors.*





# BIOREACTOR TECHNOLOGY FOR LARGE SCALE CULTIVATION OF PLANT CELL SUSPENSION CULTURES AND PRODUCTION OF BIOACTIVE COMPOUNDS

**Dr. Devanand P. Fulzele**

Nuclear Agriculture and Biotechnology Division  
Bhabha Atomic Research Centre

## *Abstract*

*A bioreactor with helix impeller has been designed and developed at Nuclear Agriculture and Biotechnology Division capable of growing high density plant cell suspension cultures. The design of this bioreactor has been transferred to Kabra Drugs Limited, Indore under a technology transfer agreement. Mixing studies revealed that the helix impeller speeds of 80 rpm to 200 rpm ensured uniform mixing of suspension cultures. Catharanthus roseus cell cultures cultivated in 100 lit bioreactor with an initial 11.5% packed cell volume to give an initial biomass to liquid ratio 42.6 g/l fresh biomass at Kabra Drugs Limited, Indore. This resulted in production of a biomass 32 Kg fresh weight within 16 days of cultivation, whereas natural grown plant produced 2.3 Kg/m<sup>2</sup>/year. This work addressed the design and development of helix impeller for 50 and 100 lit bioreactor for high density Catharanthus roseus cell suspension cultures.*

**M**EDICINAL PLANTS ARE THE most exclusive source of life saving drugs for the majority of the world's population. About 8000 herbal remedies have been codified in the Ayurveda, which is still in use in many areas today and large numbers of bioactive compounds are life saving drugs [1]. Bioactive compounds currently extracted from plants are used as food additives, pigments, dyes, fine chemicals, insecticides, cosmetics and perfumes. In view of the growing world population, increasing anthropogenic activities and rapidly eroding natural ecosystems, the natural habitats for a large number of plants are rapidly dwindling leading to extinction many valuable species. One alternative is to culture

plant cells in bioreactor under controlled defined parameters retaining the biosynthetic capacity to synthesise bioactive compounds. A number of plants such as *Catharanthus roseus* (vincristine, vinblastine, ajmalicine), *Taxus baccata* (taxol), *Nothapodytes foetida* (camptothecin), and *Artemisia annua* (artemisinin) have been screened for anti-cancer, anti-AIDS, anti-malarial and other useful bioactive compounds for therapeutic use [2-4].

India is a rich source of medicinal plants. Aromatics, essential oils and bioactive compounds bearing plant constitute an important group of the India flora. Today, one quarter of all prescribed medicines used in the

USA is of the plant origin [5]. Currently, pharmaceutical companies are manufacturing most of these compounds by cultivation of whole plants followed by extraction and purification of the desired bioactive compounds. The continuous production of the desired bioactive compounds requires repeated collection of plant material and consequently this leads to the serious problem of depletion of natural sources. Secondly, plants are not often readily available. Mass cultivation of medicinal plant species under natural conditions may not be possible due to environmental, ecological, or variable climatic conditions, length of propagation or the need to use agricultural land to produce the primary food crops. Quality and quantity of the products is also effected by unforeseen environmental conditions.

## Bioreactor

Bioreactors provide nutritional and closely controlled environment for optimum growth of plant cells in which cells perform biochemical transformation to synthesise bioactive compounds. Bioreactors have several advantages for mass cultivation of plant cells. i) it gives better control for scale up of cell suspension cultures under defined parameters for the production of bioactive compounds. ii) constant regulation of conditions at various stages of bioreactor operation is possible iii) handling of culture such as inoculation or harvest is easy and saves time iv) nutrient uptake is enhanced by submerged culture conditions which stimulate multiplication rate and higher yield of bioactive compounds. v) large number of plantlets are easily produced and can be scaled-up.



Fig. 1. Mass propagation of multiple shoot cultures of *Artemisia annua*

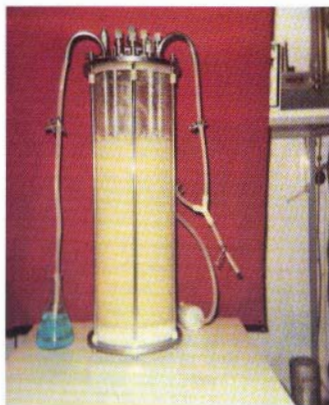


Fig. 2. Scale-up of *Catharanthus roseus* cell cultures in a 20 litre air

## Bioreactor Designed and Demonstrated for Cell and Organ Cultures

Bell-jar bioreactors designed in Nuclear Agriculture and Biotechnology Division for mass propagation of cell and organ cultures. This bioreactor demonstrated that large-scale cultivation of multiple shoots and plantlet cultures can result in production of plant secondary products at levels higher than those of whole plants. The newly designed bioreactor proved that any multiple shoot and plantlet cultures could be mass propagated under defined controlled parameters (Fig. 1). Cell cultures of *Catharanthus roseus* were performed in a 20 lit air lift bioreactor for production of ajmalicine (Fig 2).

The application of bioreactor system for large scale cultivation of plant cells for the production of valuable bioactive compounds is an active field, whose application holds great promise for pharmaceutical industry. Large scale cultivation of plant cells in bioreactor increases the biomass production much more than the whole plants are grown in the field. Culture cycles of cell suspensions in bioreactor would be a question of weeks and not of years as for example in case of shikonin plant, which usually is not harvested before the age of five years. Successful production of shikonin in bioreactor by cell cultures of *Lithospermum erythrorhizon* which was the first commercial process using plant cell cultures [6]. The commercial exploitation of bioreactor technology is an alternative and attractive area for bulk production of bioactive compounds for therapeutic use.

Plant cells in liquid suspensions offer a unique combination of physical and biological properties that must be accommodated in large scale bioreactor process aimed at exploiting their biomass and synthesis of bioactive compounds.

Some of the well-known drawbacks of the cell suspension cultures in bioreactor includes the instability of the productive cell lines, the slowness of the cell growth and production phase and limited knowledge about the secondary metabolite pathways [7]. There are indications that sufficient oxygen supply and proper mixing in air lift bioreactors may not be suitable for high density ( $\geq 300$  to  $350$  g/l fresh biomass) plant cell suspension cultures. Secondly, the problem of well-known shear sensitivity and rapid setting characteristics of plant cell aggregates and cell floating tendencies of the cell cultures have to be solved when bioreactors for plant cell cultures are designed [8].

Plant cells are 10 to 100 times larger than bacterial and fungal cells. Cultured plant cells range from 20-40  $\mu\text{m}$  in diameter and from 100-200  $\mu\text{m}$  in length and embrace vacuoles up to 95% or more of cell volume. These features have led to the belief that plant cells are shear sensitive. Also, the oxygen requirement of plant cells is low in comparison to the oxygen requirement of microbial cells. Such special features of cultured plant cells necessitate to design and develop a impeller for bioreactor, which could provide proper mixing and sufficient oxygen supply throughout the bioreactor without forming dead zones and will not damage the cells during cultivation period.

The hydrodynamic conditions in bioreactors are most strongly dependent on the impeller design. In view of this important point, a helix impeller was designed and developed for 50 and 100 lit bioreactors and *Catharanthus roseus* cultures were successfully grown at high density (Fig. 3). Bioreactors (50 and 100 lit capacity) were also designed with several options to perform continuous, semi-continuous, single and double stage operation modes with plant cell cultures.

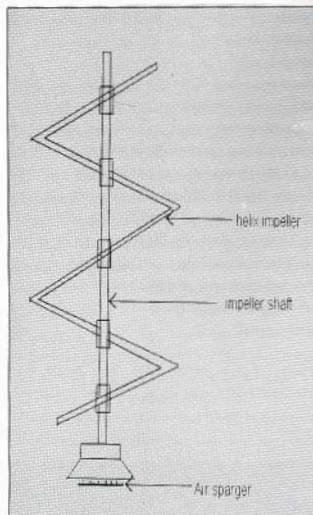


Fig 3. A schematic representation of the helix impeller used for the agitation and sufficient oxygen supply to *Catharanthus roseus* cells cultivated in 100 lit bioreactor

The geometry of the helix impeller resulted in upward liquid pumping at the blades upon counter clockwise rotation. Bioreactor with helix impeller decreases the bottom and top conical slower mixing zones generated by other types of the impellers. Agitation speeds ranging from 80 rpm to 200 rpm also improved mixing efficiency of cell suspension cultures. Large scale cultivation of *Catharanthus roseus* cell cultures has showed that the bioreactor configurations with helix impeller did not yield slower mixing zones of the impeller at speed ranging from 80 rpm and above. Impeller speed lower than 80 rpm resulted in setting of cell aggregates suspension. The viscous shear-thinning behaviour of cell

cultures, whose homogenous mixing at low shear and proper oxygenation are problematic using conventional or pneumatic agitation system for bioreactors [9].



Fig 4 A 100 lit bioreactor successfully commissioned at Kabra Drugs Limited, Indore.

Bioreactor technology was transferred to M/s. Kabra Drugs Limited, Indore, a pharmaceutical based company for large scale cultivation of plant cell cultures and production of bioactive compounds (Fig. 4). Bioreactor-grown suspension cultures in 50 and 100 l bioreactors were highly homogenous in overall appearance and compared well to those with cultured in shake flasks. Microscopic observations revealed that both bioreactor and flask grown suspensions comprised of single cells.

Cell culture experiments confirmed that the bioreactors (50 and 100 l capacity) equipped

with helix impeller is suitable for growing low to high density cell suspensions. The most resulted mixing speed was observed at 140 rpm, which was not related to cell lysis but to excessive vortexing of the suspension and biomass production at higher speed.

### Mass Propagation of *Catharanthus roseus* in 100 lit Bioreactor

Large scale cultivation of *Catharanthus roseus* cell suspension cultures were performed in 100 l bioreactor (working capacity 75 l) equipped with helix impeller. Cell suspensions were established in Murashige and Skoog's medium supplemented with 2,4-dichlorophenoxy acetic acid (9.05  $\mu\text{M}$ ) and kinetin (4.65  $\mu\text{M}$ ). Basal medium was prepared in tap water and market sugar to reduce the production costs of biomass and bioactive compounds. Two week old suspension cultures were used as inoculum giving an initial biomass to liquid ratio of 42.6 g l<sup>-1</sup> fresh biomass. The speed of the helix impeller at 140 rpm and initial dissolved oxygen (pO<sub>2</sub>) was maintained at 30%. Cell cultures showed uniform growth over a period of 15 days and than reached to stationary phase. Sucrose in the medium was completely hydrolysed within two days, and the monosaccharides were consumed thereafter by the cells. The final yield of biomass was 32 Kg fresh weight in 16 days of cultivation in bioreactor. It was shown that the 100 lit bioreactor displayed good performance in growing high density *Catharanthus roseus* cell suspension cultures (Fig. 5). The higher and more efficient upward suspension pumping capacity at low shear rate of the helix impeller, ensured sufficient and more uniform mixing of the delicate plant cell suspension and their better growth performance. This results demonstrated that large scale cultivation of plant cell cultures

in bioreactor equipped with helix impeller is a viable technology for pharmaceutical industries.

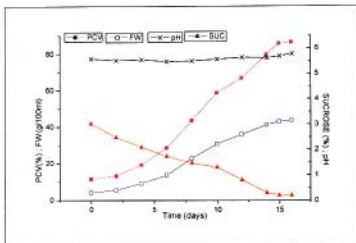


Fig. 5 Time course data for cell suspension cultures of *Catharanthus roseus* in 100 lit bioreactor equipped with helix impeller. Sucrose ▲—▲; Packed Cell Volume ■—■; Fresh weight □—□; pH x—x.

The design of the helix impeller and its mechanical feasibility and the mechanical sterile seals represent key components of successful bioreactor. The industrial use of this type of bioreactor configuration depends on the low shear mixing efficiency and dissolved oxygen (pO<sub>2</sub>) supply.

Many multinational pharmaceutical companies have started their production units in India with a view to produce bulk amounts of plant based drugs. Currently, pharmaceutical companies are using field grown plants followed by extraction and purification process to achieve the fine powder containing bioactive compounds. The continuous production of anti-cancer, anti-AIDS and other important life saving drugs requires large number of natural grown plants. Therefore, pharmaceutical companies are cutting plants from the forest. It causes the serious problem of depletion of natural sources and disappeared several elite varieties of the medicinal plants. It is the right time to take the opportunity to develop eco-friendly indigenous bioreactor technology

for large scale commercial production of bioactive compounds and to protect the natural sources.

### Acknowledgement

I would wish to thank Dr. (Ms.) Susan Eapen, Head, Plant Biotechnology and Secondary Product Section, Dr. R. K. Mitra, Head, Nuclear Agriculture and Biotechnology Division, and Dr (Smt) A.M. Samuel, Director, Biomedical Group, for their constant encouragement.

### References

1. Haung PL, Huang HI & Lee-Huang S. (1992) Developing drugs from traditional medicinal plants. Chemistry and Industry; April, 290-293
2. Fulzele DP & Heble MR. (1994) Large scale cultivation of *Catharanthus roseus* cells: Production of ajmalicine in a 20-l airlift bioreactor. Journal of Biotechnology; 35: 1-7
3. Fett-Neto AG, DiCosmo F, Reynolds WE & Sakata K. (1992) Cell culture of *Taxus* as a source of the antineoplastic drug taxol and related taxanes. Bio/Technology; 10:1527-1575
4. Fulzele DP, Heble MR & Rao PS. (1995) Production of terpenoid from *Artemisia annua* L. plantlet cultures in bioreactor. Journal of Biotechnology; 40: 139-143
5. Farnsworth NR. (1985) The role of medicinal plants in plants in drug development. In: Krooogsgard-Larsen P, Brogger Christensen S & Koford H (eds). Natural Products and Drug Development (pp 17-30) Munksgaard Copenhagen, Denmark
6. Fujita Y, Tabata M, Nishi A & Yamada Y. (1982) New medium and production of secondary compounds with the two stage culture method. In: Fujiwara (ed) Proc. 5<sup>th</sup> Intl. Cong. Plant Tissue and Cell Cultures (pp. 399-400) Maruzen Co. Tokyo
7. Panda AK, Misra S, Bisoria VS & Bhojwani SS. (1989) Plant cell reactors- A perspective. Enzy. Microbial. Technology; 11: 386-397
8. Tanaka H. (1987) Large scale cultivation of plant cells at high density. Proc. Biochem. August. 106-110
9. Tanaka H. (1982) Oxygen transfer in broth of plant cells at high density. Biotchnol. Bioeng. 24: 425-435

**Dr. Devanand P. Fulzele is the recipient of the BARC Technical Excellence Award for the year 1998.**

About the author .....



After obtaining his M.Sc. degree in Microbiology from Nagpur University, in 1982, Dr Devanand P. Fulzele joined Nuclear Agriculture and Biotechnology Division, BARC, in 1986. Since then, he has been working in the area of bioreactor system for large scale cultivation of plant cell cultures and production of bioactive compounds. Dr Fulzele obtained his Ph.D. degree in 1996 from Mumbai University for his work on regulatory aspects of secondary metabolism in medicinal plant tissue cultures. His primary contributions are the design and development of bioreactors for organ and cell cultures for product synthesis. His work also includes design and development of bioreactors at commercial levels.



# GAS DETECTORS FOR HEAVY ION EXPERIMENTAL NUCLEAR PHYSICS RESEARCH

D. C. Biswas and R. K. Choudhury

Nuclear Physics Division  
Bhabha Atomic Research Centre

## Introduction

**G**AS DETECTORS HAVE PLAYED an important role in nuclear physics experiments since many decades. With the advent of high energy heavy ion accelerators, there has been a growing need to develop different types of gas detectors to meet various experimental requirements. Gas detectors offer several advantages in comparison to other types of nuclear radiation detectors, such as versatility in construction with regard to size and shape, variety in the mode of operation, uniformity of detector thickness, flexibility in detector thickness variation by adjustment of gas pressure, immunity to radiation damage, good timing and pulse height characteristics and ease of fabrication etc. Because of the above advantages, various types of gas detectors are extensively being used as ionisation chambers, proportional counters and avalanche detectors for heavy ion reaction studies. Today, most of the detectors used for tracking and imaging in high energy physics experiments are based on gas detectors. The use of gas detectors has also spread to many different fields of applied research, such as X-ray and heavy ion astronomy, nuclear medicine and protein crystallography etc.

An energetic charged nuclear particle traversing in a gas medium interacts with the atoms of the medium in many ways. Of all possible interactions, the electromagnetic interaction is

generally many orders of magnitude more probable than the strong or weak interactions, and takes place by the incoherent Coulomb interactions between the electromagnetic fields of the incoming charged particle and of the medium, producing both excitation and ionization of the atoms of the medium. For heavy ions of energies  $\approx 1$  MeV/u and above, the energy loss is predominantly due to the inelastic collision of the ion with the medium electrons. However, at lower energies elastic collisions of the ion with the medium nucleus becomes important. These interactions leave a trail of electrons and ions in the medium, which are collected by applying suitable electric field to produce an electric signal.

## Gas Ionisation Chamber Detectors

Gas ionisation chambers are largely used for charged particle spectroscopy studies where identification of the particle is done by measurement of energy loss ( $\Delta E$ ) of an ion in a thin transmission type detector together with the residual energy ( $E_n$ ) by another detector. Such an arrangement is commonly known as a detector telescope. The particle identification is based on the equation for the rate of energy loss [1].

$$\Delta E(E_n + \Delta E) = KMZ_{eff}^2 \dots\dots\dots(1)$$

where,  $K$  is a constant,  $M$  is the mass and  $Z_{eff}$  is the effective charge of the ion. For energetic light charged particles,  $Z_{eff} = Z$ , whereas, for heavy ions  $Z_{eff}$  less than or equal to  $Z$  and depends on the energy of the ion. For fission fragments, the effective charge  $Z$  is expressed as  $Z_{eff} = \gamma Z$ . Here  $\gamma$  is the effective charge parameter and has a complicated dependence on the atomic number  $Z$  and energy of the fragment [2].

In case of heavy ions of low energy, one requires a thin and uniform transmission type  $\Delta E$  detector for carrying out particle identification. For ions of  $Z=10-40$ , at energies less than 2-3 MeV/u, it is desirable to have very thin (1-4  $\mu\text{m}$  equivalent Si thickness) detectors. With the current technology it is very difficult to produce uniform Si detectors in this range of thickness. The much greater uniformity of a thin gas transmission detector gives it an advantage over silicon detectors. Different types of detector telescopes based on  $\Delta E_{gas}-\Delta E_{Si}$  and  $\Delta E_{gas}-\Delta E_{gas}$  detectors have been developed and used by us for measuring the energy, charge and mass of charged particles and fission fragments produced in heavy ion induced reactions at the pelletron accelerator, Mumbai.

#### Hybrid $\Delta E_{gas}-E_{Si}$ detector telescope

The hybrid telescope which is developed [3] for heavy ion experiments, consists of a gas ionisation chamber for measuring  $\Delta E$  and a surface barrier detector to measure the residual energy loss ( $E_n$ ). These detectors are commonly used for identification of heavy ion reaction products to measure their energy, charge and mass. These detectors are also suitable for fission fragment measurement providing good separation between projectile like particles and fission fragments. The schematic

diagram of the hybrid detector telescope developed at B.A.R.C, is shown in Fig.1.

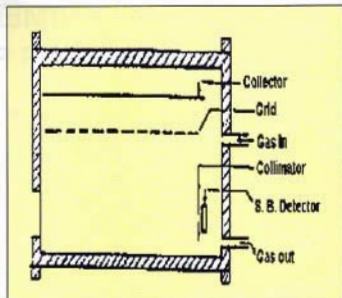


Fig.1 Schematic diagram of hybrid telescope

It consists of a gas ionization chamber (10 cm length) having a grid and a collector parallel to the ion track and a surface barrier detector (typically 500  $\mu\text{m}$  thickness) at the end inside the gas medium. The main body of the detector is machined from stainless steel material and acts as cathode. The Frisch grid is constructed by fixing a metallic mesh (95% transmission) on a rectangular frame made out of Cu-plated fibre glass. The anode plate is made of one sided Cu-plated fibre glass. The separation between the cathode and grid is 40 mm and grid to anode is 10 mm. The detector works in ionisation region so that the pulse height is proportional to primary ionisation in the gas medium. A collimator of 5 mm diameter is mounted in front of the detector and a thin (1-2  $\mu\text{m}$ ) polypropylene foil is placed as the window to allow the reaction products enter into the detector. This detector has been used for measuring fission fragment angular distributions [7] in heavy ion reactions and identification of projectile-like fragments (PLF's) produced in heavy ion reactions at energies near



the Coulomb barrier [5,6]. The  $\Delta E$ - $E_a$  plot shown in Fig. 2 demonstrates the clear separation of various projectile-like fragments ( $Z=2$  to 10) produced in  $^{19}\text{F}+^{232}\text{Th}$  reaction at 108 MeV.

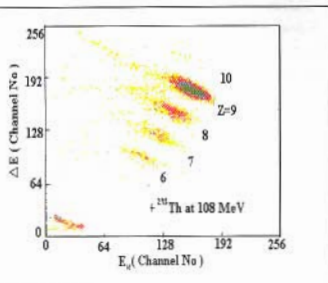


Fig. 2  $\Delta E$ - $E_a$  plot for various PLF's produced in  $^{19}\text{F}+^{232}\text{Th}$  reaction at 108 MeV.

#### Multi-angle Hybrid ( $\Delta E_{\mu}$ - $E_a$ ) detector telescope

A multi-angle particle telescope having common  $\Delta E_{\mu}$  backed by three silicon E detectors at  $9^\circ$  intervals has been developed and its principle of operation is same as the hybrid detector telescope mentioned above. This detector is specifically useful to carry out the angular distribution of fission fragments and heavy ions. Using this detector, measurements have been carried out on fission fragment angular distributions at near barrier energies [8].

#### Position sensitive ionization chamber ( $\Delta E_{\mu}$ - $E_{\mu}$ ) detector

A trapezoidal shaped gas ionisation chamber has been developed [4] for heavy ion reaction studies, which can be used for particle identification from the  $\Delta E$ - $E$  information and the position measurement is obtained by

dividing the  $\Delta E$  anode into multiple segments and employing charge division technique. The  $\Delta E$ -part of the anode plate is divided into five segments along the particle track and the alternate segments are connected together for position determination. With this detector one can identify the particle and simultaneously measure the energy as well as angle of the reaction products.



Fig. 3  $\Delta E_{\mu}$ - $E_{\mu}$  Position sensitive ionization chamber.

The main body of the detector as shown in Fig.3, is machined from stainless steel material. The detector assembly which consists of a cathode, a Frisch grid and anode plate ( $\Delta E$  path length=45 mm and  $E=90$  mm) all having trapezoidal shape and mounted at suitable separations with teflon rods and spacers, The schematic diagram of the detector assembly and anode plate is shown in Fig. 4.

The  $\Delta E_1$  and  $\Delta E_2$  pulses are summed after proper gain matching to obtain the total energy loss in the  $\Delta E$  section of the ionisation chamber. The detector has been used in heavy ion experiments for measuring fission fragments in a number of heavy ion induced reaction studies. The position in the reaction plane is measured by the charge division method. The  $\Delta E$  anode segment is splitted into three segments which are alternatively connected, so that the average  $dE/dx$  is almost equal in both

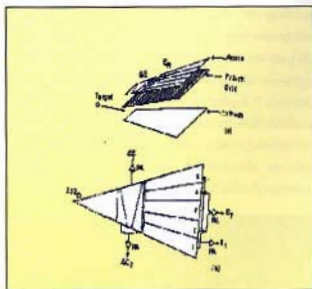


Fig. 4 Schematic diagram of (a) detector assembly, and (b) anode plate for  $\Delta E_1$ - $E_2$  position sensitive ionization chamber.

the segments for the particles entering along the central line of the detector, even for fission fragments whose specific energy varies strongly along the range[3]. Particles passing at any other angle will lose energies proportional to the path lengths in  $\Delta E_1$  and  $\Delta E_2$  segments. A position parameter defined as  $x = (\Delta E_2 - \Delta E_1) /$

$(\Delta E_2 + \Delta E_1)$  is proportional to the particle position and is related to the scattering angle of the particles in the reaction plane. The position resolution is about 1.1 mm which translates to  $0.75^\circ$  (FWHM) in the angle resolution of the detector which is quite good for studying the angular distribution of fission fragments in heavy ion reactions.

Fig. 5 shows a scatter plot of  $\Delta E_1$  vs  $\Delta E_2$  for  $^{252}\text{Cf}$  fission fragments obtained for a mask having five slits each 1mm wide and separated by 5mm, fixed in front of the detector. Different bands are seen corresponding to slit openings. The position spectrum was obtained separately for the light and heavy fission fragment groups and is shown in Fig.6. In this geometry, the angular coverage of the detector is  $30^\circ$  and the detector is useful for angular distribution studies. In this configuration of the anode plate, one can carry out online calibration of the position signal of the detector, which is quite useful during the experiments.

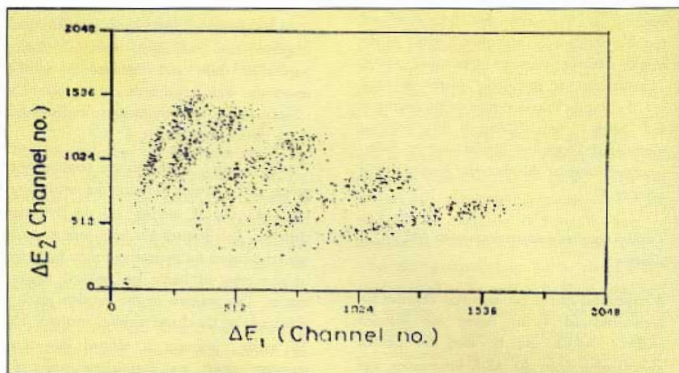


Fig. 5  $\Delta E_2$ - $\Delta E_1$  plot for  $^{252}\text{Cf}$  fission fragments using a mask with five slits.

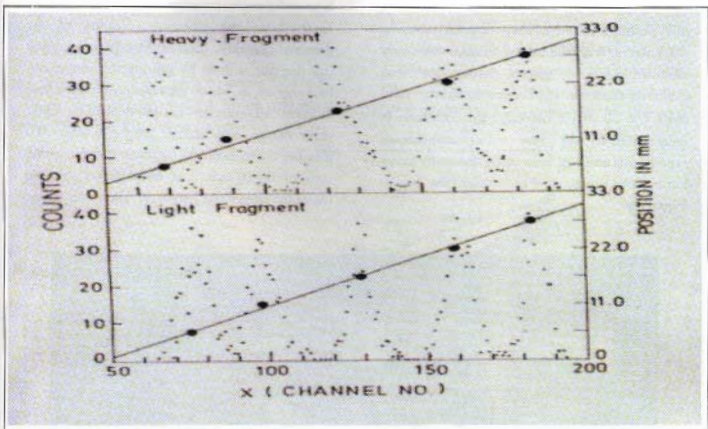


Fig.6 Position spectrum for light and heavy fragment groups.

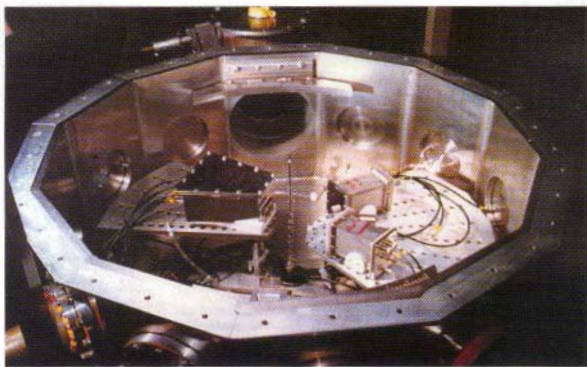


Fig.7 Gas detectors mounted inside the scattering chamber.

Several experiments have been carried out using this position sensitive ionization chamber in combination with the hybrid detector telescopes mounted inside the general purpose scattering chambers shown in Fig.7. Because of large solid angle ( $\approx 70 \text{ mSr}$ ) coverage, this detector is most suitable for low count coincidence experiments and has been used for many heavy ion induced experiments to measure the fission fragments.

large solid angle coverage of about  $50 \text{ mSr}$  [9]. Fig.9 shows the schematic diagram of the detector assembly. Particle identification using this detector is done by splitting the anode into four regions, in which the reaction products lose different amounts of energy depending upon their charge and initial kinetic energy. To measure the mass of the reaction products, the time of flight technique is employed making use of the large flight length of about  $1 \text{ m}$  from



*Fig.8 Large Area Position Sensitive Ionization Chamber*

#### ***Large Area Position Sensitive Ionisation Chamber (LAPSIC)***

A large area position sensitive ionisation chamber (LAPSIC) shown in Fig.8, has been developed as one of the experimental facilities for heavy ion reaction studies. The main features of the detector are wide dynamic range, good charge and mass resolution, position sensitivity both in and out of reaction plane and

the scattering chamber to the entrance of the ionisation chamber. The angular coverage in the reaction plane is  $22^\circ$  and the position measurement is carried out by using the delay line method. The out of plane angle information is obtained by measuring the drift time of the electrons between cathode and anode. This detector has been used for studying deep inelastic reactions and

measurement of fission fragment energy as well as time of flight in heavy ion induced reactions to obtain the fission fragment mass distributions.

A typical  $\Delta E_1$  vs  $\Delta E_2$  plot is shown in Fig.10 shows a clear separation of fission fragments from projectile-like fragments.

thin structure, these detectors have excellent inherent discrimination for low atomic number ions, ultra fast timing and very good position resolution. The detector was tested with fission fragments and the position resolution of 0.5 mm has been obtained. For the target

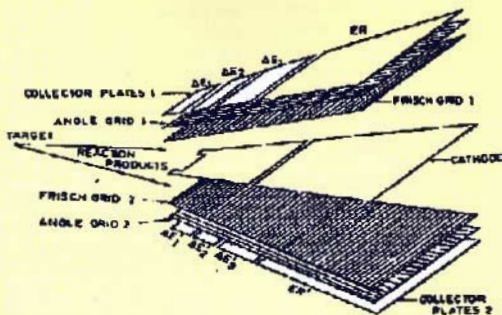


Fig. 9 Schematic diagram of LAPSIC detector assembly.

### Position Sensitive Multistep Parallel Plate Avalanche Counter

Large area position sensitive multistep avalanche counters have been developed in collaboration with Saha Institute of Nuclear Physics, Calcutta and used for detecting fission fragments produced in heavy ion induced reactions at Pelletron accelerator facility, Mumbai. The position information both in x and y directions are obtained by the delay line method. Because of very low operating gas pressures and

detector distance of about 15 cm, the angular resolution is about  $0.15^\circ$ . A typical x position spectrum obtained for fission fragments is shown in Fig.11. The dips in the spectrum indicate the positions of nylon support wires of 0.6 mm diameter.

As the angular resolution of these detectors is excellent, two such detectors were used for detecting the correlated fission fragments [10]. By employing the folding angle technique, various experiments have been carried out to separate the complete fusion and transfer

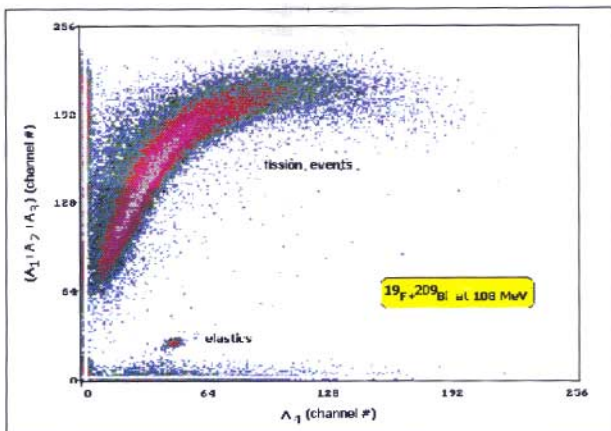


Fig.10 Energy loss in the anode plates showing separation of fission fragments from PLFs.

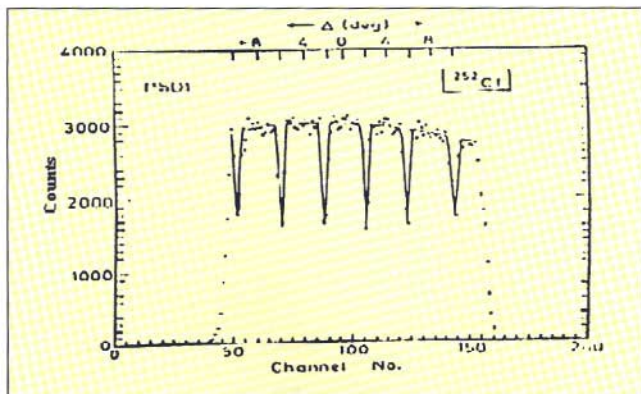


Fig.11 Position spectrum for  $^{252}\text{Cf}$  fission fragments measured by avalanche counter.

induced fission events for studying the angular distribution of fission fragments at near barrier and sub barrier energies.

## Use of the Gas Detectors in Nuclear Physics Experiments

All the gas detectors mentioned above are extensively used in heavy ion experiments at Pelletron accelerator facility, Mumbai and have given significant boost to gas detector technology for nuclear physics studies. The important results obtained using these detectors are:

- (i) Measurement of fission fragment energy, charge and mass to study the specific energy loss behaviour of fission fragments along the track [2,3].
- (ii) The angular distribution of projectile like particles have been studied to understand the role of projectile structure in multinucleon transfer and their importance in explaining "slope anomaly", which was observed in the single and multi-nucleon transfer reaction probabilities for many target-projectile systems [5,6].
- (iii) Using the gas detectors, measurements have been carried out on heavy ion induced fusion-fission and transfer induced fission reaction studies, for explaining the observed anomalous angular anisotropies for several systems at energies around the Coulomb barrier [11-12]. It is observed that the orientation dependent quasifission model could explain the observed anomalous peaklike structure in angular anisotropies at deep sub-barrier energies [13].

The measurements on fusion-fission and transfer induced fission reactions have also yielded many new results, which are of fundamental importance for an understanding of the mechanism of mass, energy and angular

momentum transfer in heavy ion induced reactions leading to fission in heavy target nuclei. These experiments, have provided important information to understand the dynamics of the fission process [14-16].

## Conclusions

Various gas detectors have been developed over more than a decade for their use in experimental nuclear physics at pelletron accelerator, Mumbai. Using these detectors it is possible to measure the energy, charge, mass and position information which are very useful parameters to identify a heavy charged particle. Several measurements have been carried out to understand the multinucleon transfer processes and dynamics of heavy ion induced fusion-fission reactions. Developments are still in progress to improvise these detectors, design and fabrication of new ionisation chambers as well as cathode strip detectors. With the experience in gas detectors in low energy nuclear physics experiments, collaborative experiments are also being carried out in intermediate nuclear physics experiments at LNL, Italy and in high energy physics experiments using PHENIX detector at BNL, USA.

## Acknowledgement

The authors gratefully acknowledge Dr. S. S. Kapoor for many illuminating discussions and suggestions on this work. We are thankful to Mr. L. M. Pant, Mr. B. V. Dinesh, Dr. B. K. Nayak and Dr. A. Saxena for their involvements during the various developments of the various gas detectors.

## References

1. F. S. Goulding and Bernard G. Harvey, *Ann. Rev. Nucl. Sci.*, **25**, 167 (1975).

2. M.N. Rao, D.C. Biswas and R.K. Choudhury, Nucl. Instr. and Meth. B51 102(1990).
3. D.C. Biswas, M.N. Rao, and R.K. Choudhury, Nucl. Instr. and Meth. B53 251(1991).
4. D.C. Biswas, V.S. Ambekar, L.M. Pant, B.V. Dinesh and R.K. Choudhury, Nucl. Instr. and Meth. A340 551 (1994).
5. D. C. Biswas, R. K. Choudhury, B. K. Nayak, D. M. Nadkarni, and V. S. Ramamurthy, Phys. Rev. C 56 1926 (1997).
6. D.C. Biswas, R.K. Choudhury, D.M. Nadkarni, and V.S. Ramamurthy, Phys. Rev. C52 2827 (1995).
7. S. Kailas, A. Navin, A. Chatterjee, P. Singh, A. Saxena, D.M. Nadkarni, D.C. Biswas, R.K. Choudhury and S.S. Kapoor, Pramana J. Phys 41, 339 (1993).
8. A. Karnik, S. Kailas, A. Chatterjee, P. Singh, A. Navin, D.C. Biswas, D.M. Nadkarni, A. Shrivastava and S.S. Kapoor Z. Phys. A 351 195 (1995).
9. Deep inelastic collisions of  $^{32}\text{S}+^{27}\text{Al}$  reaction at 130 MeV bombarding energy, R.K. Choudhury, D.M. Nadkarni, V.S. Ambekar, B.V. Dinesh, A. Saxena, M.S. Samant, D.C. Biswas, and L.M. Pant, Pramana, Vol 44, 177(1995).
10. N. Majumdar, P. Basu, M.L. Chatterjee, .C. Biswas, A. Saxena, V.S. Ambekar, R.K. Choudhury and D.M. Nadkarni, Nuovo Cimento, 188A, (1995)817.
11. N. Majumdar. P. Bhattacharya, D.C. Biswas], R.K. Choudhury, D.M. Nadkarni and A. Saxena, Phys. Rev. C51, 3109 (1995).
12. N. Majumdar, P. Bhattacharya, D.C. Biswas, R.K. Choudhury, D.M. Nadkarni and A. Saxena, Phys. Rev. C 53 R544 (1996).
13. N. Majumdar, P. Bhattacharya, D. C. Biswas, R. K. Choudhury, D. M. Nadkarni and Alok Saxena, Phys. Rev. Lett. 77, 25 (1996).
14. A. Chatterjee, A. Navin, S. Kailas, P.Singh, D.C. Biswas, A. Karnik, and S.S. Kapoor, Phys. Rev. C52 3167 (1995).
15. D.M. Nadkarni, A. Saxena, D.C. Biswas, R.K. Choudhury, S. S. Kapoor, N. Majumdar, and P. Bhattacharya Phys. Rev. C59 R580 (1999).
16. D. C. Biswas, R. K. Choudhury, A. Saxena, D. M. Nadkarni and V. S. Ramamurthy, Submitted to Phys. Rev. C (2000).

*Dr. D. C. Biswas is the recipient of the "S. N. Seshadri Memorial Instrumentation Award" in 1997.*

*About the Author ....*



*Dr. D. C. Biswas joined the 27<sup>th</sup> batch of BARC Training School in 1983 after obtaining M. Sc. degree in Physics from Calcutta University. Since then, he is working in Nuclear Physics Division, BARC, in various experimental activities using the Pelletron accelerator facility. He is involved in the developments of various gas detectors for their use in heavy ion induced nuclear physics experiments. He has made significant contributions in "Multinucleon transfer and heavy ion induced fusion-fission as well as sequential fission reaction studies". He has participated in several international collaboration experiments and has made important contributions in the field of spectroscopy of fission fragments using large gamma detector setup ( GASP ) at LNL, Italy.*





# SIMULATION AND EXPERIMENTAL VERIFICATION OF HYPERFINE SPECTRUM OF U-233

**B.N. Jagatap, L.M. Gantayet and A.P. Marathe**

Laser & Plasma Technology Division

**S.A. Ahmad, A. Venugopalan and B.K. Ankush**

Spectroscopy Division

and

**A. Ramanujam**

Process Development Division

Bhabha Atomic Research Centre

## Abstract

Knowledge of hyperfine structure (hfs) of lines of U-233 is of paramount importance in configuring an isotope selective multi-step photoionisation scheme for the clean-up process. Since the isotope shift (IS)  $\delta\nu(233, 232)$  is small (a few tens of millikayser), the spectral overlap between U-232 and U-233 is governed by the hfs pattern of U-233. It is imperative that the spectral transitions to be chosen for selective photoionisation must have smaller hfs extent to ensure high selectivity in the Clean-up process. In this paper, we present our theoretical and experimental work on the hfs of U-233. In what follows we discuss the hfs of 5915 Å line [ $0\text{ cm}^{-1} \text{ } ^5L_6 \rightarrow 16900\text{ cm}^{-1} \text{ } ^6K_7$ ] of U-233 as a case study.

## Theoretical

THE HFS OF AN ATOMIC LINE IS A result of splitting of energy level caused by the interaction of the electron with the nuclear magnetisation and nonspherical charge distribution. The parameters governing the splitting are hfs constants A and B that respectively signify the magnetic dipole and electric quadrupole interactions. For the spectral line under study the hfs constants are reported in the literature for U-235 isotope [1]. This information along with the nuclear parameters [2] (see Table-1) was used to construct the constants A and B for U-233 isotope and obtain the splitting patterns of the lower and excited levels. The intensities of the hfs components

were obtained using Racah algebra. The hfs line spectrum thus obtained was broadened using Doppler function to represent a high resolution spectrum obtained from a source at a given temperature. In Fig. 1, we give the simulated hfs spectrum of 5915 Å line of U-233. We may note here that since  $|\mu_{233}| > |\mu_{235}|$ , the hfs of U-233 has a wider width than that of U-235. Furthermore, the splitting pattern in U-233 is regular as against inverted in case of U-235.

Table 1: Nuclear Data for Uranium Isotopes

Isotope	Spin	$\mu$ (nm)	Q (b)
U-233	5/2	+0.55	+3.5
U-235	7/2	-0.35	+4.55

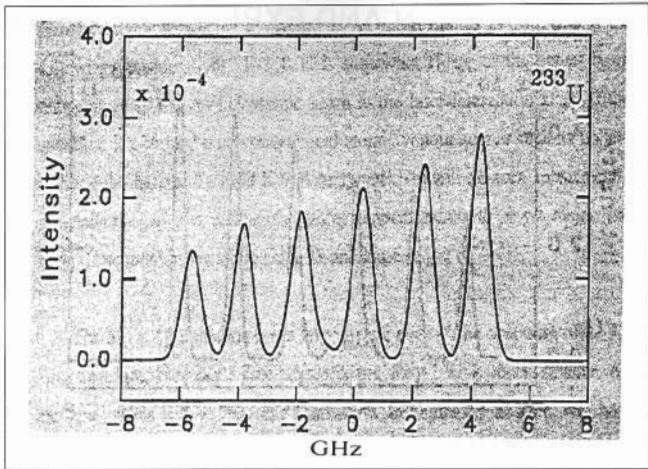


Fig. 1. Simulated hyperfine spectrum of 5915 Å of U-233

## Experimental

The simulated spectrum provides several guidelines to obtain the spectrum experimentally. Specifically, a resolution of  $\sim 10^6$  is sufficient to resolve the hfs as shown in Fig. 1.

Such resolution is conveniently offered by recording Fabry-Perot optical spectrometer (REFPOS). To record a high resolution spectrum of a line of an element on REFPOS, a hollow cathode discharge lamp (HCDL) is used as a source of narrow atomic lines, especially of refractory elements. Usual HCDLs consist of a cylindrical hollow cathode, made up of element under investigation in a glass enclosure fitted with optical windows and appropriate anode. This design, although convenient for common elements, is not at all suitable for spectroscopy of

radioactive elements. The amount of metal used for making a cylindrical hollow cathode is generally in the range of 100-200 gm. Such amounts are prohibitively large for radioactive isotopes, and give rise to severe radiological safety problems. In addition, the integrity of the entire HCDL assembly is questionable owing to the glass enclosure

For the spectroscopy of U-233 (U-232 @ 2 ppm), we have developed a liquid nitrogen cooled all metal HCDL which incorporates several novel ideas and take into consideration problems of handling rare and radioactive elements [3]. This new HCDL uses  $\sim 10$  mg of U-233 oxide which lasts for about 50 hours of operation. The HCDL is sturdy and intrinsically safe. In addition, it can be conveniently loaded with a radioactive material sealed hermetically in

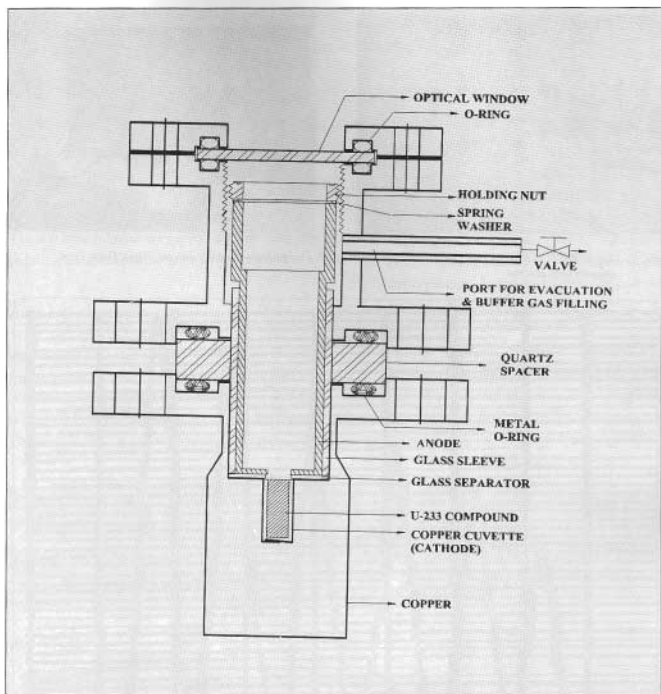


Fig. 2. Schematic design of all metal hollow cathode discharge lamp for high resolution spectroscopy of U-233.

an  $\alpha$ -protected facility and transported to an inactive area housing spectroscopic instruments satisfying all the safety requirements. In Fig. 2, we show schematically the design of this new HCDL. This HCDL, operated with neon as the buffer gas, was used as a source of U-233 atomic lines. The gamma radiation level was continuously monitored all along the

spectroscopic experiment and was found to be at the normal background level. The high resolution spectrum was recorded on indigenously built REFPOS. Fig. 3 shows a view of REFPOS facility which consists of a high resolution monochromator, Fabry Perot assembly and photon counting system. All these systems are fabricated and assembled in BARC.



Fig. 3. View of REFPOS Facility. Left : Entrance slit of high resolution monochromator with detector. Right: Fabry Perot assembly with detector.

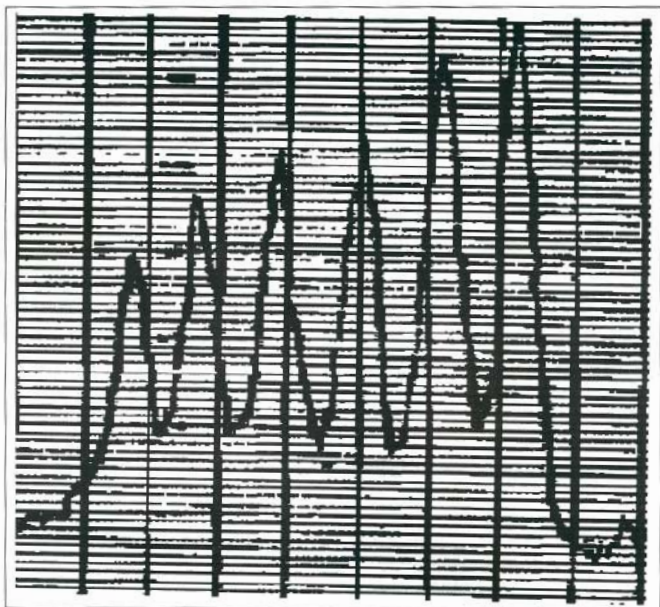


Fig. 4. HfI spectrum of  $5915 \text{ \AA}$  of U-233 recorded on REFPOS

In Fig. 4, we show the experimental spectrum of the 5915 Å line of U-233 as recorded on REFPOS. This may be compared with the simulated spectrum of Fig. 1. The separations and relative intensities of the hfs components are in very close agreement in these two spectra.

In conclusion, we have demonstrated experimentally the hyperfine spectrum of a line of U-233 and verified the simulation of same spectrum based on the knowledge of U-235. These methodologies are useful in generating the requisite database for the laser clean-up process.

### Acknowledgement

Authors thank Dr. A.B. Patwardhan for lending his expertise in handling and loading of U-233. The alpha protected facility for leak testing and gas filling of HCDL, provided by Radiometallurgy Division, BARC is gratefully acknowledged.

*This paper received the Best paper award in the category "New Technologies for Thorium Fuel Cycle" in the Annual Conference of Indian Nuclear Society (INSAC-2000) on "Power from Thorium : Status, Strategies and Directions", held at BARC, Mumbai, during June 1-2, 2000,*

*About the authors ....*



*Dr B.N. Jagatap graduated from the 20<sup>th</sup> batch of BARC Training School and obtained his Ph.D (Physics) from University of Mumbai in 1988. He has been associated with the Interdisciplinary Centre for Chemical Physics, University of Western Ontario, Canada, as Post Doctoral Fellow (1993-94) and Visiting Scientist (1999 and 2000-2001).*



*Mr L.M. Gantayet, a chemical engineer, joined BARC in 1972. He was awarded the Homi Bhabha prize in the 1971-72, 15<sup>th</sup> batch of BARC Training School. He has worked from the concept to development of total technology of the isotope separation processes. His current interests include development of laser-based separation processes.*

### References

1. W.J. Childs, O. Poulsen, L.S. Goodman; Opt. Lett., 4, 35 (1979).
2. V.S. Shirley and C.W. Lederer, Tables of Nuclear Moments, Laurence Berkeley Laboratory (1974).
3. S.G. Nakhate, A.P. Marathe, B.K. Ankush, A. Venugopalan, B.N. Jagatap, L.M. Gantayet, S.A. Ahmad, U.K. Charterjee, A.P. Roy, Proceedings of Seminar on Spectroscopy, Lasers and Laser Applications, (CUST, Kochi, March 23-26, 1998) p. 47. See also p. 77 in the same volume.
4. A.P. Marathe, B.K. Ankush, A. Venugopalan, A.B. Patwardhan, B.N. Jagatap, A. Ramanujam, L.M. Gantayet, S.A. Ahmad, Proceedings of Symposium on Spectroscopy of Lanthanides and Actinides (BARC, Nov. 16-19, 1999) p. 109.



*Ms Asawari Marathe joined the 40<sup>th</sup> batch of the BARC Training School after doing her post graduation in Physics from Indian Institute of Technology, Mumbai. She is currently working in the projects U<sup>235</sup> Clean-up and Laser Cooling of Atoms in Laser & Plasma Technology Division.*



*Dr S.A. Ahmad, formerly Head, Atomic Spectroscopy Section, started his scientific career in 1962, when he joined BARC from the then Atomic Energy Training School. He has made very significant contributions to several areas in atomic spectroscopy and is India's leading specialist in studies related to nuclear effects in atomic spectra. He has more than 70 publications, mostly in reputed international journals. Dr Ahmad, during his two years (1982-84) stay at CERN, Geneva, was involved in the investigations of nuclear properties of more than 100 short lived isotopes/isomers, using collinear fast beam laser spectroscopy, at the ISOLDE facility. Presently, he is pursuing his interest in high-resolution spectroscopy of lanthanides and actinides. Dr Ahmed is the President of the Indian Society of Atomic and Molecular Physics.*



*Dr A. Venugopalan joined Spectroscopy Division, BARC in 1970 after graduation from Kerala University. He did his Ph.D in Physics from the University of Mumbai in 1982. He has worked as visiting scientist at the ISOLDE facility at CERN, Geneva, in 1985 and was a collaborator in the first time on line measurement of isotope shift and hyperfine structure of short lived gold isotopes using Resonance Ionisation Spectroscopic technique. He also worked as visiting scientist at the Institute of Physics, University of Mainz, Germany, in 1989 - 1990. His field of specialisation is High Resolution Atomic Spectroscopy. Presently he is involved in the spectroscopy of lanthanides and actinides. He has more than 50 publications, mostly in international journals.*



*Mr B.K. Ankush joined Spectroscopy Division, BARC, in 1990 after completion of postgraduation in Chemistry from Shri Chhatrapati Shivaji University, Kolhapur. His field of research is 'High Resolution Studies of Spectra of Lanthanides and Actinides'. His research articles have been published in national and international conferences and journals.*



*Dr A. Ramanujam has been associated with the Trombay Plutonium Plant since its inception. In 1970, he has specialized in the reprocessing of fast reactor fuels at CEA, France. As Head, PDD, he is responsible for plutonium processing and process control analytical operations at the Trombay Plant and for setting up the laboratory systems in the new processing projects like KARP, FUS, etc. His R&D interests include PUREX and THOREX process development, automation in Pu and <sup>235</sup>U product processing, partitioning and recovery of minor actinides and important fission products under P&T program.*



# ELECTRON BEAM WELDING OF COPPER TO AISI-304 SS

T.K.Saha and A.K.Ray

Laser and Plasma Technology Division

B.K. Shah

Atomic Fuels Division

and

K. Bhanumurthy and G. B.Kale

Materials Science Division

Bhabha Atomic Research Centre

## Abstract

*Copper, when welded to Stainless Steel, causes hot cracking in the heat affected zone (HAZ). The amount of copper that melts and mixes with the SS in the weld pool does not cause much problem. However the Copper enriched HAZ on the SS side can reach a temperature at which Copper melts and penetrates the grain boundaries of SS. This phenomenon may result in grain boundaries weakening and may cause cracking. Electron Beam (EB) Welding which is having extremely low HAZ because of its very low heat input, can be well suited for the fusion welding of Copper to SS. EB welding of Copper to SS was carried out for the fabrication of Rotating Anode of X-ray generator to be used in Linear Accelerator at Center for Advance Technology, Indore. A number of dummy pieces were welded initially with different weld parameters. Some of the weldings that were carried out at lower weld speed showed micro-cracks. Metallography of these specimens has traced grain boundary liquation of the Copper in SS. The authors will discuss the weld procedure, the mechanical and metallographic evaluations of the welds and some of the techniques adapted to achieve defect free EB welding of the above dissimilar material.*

## Introduction

EB WELDING IS THE BEST choice for welding of dissimilar materials because of its low heat input, high power density and precisely controlled beam. Moreover, EBW can provide purest welding environment since the welding is normally carried out in vacuum. Copper to SS weld joint has significant roles to play in the fields of heat transfer, power generation and transmission, cryogenics,

electrical and electronics. Rotating anode (Fig. 1), which consists of two copper to SS joints is a component of X-ray generation equipment, being used in Linear Accelerator, that has been developed in Center for Advance Technology. During EB welding trial of the above component, problems like heavy sputtering, bending of the beam and micro-cracks were noticed. Sputtering and bending problem was eliminated by proper focusing and by off-setting of the electron beam. Most probable cause of the micro-

cracks seems to be the grain boundary liquation of HAZ of stainless steel by liquid copper as suggested by Savage<sup>1</sup>. Several EB welded test specimens were prepared at various powers and speeds to investigate actual reasons of cracking and to find out the solution of the problem.

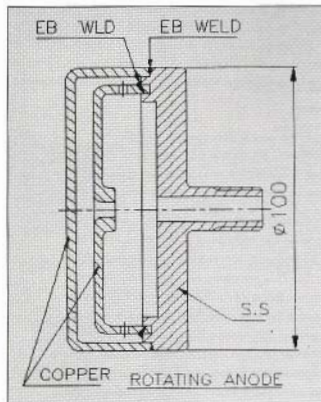


Fig. 1 Schematic of rotating anode



Fig. 1b Welded rotating anode

## Experimental Set Up

All the weldings have been carried out by using an EB welding machine, developed indigenously in BARC, that is working since last 18 years.

*Specifications of the machine :* Specifications of the EB welder is as follows:

Capacity:	6 kW
Accelerating voltage:	150 kV
Electron Gun vacuum:	$5 \times 10^{-6}$ mbar
Chamber vacuum:	$5 \times 10^{-4}$ mbar
Chamber size:	1500 x 1000 x 1000 mm <sup>3</sup>
Speed, X-Y table:	20 – 2000 mm per min.
Speed, rotary table:	0.5 – 20 rpm

Movements of X-Y table and rotary manipulator are programmable. Focused beam diameter is about 0.5mm at moderate power and about 2mm at maximum power.

*Mounting of the test specimen :* Rotating anode was mounted on the rotary table of the work chamber at an angle of 45 degree for the first weld and then horizontally for the second. The test specimens, that are essentially 3mm thick plates, were mounted on specially designed holding fixtures. Copper end-taps have been provided at starting and finishing ends of the test specimens. One millimeter thick tantalum backing plate was used for the test coupons to avoid excessive penetration. Tantalum has been chosen because of its good behavior as backing plate<sup>3</sup> attributed to its high melting point, good thermal conductivity and non-contaminating nature.



**Table I : Initial weld parameters for rotating anode**

SL. No.	Beam energy	Beam current	Job speed	Beam power
1.	90 kV	15 mA	15 cm/min.	1.35 kW
2..	120 kV	25 mA	90 cm/min.	3.0 kW

**Table II : Weld parameters for test coupons**

Sample. No.	Beam Energy (kV)	Beam Current(mA)	Speed (cm/min.)	Beam off-set on Cu (mm)	Penetration (mm)
1	120	16	30	0.5--1.0	3.0
2	120	24	100	0.5--1.0	3.0
3	120	20	100	0.2	3.0
4	120	28	120	1.0	3.0
5	120	14	20	1.0	3.0
6	120	18	100	nil	2.85

### Weld Parameters

The weld penetration requirement for the Rotating anode was 3 mm. The following weld parameters were selected to provide 3mm penetration on copper at low and high powers.

**Table III : Tensile test result**

U.T.S. (MPa)	Sample No.	Failure location	0.2% YS (MPa)
135	1	weld fail	98
160.10	2	weld fail	104.60
156	3	weld fail	88
228.30	4	weld fail	124.90
168.10	5	P/M(SS) fail	78.90

*Parameters for Test Coupons* : Table II recorded the various weld parameters with which the weldings of the test specimens were carried out.

The above test coupons were prepared for Tensile test, Micro hardness analysis, Micrography including SEM and for Electron probe micro analysis (EPMA). Pre-heat passes at low current were carried out before all the welding. Post-weld cosmetic passes were provided in a few cases where sputtering or undercut had taken place. Vacuum in electron gun and inside the work chamber was  $5 \times 10^{-4}$  mbar and  $5 \times 10^{-4}$  mbar respectively during the welding operation.

### Results

*Tensile test* : From the results of the tensile test, given in Table-III, it is observed that the welds, that were carried out at higher speeds (sample no: 2,3 and 4) have shown higher Yield strength. Sample no. 3, which was welded with off-setting the beam by less than 0.5mm on copper side, has shown lowest UTS. In case of sample no. 6, the electron beam was aligned at exactly on the joint.

The weld pool in this case had diverted towards SS side and the specimen did not have full penetration hence its tensile strength was not tested.

**Micro-hardness analysis:** The micro hardness analysis were carried out for sample no. 2, 3 and 5. Two lines were selected on each welded section, near the top bead and near the weld root. V.P.N. values were recorded at an interval of 0.1mm along this line from the center, until the readings stabilized. Fifteen to twenty readings

were taken for each side of the welds among which the maximum and the minimum values are recorded in Table-IV. It could be observed from the table, there is no significant change in hardness values on SS side. However on Cu side, variation in sample number 3, and 5 is significant. Whereas sample number 2, that has been welded at higher speed did not suffer much change in hardness.

Table III: Tensile test result

Sample No.	Failure location	0.2% YS (MPa)	U.T.S. (MPa)
1	weld fail	98	135
2	weld fail	104.60	160.10
3	weld fail	88	156
4	weld fail	124.90	228.30
5	P/M(SS) fail	78.90	168.10

Table IV: Vickers pyramid test load: 100gms. 20x

Sample No.	Reading No.	Max. Value	Min. Value	Max. Value	Min. Value
		SS (V.P.N.)	SS (V.P.N.)	Cu (V.P.N.)	Cu (V.P.N.)
2	1. Top line	221	198	94	79
	2. Root line	235	172	105	62
3	1. Top line	231	202	158	126
	2. Root line	231	194	168	104
5	1. Top line	226	205	143	102
	2. Root line	235	190	100	58

## Microstructural Investigation of the Weld

The typical optical micrographs for the welded specimens 3, 4 and 5 are shown in Fig.2, 3 and 4 respectively. The optical micrograph corresponding to Fig. 2 shows the presence of micro cracks originating at the Cu HAZ and propagating into the weld pool. There are no such kind of cracks or micropores visible in sample no 4(Fig.3). This interface is rather sharp and devoid of any

microcracks. However for the specimen 5, the micrograph indicated microcracks. A typical scanning electron micrograph for the specimen 5 is shown Fig. 4. This micrograph clearly indicated the narrow HAZ, typical of EB welded specimens. In addition, the micrograph also indicates microcracks originating at HAZ and propagating into the stainless steel. The migration of the liquid copper into these cracks could also be noticed.

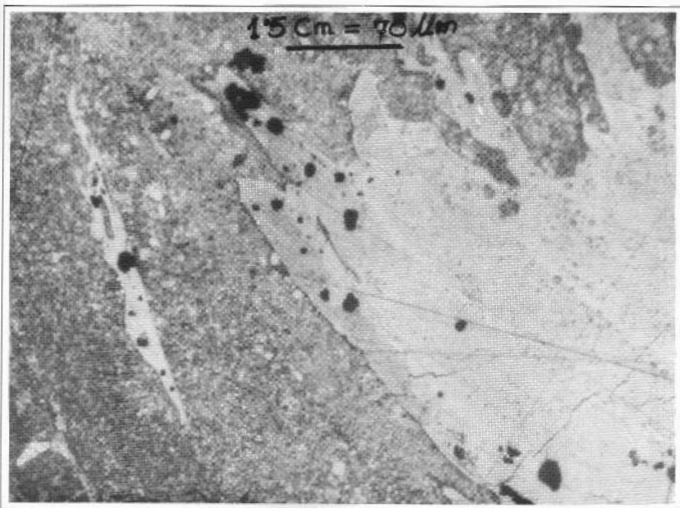
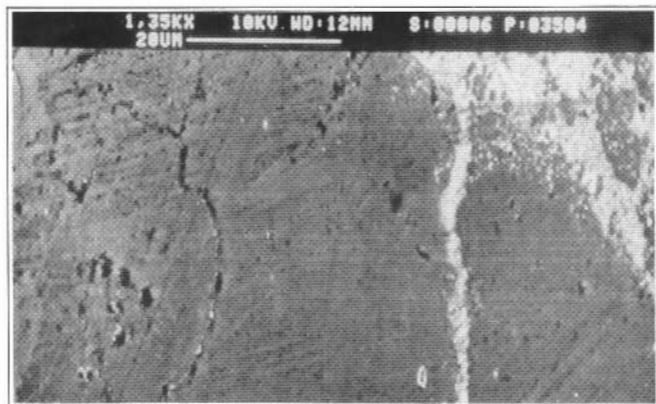


Fig. 2 Microcracks developed in weld (sample no. 3, low off-set).



*Fig. 3 Micro-structure in specimen no. 4 (welded at 100 cm/min.)*



*Fig. 4 SEM study of propagation of micro-cracks in Grain Boundary during low speed EB welding*

**Electron probe micro analysis:** Both point counting and intensity profiles for the Fe(K-alpha), Cr(K-alpha), Ni(K-alpha) and Cu(K-alpha), elements across the interface have been established by EPMA. The electron gun of EPMA was operated 15 keV and a stabilized beam current of 20nA. ZAF software<sup>4</sup> has been used to convert the intensity to atomic concentrations. A typical elemental distribution corresponding to the specimen no. 2 is shown in Fig. 5.

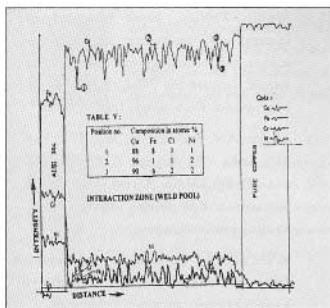


Fig. 5 EPMA profiles for specimen no. 2

A nearly homogenous distribution of Fe, Cr, Ni, and Cu could be seen from this profiles. However the behavior of Cu-Ni binary is quite complimentary to Fe-Cr system<sup>5</sup>. Point count analysis corresponding to three regions marked (1), (2) and (3) in Fig. have been corrected by ZAF procedure and these results are listed in Table V. The weld pool essentially consists of Cu (90 to 92 at.%). There is also some dissolution of Fe (6.5 at %) and very small quantity Of Cr. and Ni. It can be seen from this table that the composition of Cu and Ni goes down and the

same of the Fe and Cr goes up at point(1) and (3) as compared to corresponding composition at point(2).

## Discussion

During the welding operation, it was observed that if the beam is aligned exactly on the joint, a negligible amount of Cu melts whereas most of the melting takes place on SS side. From the beam profile, it seems the beam might have changed its path towards stainless steel. These phenomena may be attributed to the following reasons: (a): Large difference of thermal conductivities between Cu and SS. (b): Development of magnetism in non magnetic steel due to phase change.i.e ferrite formation during the melting process. (c): Production of electro motive force due to dissimilar metal welding by EB.

However in this case the first reason is predominant. To eliminate the problem, it was decided to shift the EB towards the Cu side of the joint. Two off-setting parameters, a)0.2mm and b)0.5mm to 1mm were (both at higher speed) chosen. Tensile test result shows that the welded specimen with 0.2mm off-setting (specimen no. 3) possessed poor yield strength(YS) and ultimate tensile strength(UTS). Whereas specimens that have been welded by off-setting the beam more than 0.5mm, possessed good YS and UTS. Micro hardness test (Table-IV), also revealed that there is a large variation in hardness value on Cu side of the weld pool for specimen no.3, whereas for the specimens, with more beam off set, this variation is negligible. This fact was confirmed by the microstructural investigation of specimen no. 3(Fig.2), which shows presence of smaller microcracks. Microstructural investigations confirmed

absence of microcracks in specimens welded at higher weld speeds (100cm/min. or more). Whereas during the low speed weldings, microcracks appeared at HAZ and propagated through stainless steel parent metal (Fig. 4). This fact has been confirmed by tensile test results and micro hardness examinations. This result could be attributed to the fact that at higher speed there may be very limited time for diffusion and segregation of solute element during the cooling cycle.

## Conclusion

Autogenous sound welding of Cu to AISI 304 SS is feasible by EBW process. Fabrication of a number of rotating anodes have been carried out with 120kV and 26mA focused beam. The linear speed of the job was selected at 100cm/min. The electron beam was aligned at a distance of 1mm from the joint on Cu side. Low power pre-heat pass was provided for every job. Pressure test as well as He-leak detection test were carried out on all the jobs and integrity of weld joints were found to be satisfactory.

## Acknowledgement

Authors are thankful to Dr.N.Venkatramani, Head, Laser & Plasma Technology Division for his constant encouragement for this work.

Authors are grateful to Dr.S.Banerjee, Associate Director, Metallurgy Group, BARC, for his support.

## References

1. Savage W.F, Nipples and Fetal E, Intergranular attack of steel by molten copper, Welding Journal, Vol.57.1.
2. T.K.Saha, A.R.Biswas and A.K.Ray :Effect of Backing Plate Material on SS 304EB Welding, paper presented in International conference on Vacuum science and technology and SRS Vacuum system, January 30- Feb2, 1995, Centre For Advance Technology, Indore, India.
3. Thakur A.V, Kumar S.C, Raju P.T, Ray A.K, Sinha A.K, Varghese P.M, Vijayan T and Roatgi V.K, Report on Partial vacuum E.B.Welding Machine for welding precise components.
4. R.W.Cahm, P.Hassan, E.J.Kumar, Editor, Material Science and Technology, a comprehensive treatment, Volume:2B.
5. P.B.Massalski, Editor, Binary alloy phase diagram, 2nd edition, American Society For Metals, Metalspark, Ohio, 1990.

*This paper presented during the International Welding Conference - IWC'99 at New Delhi during February 15-17, 1999 has been adjudged the winner of the KCP Award 2000.*



Mr T.K. Saha joined BARC in 1980. He graduated from the Institution of Engineers (India) in mechanical engineering. Presently he is working in Laser and Plasma Technology Division and is engaged in electron beam welding activities. He is responsible for development of welding procedure for some important components such as canned motor, centrifuge, coronet, rotary anode, Ni-electrode, reflector and shut-off plate for KAMINI. He has 12 publications to his credit.



Dr A.K. Ray graduated from IIT, Karaghpur, and obtained his M.Sc. Tech and Ph.D. from IIT, Powai. He joined the 11<sup>th</sup> Batch of BARC Training School. Since then he is engaged in the development of electron beam melting, welding and evaporation equipment. He has about 25 publications to his credit.



Mr B.K. Shah graduated from R.I.T., Jamshedpur, in metallurgy. He did M.Tech. from IIT, Bombay, in Corrosion Science & Engineering. He is having work experience in fabrication of nuclear fuel and reactor components, metallurgical evaluation and failure analysis, metallurgical characterization by NDT and corrosion study for alloys. He has about 90 technical papers published in various proceedings and journals.

Dr K. Bhanumurthy did his Ph.D. in metallurgy and is having 20 years of experience in the field of diffusion and application of EPMA. He has worked in Germany on Humboldt Foundation Fellowship.



Dr G.B. Kale did his B.E., M.Sc. Tech. and Ph.D. in metallurgy. He joined the 15<sup>th</sup> Batch of BARC Training School. He has 28 years of experience in the field of diffusion and application of EPMA. He has worked as a visiting scientist in Germany under Indo-FRG bilateral programme.



# PHOSPHORUS DETERMINATION BY DERIVATIVE NEUTRON ACTIVATION ANALYSIS

Y. M. Scindia, A. G. C. Nair, A. V. R. Reddy and S. B. Manohar

Radiochemistry Division  
Bhabha Atomic Research Centre

## Introduction

PHOSPHORUS IS AN IMPORTANT element in biological, physiological and environmental sciences. It is one of the few elements, which is not amenable for direct Neutron Activation Analysis (NAA). This problem is circumvented using Derivative Neutron Activation Analysis (DNAA) method (Ehmann 1987). Phosphorus is stoichiometrically complexed with a surrogate element having superior nuclear properties, which can be easily assayed by NAA. The procedure involves selectively complexing phosphorus with vanadium and molybdenum in acidic medium as molybdovanadophosphoric acid (MVPA) and extracting the complex into methyl isobutyl ketone (MIBK). The organic phase was analyzed by UV-Visible spectroscopy and NAA. Studies were carried out on the complexation and extraction behavior of the MVPA complex in order to carry out DNAA. This method is tested to estimate phosphorus in Certified Reference Materials and water samples

## Experimental

All the reagents used were of AR grade. A stock solution of phosphorus was prepared from potassium dihydrogen phosphate ( $\text{KH}_2\text{PO}_4$ ) and from this a standard containing 0.025 mg/ml of phosphorus was prepared by dilution. Vanadium carriers of 0.01M and molybdenum

carrier of 0.1M were prepared from ammonium metavanadate and ammonium molybdate 4-hydrate respectively. Methyl Isobutyl Ketone (MIBK) used for preconcentration of the complex was of BDH make. All the standard water samples were prepared using de-ionized water. The concentration of phosphorus ranged from 0.02 to 20  $\mu\text{g/g}$ . Two Certified Reference Materials (CRMs), namely, A-13 (frozen animal blood), V-10 (hay sample) obtained from IAEA were dissolved in 3 ml of conc.  $\text{HNO}_3$  and 0.5 ml of conc.  $\text{HClO}_4$ . These were made up to 25 ml in 0.1M.  $\text{HNO}_3$ . Sample solutions were transferred by weight basis.

## Results and Discussion

In order to determine the stoichiometry of the MVPA complex, two sets of experiments were carried out. In the first set of experiments, vanadium concentration was kept constant (250  $\mu\text{g}$ ), with molybdenum in excess (2500  $\mu\text{g}$ ) and the concentration of phosphorus was varied. The extracted MVPA complex was analyzed using UV-Visible spectrophotometer. Fig. 1 shows the variation of optical density as a function of phosphorus concentration from which vanadium to phosphorus ratio was found to be 2:1. In the second set of experiment vanadium and phosphorus concentrations were kept constant in the ratio of 2:1 and the concentration of molybdenum was varied.



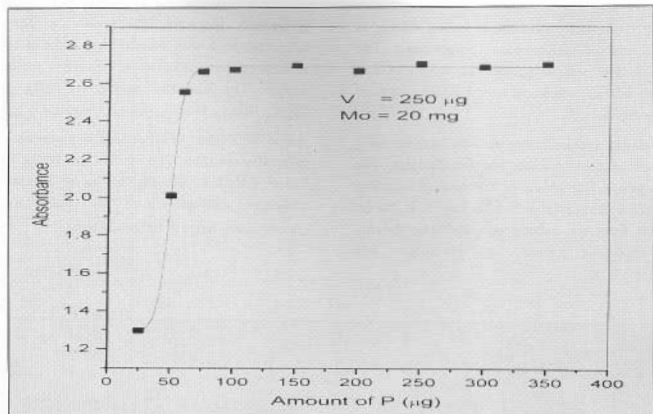


Fig. 1. Variation of absorbance with phosphorus concentration

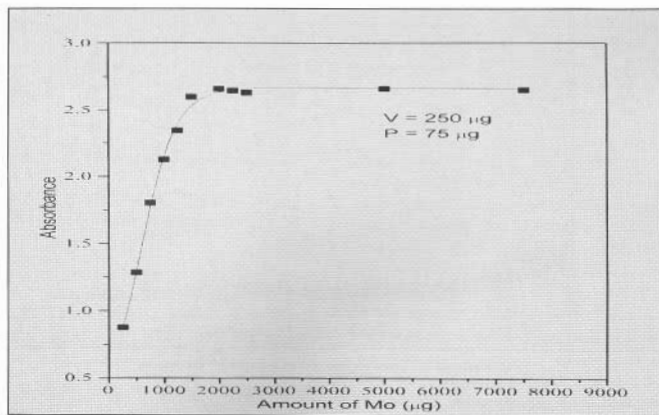


Fig. 2. Variation of absorbance with molybdenum concentration

Fig. 2 shows the variation of optical density as function of molybdenum concentration. The mole ratio between phosphorus, vanadium, and molybdenum was found to be 1:2:10 under these conditions.

Neutron activated samples were assayed using high-resolution gamma ray spectrometer. The gamma ray spectrum of the neutron activated MVPA complex is shown in Fig. 3. It can be seen from the gamma ray spectrum that the characteristic gamma rays of silicon and

germanium that are also known to form heteropoly acids with molybdenum and that are present in the matrix, do not interfere in the analysis. The extraneous gamma ray peaks are due to  $^{101}\text{Mo}$ - $^{101}\text{Tc}$  (191 keV, 307 keV) and that of  $^{38}\text{Cl}$  (1642 keV) present as impurities in polypropylene tube. The method was tested for linear analytical response by using standard addition method over a phosphorus concentration range of 0.02-0.20  $\mu\text{g/g}$ .

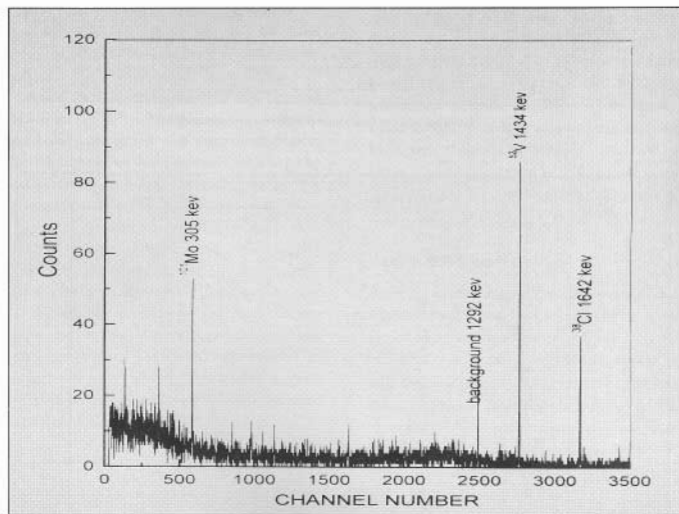


Fig. 3. Gamma-ray spectrum of the neutron activated MVPA complex

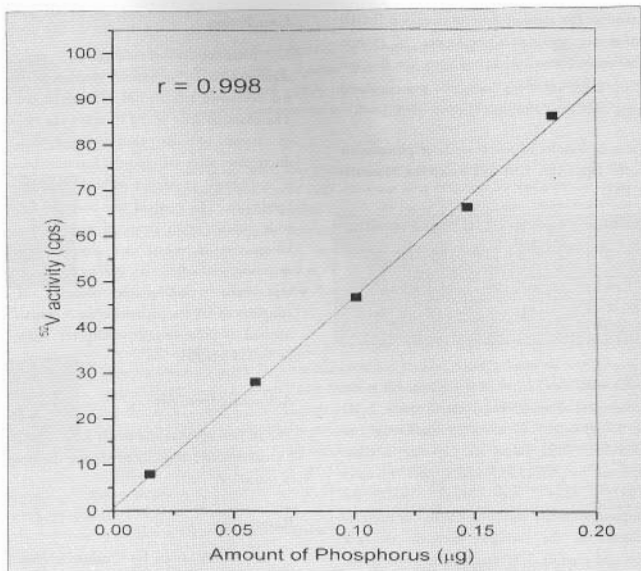


Fig. 4. Phosphorus concentration vs <sup>52</sup>V activity

Table 1 : Result of standard water samples

Amount of Phosphorus added in (µg P/ml)	Amount of Phosphorus determined in mg P/ml
0.02	0.030 ± 0.002
0.054	0.057 ± 0.003
0.075	0.078 ± 0.003
0.100	0.121 ± 0.005
0.180	0.190 ± 0.004

In Fig. 4 <sup>52</sup>V activity was plotted as a function of phosphorus concentration. The relationship between <sup>52</sup>V activity and phosphorus content was

found to be linear, with a correlation coefficient ( $r$ ) of 0.998. Table 1 shows the results of phosphorus concentration in standard water samples analyzed. Up to 25-ml of water could be preconcentrated effectively using 5 ml of MIBK. The measured phosphorus content in the CRMs, namely A-13 (animal blood) and V-10 (Hay sample) are given in Table 2. The error quoted is the standard deviation ( $1\sigma$ ) from triplicate measurements. The percent relative standard deviation ( $r_{std}$ ) obtained by this method is 3-7 % and the percentage deviation from the reported value is of the order of 4-8 %. The main errors are associated with the counting

statistics. The absolute limit of detection [LOD] under our experimental conditions of 15 min irradiation, 5 min cooling and a neutron flux was of the order  $10^{12} \text{ n cm}^{-2} \text{ s}^{-1}$  was calculated using the Currie's formula (Currie, 1968)]

**Table 2: Results of the analysis of phosphorus in the two IAEA Certified Reference Materials (CRM)**

CRM	Amount Reported	Amount determined
A-13	940 µg/g	980 ± 35 µg/g
V-10	2.3 mg/g	2.1 ± 0.2 mg/g
SRM 1577a	1.1%	1.03 ± 0.3%

$LOD = 2.71 + 3.29 \sqrt{C_b / L_t}$ , where  $C_b$  is the background counts and  $L_t$  is the live time. LOD was found to be 0.07 ng in an interference free condition. These values are superior to those reported by Allen and Hahn, and Ehmann (1987). Allen and Hahn used the tungstophosphoric acid complex. In this complex tungsten is the surrogate element and the activated product  $^{187}W$  was used to arrive at the phosphorus concentration. They have reported a detection limit of 4 ng and 1 ng respectively. These values are much lower than the method using the fast neutron reaction  $^{31}P(n,\alpha)^{28}Al$  and the limit quoted for ion selective electrode (4 µg) and spectrophotometry (10 µg). Our value compares better with the reported data.

## Conclusion

A preconcentration chemical procedure accompanied by derivative neutron activation was developed and used to estimate phosphorus. The characteristics of the complex are evaluated in terms of the stoichiometry and the discrepancy with the reported literature observed is attributed to different acid concentration conditions. The method can be applied over a wide concentration range in varying matrices. Using this technique the absolute limit of detection achieved is 0.07ng. The entire experiment including the counting of the samples can be completed within 3 hours. The method is promising especially for water and biological samples.

## Acknowledgement

The authors are thankful to Mr R.N. Acharya for his constructive suggestions during the progress of this work.

## References

1. Currie LA Limits for Qualitative Detection and quantitative Determination, Anal. Chem. (1968) 40: 586.
2. Ehmann WD, Young RC, Koppelaar DW, Jones WC, and Prasad MN. Derivative techniques in Activation Analysis, J. Radioanal. Nucl. Chem (1987) 112: 71-87.

*This paper was adjudged as the Best paper presented in the 18<sup>th</sup> National Conference of Indian Council of Chemists held at Jalgaon during December 26-29, 1999.*



Mr Yogesh M. Scindia obtained his M.Sc. in Chemistry from Mumbai University in 1998. He joined BARC in January 1999 as a Junior Research Fellow under the Mumbai University-DAE fellowship scheme and is presently working in Radiochemistry Division. His research fields are Trace Elements Determination in Environmental and Biological Matrices using Activation Techniques.



Dr A. G. C. Nair joined BARC after graduation from Kerala University in 1969 and obtained his Ph.D. from Mumbai University in 1989. His main areas of interest are radiochemical studies of fission and neutron activation analysis. During the course of these studies, several radiochemical separation procedures for fission products like Mo, Xe, In, Pd, etc. were developed. Another field where he has been interested is  $k_p$  standardized neutron activation analysis and radiotracer applications. Presently he is engaged in Prompt Gamma Ray Activation Analysis technique. He has been an IAEA expert to the Ghana Atomic Energy Commission, Ghana. He has more than 70 publications in international journals and symposia.



Dr A.V.R. Reddy obtained his M.Sc. in Chemistry in 1974 from Sri Venkateswara University, Tirupati, Andhra Pradesh. He joined Radiochemistry Division, BARC, through the BARC Training School in 1977 and is at present Head, Nuclear Chemistry Section. His areas of research are nuclear fission, nuclear reactions, nuclear spectroscopy, heavy element chemistry, activation analysis, nondestructive assay methods and preparation of special radioactive targets. He has more than 100 publications to his credit. Dr Reddy has co-authored three books and has edited five volumes. Since 1996, he has been a member of IUPAC's Commission on "Radiochemistry and Nuclear Techniques". He worked during 1992-93 in the Institut fuer Kernchemie, University of Mainz, Germany, on the chemistry of transactinide elements. During 1999-2000, as a technical officer in International Atomic Energy Agency, Vienna, he worked on Radiochemistry and Nuclear Analytical techniques.



Dr S.B. Manohar obtained his Master's degree in Chemistry from the University of Poona in 1965. He joined Radiochemistry Division, BARC through the BARC Training School and is at present Head, Radiochemistry Division. His areas of research are nuclear fusion, nuclear reaction, nuclear spectroscopy, radiochemical separations, neutron activation analysis, nuclear probes, radioactivity in the environment and development of non-destructive assay (NDA) techniques. He has published 70 scientific papers in international journals and more than 100 in symposia. He has authored a book "Experiments in Radiochemistry" and has edited the Symposium proceedings NUCAR 95 and NUCAR 99. Dr. Manohar was involved in an IAEA intercomparison measurements of radionuclides in grass samples collected after Chernobyl accident. In this connection he attended the IAEA consultants meeting at Cadarach, France during 15-17 July, 1987 and has contributed to preparation of technical report 295 titled "Measurement of radionuclides in food and environment", IAEA (1989). Dr Manohar is Ph.D. guide for Mumbai University and five of his students have been awarded Ph.D. degree in the last four years. He is a member of many scientific associations and President (elect) of Indian Association of Nuclear Chemists and Allied Scientists (IANCAS).

# DETERMINATION OF H<sub>2</sub> CONTENT IN ZIRCALOY USING HOT VACUUM EXTRACTION –QUADRUPOLE MASS SPECTROMETRY (HVE-QMS)

Y.S. Sayi, Rajendra Prasad, K.L. Ramakumar, C.S. Yadav, P.S. Shankaran,  
G.C. Chhapru, V. Venugopal, S.K. Aggarwal, H.C. Jain and D.D. Sood

Fuel Chemistry Division  
Bhabha Atomic Research Centre

## Introduction

**H**YDROGEN HAS VERY LOW solubility (< 1 ppmw at room temperature) in zircaloy which is widely used in nuclear technology. Consequently, the presence of hydrogen exceeding a certain specification limit in zircaloy components in thermal reactors eventually leads to the formation of zirconium hydride ultimately resulting in hydrogen embrittlement [1,2]. Determination of hydrogen/deuterium content in zircaloy coolant channels of pressurised heavy water reactors (PHWRs) has, therefore, been identified as one of the crucial post irradiation examination tasks for evaluating the integrity of the coolant channels for sustained, trouble-free use [3].

This paper gives the details of a hot vacuum extraction technique coupled to an on-line quadrupole mass spectrometer for the determination of hydrogen in zircaloy samples.

## Experimental

A high vacuum system has been fabricated for hydrogen extraction and determination. In a typical analysis, the sample weighing about 20

mg is taken in the quartz reaction tube. The entire system is evacuated to a vacuum better than 10<sup>-4</sup> mbar. The sample in the quartz tube is heated by a resistance furnace. Degassing of the sample is carried out at 450°C for 15 min. The valve at the outlet end of the quartz tube is closed and the temperature is slowly raised at 10<sup>0</sup>/min to a temperature of 1050°C and maintained for 15 min. The valve is then opened and the evolved gases are extracted out of the quartz tube by an ejector pump for 15 min and allowed to expand to a known volume. Pressure in the system is measured by a McLeod gauge. The evolved gas composition is determined by feeding the gases to the on-line quadrupole mass spectrometer (DATAQUAD Model DXM from M/s Anglo Scientific, UK) through a microleak valve.

Prior to the actual sample analysis, the expansion volume was calibrated by analysing titanium steel LECO analysed standard with known hydrogen concentration (28.1±5.1 ppmw)

## Results and Discussion

A typical mass spectrum of the evolved gases indicated the presence, in addition to hydrogen ion peaks ( $m/z = 1, 2, 3,$  and  $4$ ), of moisture

Table 1 : Concentration of hydrogen in zircaloy samples determined by HVE-QMS

Sample weight (g)	Total Pressure (mbar)	Total Intensity	Relative $H_1/2+H_2$ Intensity	$P(H_2)$ (atm.)	Conc. Of $H_1$ (ppmw)
0.10838	$4.8 \times 10^{-2}$	$9.44 \times 10^4$	27.03%	$1.20 \times 10^{-5}$	9.0
0.12961	$6.0 \times 10^{-2}$	$9.89 \times 10^4$	28.55%	$1.69 \times 10^{-5}$	10.6
0.11720	$6.5 \times 10^{-2}$	$2.61 \times 10^4$	22.66%	$1.45 \times 10^{-5}$	10.1
0.12466	$6.3 \times 10^{-2}$	$6.78 \times 10^4$	28.71%	$1.79 \times 10^{-5}$	11.7
0.12625	$6.5 \times 10^{-2}$	$1.77 \times 10^4$	29.35%	$1.89 \times 10^{-5}$	12.0
0.13571	$6.7 \times 10^{-2}$	$3.90 \times 10^4$	25.34%	$1.68 \times 10^{-5}$	10.1
0.04775	$3.3 \times 10^{-2}$	$4.19 \times 10^4$	16.45%	$5.30 \times 10^{-6}$	9.0
0.12986	$6.5 \times 10^{-2}$	$7.88 \times 10^4$	27.41%	$1.80 \times 10^{-5}$	11.0
				Mean	10.4±0.6

Concentration from inert gas fusion :  $10 \pm 1$  ppmw

$m/z = 18$ ),  $CO+N_2$  ( $m/z = 28$ ),  $O_2$  ( $m/z = 32$ ) and  $CO_2$  ( $m/z = 44$ ).

Prior to each sample analysis, a blank spectrum was recorded for all the masses of interest. The signal intensities at different  $m/z$  values were corrected for the corresponding blank contribution. The total intensity of hydrogen ( $I(Hydrogen)$ ) is given by  $I[H]/2+I[H_2]$ . If deuterium is also present, the intensities at  $m/z = 3$  ( $I[HD]$ ) and  $4$  ( $I[D_2]$ ) are also added. Relative intensity of hydrogen to the total intensity ( $I(Hydrogen)+I(H_2O)+I(CO)+I(O_2)+I(CO_2)$ ) was used to obtain the partial pressure due to hydrogen isotopes as a fraction of total pressure of the evolved gases. Table 1 gives the hydrogen content in a zircaloy sample in replicate analyses employing HVE-QMS. The same sample has been analysed by employing inert gas fusion (IGF) method using a commercial hydrogen determinator, the results of which are also given in the same Table. It is clearly seen that the agreement between the results is good.

## Conclusions

It is possible to get isotopic information and also the composition of evolved gases using HVE-

QMS technique. The information on hydrogen and deuterium contents in zircaloy would help in the evaluation of its "health" particularly with respect to hydrogen embrittlement.

## References

1. W.L. Mudge Jr., in Zirconium Alloys, American Society Of Metals, Ohio (1953) p 146.
2. B. Watkins, A. Cowan, C.W. Parry and B.W. Pickles, in Application - Related Phenomena in Zirconium and its Alloys, ASTM Special Pub. 458, American Society for Testing and Materials, Philadelphia (1968) p 141.
3. G.J. Field, J.T. Dunn and B.A. Cheadle, Canadian Metallurgical Quarterly, 24 (1985) 181 and other papers

*This paper was awarded the Best Paper Prize in the Seventh National Symposium on Mass Spectrometry, November 26-28, 1996 held at DRDE, Gwalior*



Dr Yelkar Seshu Saiji joined BARC in 1978 after obtaining M.Sc. (Physical Chemistry in 1972) and Ph.D. (1977) from Sri Venkateswara University. He is mainly involved in chemical quality control of nuclear fuels. He has also carried out some thermodynamic studies on carbide fuels.



Mr Rajendra Prasad obtained his M.Sc. in Chemistry from Allahabad University in 1966 and graduated from 10<sup>th</sup> Batch of BARC Training School. His area of interest is thermodynamics of nuclear materials.



Dr K.L. Ramakumar's field of interest include development of methodologies for trace analysis and separation procedures.



Mr C.S. Yadav obtained his M.Sc. in Inorganic Chemistry from Bombay University in 1979. He joined BARC in 1982. His is mainly involved in the chemical quality control and thermodynamic studies of nuclear fuels.



Mr P.S. Shankaran completed post graduation in Physical Chemistry from Bombay University in 1979. He is mainly involved in the chemical quality control and thermodynamic studies of nuclear fuels.



Mr G.C. Chhapru joined BARC after graduating in Chemistry from Bombay University (1973). He is mainly involved in the chemical quality control and thermodynamic studies of nuclear fuels.



Dr V. Venugopal is the Head of Fuel Chemistry Division, BARC. He is from 14<sup>th</sup> Batch of BARC Training School. He is a Ph.D. guide of Mumbai University. His main area of interest is thermodynamics of nuclear materials. He has more than 180 publications in reputed international journals.



Dr Suresh Kumar Aggarwal, born in 1953, is currently Head, Mass Spectrometry Section of the Fuel Chemistry Division, BARC. He received his B.Sc. (Hons.) from Guru Nanak Dev University, Amritsar, in 1972 with two Gold Medals. He joined the 16<sup>th</sup> Batch of BARC Training School in 1972 and received the Homi Bhabha Award. He did his Ph.D. from Bombay University in 1980. He worked at the University of Antwerp, Belgium, on Spark Source Mass Spectrometry (SSMS) for 6 months during 1982-83. He had his Post-doctoral training (1987-89) in GC-MS for trace elements determination in biological samples at the University of Virginia Health Sciences Centre, USA. He is a coauthor of 300 scientific publications which include 100 articles published in reputed journals. Dr Aggarwal has participated in several international and national conferences and in different international intercomparison experiments on TIMS and alpha spectrometry of Pu and U. He is a specialist in the field of atomic mass spectrometry and alpha spectrometry and is interested in various atomic mass spectrometric techniques. His other areas of interest include electrochemistry and solvent extraction. He served ISMAS as a Secretary during 1992-1997 and is presently, Vice-President (HQ) of ISMAS. He represents India in the Executive Committee of International Mass Spectrometric Conference. He has visited several countries in America, Europe and Australia as an expert as well as for delivering lectures. He is one of the editors of three books and is a recognised Ph.D. Guide of the Mumbai University.

Dr.H.C.Jain was formerly, Head, Fuel Chemistry Division, BARC. His specialisations are Mass Spectrometry, Alpha Spectrometry, Radioanalytical and Nuclear Chemistry. He has coauthored more than 300 publications.

Dr.D.D.Sood is presently Director, Division of Physical and Chemical Sciences, IAEA, Vienna. He was formerly Director, Radiochemistry & Isotope Group, BARC. He has made pioneering contributions to the chemistry of plutonium and other actinides. Dr.Sood is the author of four books on Nuclear and Radiochemistry.





# UPTAKE OF METAL IONS BY EXTRACTION CHROMATOGRAPHY USING DMDBTDMA AS THE STATIONARY PHASE

S.Sriram, P.K.Mohapatra and V.K.Manchanda

Radiochemistry Division

and

L.P.Badheka

Bio-organic Division

Bhabha Atomic Research Centre

## Abstract

*The uptake of U(VI), Pu(IV), Am(III), Eu(III), Cs(I) and Sr(II) from nitric acid solutions by a novel extraction chromatographic resin with dimethyldibutyltetradecyl-1,3-malonamide (DMDBTDMA) as stationary phase has been investigated. The order of uptake is Pu(IV) > U(VI) >> Am(III) > Eu(III) > Sr(II) > Cs(I). Batch and column studies have been carried out for the sorption behaviour of Nd (Am) from nitric acid solution. The uptake of Nd (Am) in the presence of macro concentration of Fe(III) has also been investigated.*

## Introduction

Due to their chelating effect pentaalkyl malonamides like DMDBTDMA are promising extractants for a host of tri, tetra and hexavalent actinides from nitric acid medium [1] and thus are useful for actinide partitioning from high level waste. The main advantages of this class of extractants are their innocuous radiolytic and chemical degradation products and their easy incinerability which make them promising for waste treatment [2].

Extraction chromatographic separation methods combine the advantages of both solvent extraction and ion-exchange techniques efficiently [3]. The present work deals with preparation, characterisation and use of novel

chromatographic resin material with DMDBTDMA as stationary phase and chromosorb -W as the inert support. Distribution behaviour of several actinides and fission products was investigated using this resin material in batch as well as column studies. The effect of macro concentrations of Fe(III) on the uptake of Am(III) has also been evaluated in batch as well as column studies in 4 M HNO<sub>3</sub> medium. Column studies also involve the determination of breakthrough capacity of Nd (Am) under varying acidity conditions.

## Experimental

The ligand DMDBTDMA was synthesised in the laboratory following a reported method [4].

The extraction chromatographic resin was prepared by equilibrating equal amount of (1:1 wt/wt) Chromosorb W obtained from John's Manville and DMDBTMA in acetone for about 24 hrs. After blowing off the solvent by passing  $N_2$  gas the material was vacuum dried to constant weight. Radiometric assay of  $^{241}Am$ ,  $^{152,154}Eu$ ,  $^{137}Cs$  and  $^{85,87}Sr$  was carried out by gamma counting in a NaI (Tl) scintillation detector.  $^{235}U$  and  $^{239}Pu$  were estimated by alpha scintillation counting employing toluene based extractive scintillator.

The sorption of the radionuclides from nitric acid medium was measured by contacting a known amount of the resin material (- 15-20 mg) with a known volume of the desired acid containing the radiotracer in a thermostated water bath for 1 hour. Distribution ratio ( $D_M$ ) was evaluated as the ratio of the activity per gram

of the resin material to the activity per ml of the aqueous phase. The columns were prepared by packing about 500 mg of the resin material in a glass column (4mm x 10mm). The flow rate was adjusted to 4 to 6 drops per minute.

## Results and Discussion

Fig.1 shows the plot of  $D_M$  with varying  $HNO_3$  concentration suggesting that the order of extraction is  $Pu^{4+} > UO_2^{2+} > Am^{3+} > Eu^{3+} > Sr^{2+} > Cs^+$ . Nitric acid uptake was found to be  $- 6.0 \pm 1.0\%$  by the resin material in the range 1-6M. These observations are in conformity with the solvent extraction studies reported earlier [5]. Batch studies for the sorption behaviour of Am(III) at 4M  $HNO_3$  under varying Nd loading conditions (1.8-18.2 g/L) indicate decrease in  $D_{Am}$  to  $- 4.0$  at 18.25 g/L of Nd (Table 1).

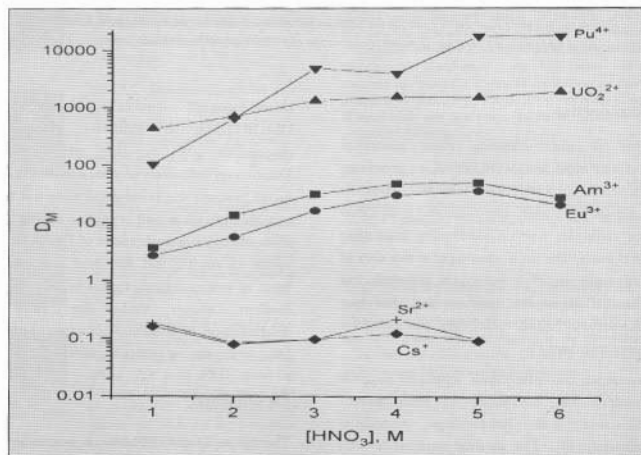


Fig. 1 Variation of  $D_M$  values with  $HNO_3$  concentration for several actinides and fission products

**Table 1: Am uptake from 4.0M HNO<sub>3</sub> under varying Nd loading conditions**

U concentration (g/L)	D <sub>Am</sub>
1.82	21.7
3.65	19.5
5.47	15.5
7.30	8.1
10.95	5.8
14.60	4.2
18.25	4.0

**Table 2: Am uptake from 4.0M HNO<sub>3</sub> at macro concentration of Fe(III)**

Fe concentration g/L	D <sub>Am</sub>
0.50	22.9
1.01	12.3
2.02	5.8
3.03	3.6
4.04	3.2
6.06	1.8

The presence of Fe(III) affects the americium ion extraction significantly [6]. The effect of macro concentration (0.5 -6 g/L) of Fe(III) on Am(III) sorption was investigated at 4.0M HNO<sub>3</sub> (Table2). A significant decrease in D<sub>Am</sub> was observed from -48 (as pure tracer) to 1.85 in presence of 6g/L of Fe(III). Breakthrough capacity of the column material for Am(III) (using 1mg/mL Nd(III) + <sup>241</sup>Am tracer) was determined at various nitric acid concentrations (1-6M HNO<sub>3</sub>) (Table 3). An increasing trend in breakthrough capacity was found with acidity upto 5M HNO<sub>3</sub>. Effect of macro amounts of Fe(III) on the Nd(Am) loading was evaluated at 4M HNO<sub>3</sub> (Table 4). Column studies on the effect of macroconcentration of Fe(III) on Nd(Am) loading indicate decrease in Am loading similar to the batch studies. 6mL of 0.01M

HNO<sub>3</sub> was sufficient to elute >95% of the loaded Nd(Am).

**Table 3: Variation of breakthrough capacity of Nd(Am) at various nitric acid concentrations**

[HNO <sub>3</sub> ], M	Breakthrough capacity of Nd (Am) mg/gm of resin
1	2
2	4
3	7
4	10
5	11
6	7

**Table 4: Effect of macro amounts of Fe(III) on Nd(Am) loading at 4M HNO<sub>3</sub>**

Fe(III) mg/mL	Breakthrough capacity of Nd(Am) mg/gm of resin
0.5	9
1.0	8
2.0	7
3.0	6
5.0	5

## References

1. C.Musikas; in the Proceedings of the Nuclear and Radiochemistry Symposium, NUCAR -95, p.12.
2. Siddall T.H. III; J.Inorg and Nucl Chem., 25, 883 (1963).
3. T.Braun and G.Ghersini (Eds) in "Extraction Chromatography", Vol. 2, Elsevier, New York (1975).
4. G.Thiollet and C.Musikas; Solv Ext and Ion Exch., 7(5), 813 (1989).
5. G.R.Mahajan, D.R.Prabhu, V.K.Manchara and L.P.Badheka; Waste Management (in press).
6. C.Cuillerdier, C.Musikas and L.Nigond; Sep. Sci. Tech., 28 155 (1993).

*This paper was given the Best Paper award for presentation at Nuclear & Radiochemistry Symposium 1999 (NUCAR-99) by Indian Association of Nuclear Chemists & Allied Scientists (LANCAS), Mumbai*



After obtaining his M.Sc. (Analytical Chemistry) from Mumbai University, Mr S. Sriram joined Radiochemistry Division, BARC in 1996 as Junior Research Fellow under the BARC - Mumbai University Collaboration Scheme for Ph.D (Chemistry). His main area of research includes the studies on liquid - liquid extraction, extraction chromatography and liquid membrane based separations of actinides and fission products using novel extractants.

Mr S. Sriram has to his credit over 18 publications in leading international journals and conferences/symposia.



Dr P. K. Mohapatra joined the Radiochemistry Division, BARC in 1987 after completing his M.Sc. in Inorganic Chemistry from Utkal University and graduating from the 30<sup>th</sup> batch of the BARC Training School. He was awarded Ph.D. by Bombay University in 1994. Dr Mohapatra carried out Post-Doctoral research work at University of Liege, Belgium, under BOYSCAST Fellowship, DST (1998 - 1999) and University of Mainz, Germany, under Humboldt Fellowship (1999 - 2000) on MRI contrast agents and chemistry of super

heavy elements, respectively. His research interests includes the chemistry of macrocyclic compounds and separation studies of actinides and fission products using novel extractants. Dr. Mohapatra has to his credit over 100 publications in international journals and conferences.



Dr V. K. Manchanda joined the Radiochemistry Division, BARC in 1969 after graduating from Delhi University and from the 12<sup>th</sup> batch of the BARC Training school. He was awarded Ph.D. by Bombay University in 1975 and carried out Post-Doctoral work at UTEP, Texas, U.S.A. as Fulbright Scholar (1985-87). His research interests include thermodynamics and kinetics of complexes of macrocyclic ligands with lanthanides and actinides, physico-chemical studies on actinide complexes, design and synthesis of novel extractants for actinides and chemical quality control of Pu based fuels. A recognised Guide in Chemistry for M.Sc. and Ph.D. by University of Mumbai, Dr. Manchanda currently heads the Actinide Chemistry Section, Radiochemistry Division. Dr. Manchanda has over 200 publications to his credit.



Dr L.P.Badhka (Ph.D, chemistry, Bombay University, 1989) joined the Bio-organic Division, BARC, in 1967. He carried out post doctoral research at the Institute for Pharmaceutical Biology at the University of Munich (1994-95). His current interests include the synthesis of organic ligands for actinide extraction.



# PREPARATION AND THERMAL STUDIES ON $\text{Pu}(\text{MoO}_4)_2$ AND $\text{Na}_2\text{Pu}(\text{MoO}_4)_3$

N.D.Dahale, Meera Keskar, K.D.Singh Mudher, R.Prasad and V.Venugopal

Fuel Chemistry Division  
Bhabha Atomic Research Centre

## Summary

THE SOLID STATE REACTIONS OF  $\text{Na}_2\text{MoO}_4$  with  $\text{Pu}(\text{MoO}_4)_2$  were carried out in different molar proportions at various temperatures. Thermal studies of the compounds have been studied using thermogravimetric (TG) and differential thermal analysis (DTA) techniques. The products formed during the thermal decomposition of the reactants were identified by X-ray diffraction method. XRD data of  $\text{Pu}(\text{MoO}_4)_2$  and  $\text{Na}_2\text{Pu}(\text{MoO}_4)_3$  were indexed on orthorhombic and tetragonal system respectively. On heating isothermally at  $1200^\circ\text{C}$ ,  $\text{Pu}(\text{MoO}_4)_2$  gave  $\text{PuO}_2$  whereas  $\text{Na}_2\text{Pu}(\text{MoO}_4)_3$  formed a mixture of  $\text{PuO}_2$  and  $\text{Na}_4\text{PuO}_7$  at  $1400^\circ\text{C}$ .

## Introduction

Molybdenum is an important fission product formed in large quantity in the nuclear reactor. Reaction of molybdenum with other fission products changes the behaviour of the fuel. Sodium metal is used as a coolant in liquid metal fast breeder reactors (LMFBR). Uranium, thorium and plutonium are used as nuclear fuels. In accidental condition, sodium, actinides and Mo may interact among themselves and form

different compounds. A systematic study to prepare and characterize some compounds in alkali metal-actinide-molybdenum-oxygen system had been carried out by Dion [1,2]. Tabuteau et.al had studied alkali-metal-plutonium-molybdenum-oxygen quaternary system by means of liquid-solid equilibrium diagrams and X-ray diffraction [3]. However, thermal studies on sodium plutonium molybdates has not been reported so far. Earlier we have reported X-ray diffraction and thermal studies on Th-Th-Mo-O and Na-U-Mo-O systems [4,5]. In continuation of our earlier work, the present work has been carried out to study the thermal behaviour of  $\text{Pu}(\text{MoO}_4)_2$  and  $\text{Na}_2\text{Pu}(\text{MoO}_4)_3$ .

## Experimental

$\text{Pu}(\text{MoO}_4)_2$  was prepared by heating the mixture of  $\text{PuO}_2$  and  $\text{MoO}_3$  in 1:2 molar ratio in platinum boat in air, initially at  $500^\circ\text{C}$  for 2 hours and then further at  $800^\circ\text{C}$  for 15 hours.  $\text{Pu}(\text{MoO}_4)_2$  and  $\text{Na}_2\text{MoO}_4$  were mixed in different molar ratios and heated upto  $600^\circ\text{C}$  in air. TG and DTA patterns of the compounds were recorded in platinum cups in Mettler Thermoanalyzer at the rate of  $10^\circ\text{C}/\text{min}$  in a flowing stream of dry air. Preheated alumina was

used as reference material for DTA measurements. The progress of the reaction and purity of the product after each heating was monitored by taking X-ray diffraction patterns of the products on DIANO X-ray diffractometer using  $\text{CuK}\alpha$  radiation ( $\lambda = 1.54178 \text{ \AA}$ )

## Results and Discussion

The XRD data of  $\text{Pu}(\text{MoO}_4)_2$  was indexed on orthorhombic system with lattice parameters  $a = 9.42 \text{ \AA}$ ,  $b = 10.05 \text{ \AA}$  and  $c = 13.98 \text{ \AA}$  and data

of  $\text{Na}_2\text{Pu}(\text{MoO}_4)_2$  was indexed on tetragonal system with  $a = 5.18 \text{ \AA}$  and  $c = 11.28 \text{ \AA}$ .

TG and DTA curves of  $\text{Pu}(\text{MoO}_4)_2$  is shown in Fig.1. TG curve showed no weight loss upto  $900^\circ\text{C}$ , showing the thermal stability of the compound. An endothermic DTA peak was observed at  $950^\circ\text{C}$  due to the melting of the compound. The end product formed at  $1200^\circ\text{C}$  was confirmed as  $\text{PuO}_2$  by weight loss calculation and by X-ray diffraction method.

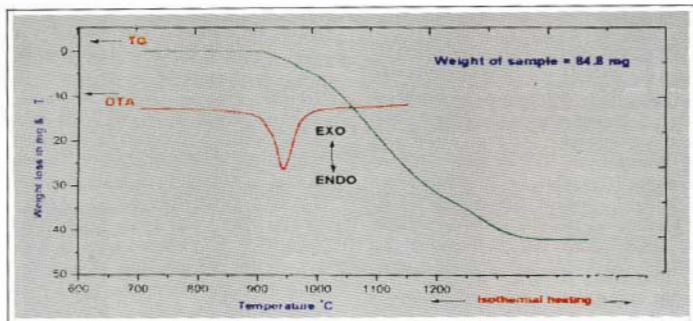


Fig.1. TG and DTA curves of  $\text{Pu}(\text{MoO}_4)_2$  in air

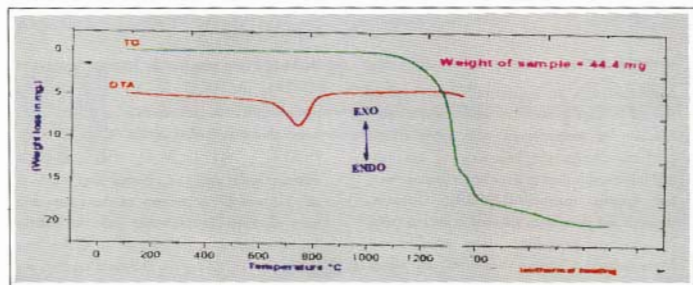
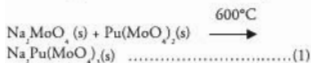
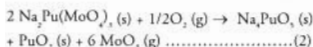


Fig.2. TG and DTA curves of  $\text{Na}_2\text{Pu}(\text{MoO}_4)_2$  in air

$\text{Pu}(\text{MoO}_4)_2$  and  $\text{Na}_2\text{MoO}_4$  mixed in equimolar proportion and heated in air upto  $600^\circ\text{C}$ , leads to the formation of  $\text{Na}_2\text{Pu}(\text{MoO}_4)_2$ . Formation of the compound can be described by Eq. (1).



Thermogram of  $\text{Na}_2\text{Pu}(\text{MoO}_4)_2$  is given in Fig.2. TG curve did not show any weight change up to  $1000^\circ\text{C}$ . The DTA curve showed an endothermic peak at  $740^\circ\text{C}$  due to the melting of the compound. The X-ray diffraction patterns of the compound before and after melting were identical, suggesting the congruent melting of the compound. Further heating of  $\text{Na}_2\text{Pu}(\text{MoO}_4)_2$  upto  $1400^\circ\text{C}$  led to the formation of mixture of  $\text{Na}_4\text{PuO}_5$  and  $\text{PuO}_2$ . The decomposition of  $\text{Na}_2\text{Pu}(\text{MoO}_4)_2$  in air can be shown by the following Eq. (2).



The formation of  $\text{Na}_4\text{PuO}_5(\text{s})$  and  $\text{PuO}_2(\text{s})$  was identified by weight loss calculation as well as by X-ray diffraction analysis.

The reaction of  $\text{Pu}(\text{MoO}_4)_2$  and  $\text{Na}_2\text{MoO}_4$  in 2:1 molar ratio at  $600^\circ\text{C}$  did not form higher molybdate. However, the XRD pattern of product was identified as mixture of  $\text{Na}_2\text{Pu}(\text{MoO}_4)_2$  and  $\text{Pu}(\text{MoO}_4)_2$ .

## References

1. C. Dion and A. Noel, Bull. Soc. Chim. France, (1983) 1-257.
2. C. Dion, Bull. Soc. Chim. France, (1981) 371.
3. A. Tabuteau, M. Pages and W. Freundlich, Mat. Res. Bull., 7 (1972) 691.
4. N.D. Dahale, K.L. Chawla and N.C. Jayadevan, NUCAR - 95, Kalpakkam, Feb.21-24.
5. D. Dahale, Meera Keskar, K.D. Singh Mudher, K.L. Chawla and V. Venugopal, ISAT - 98, Bangalore, Nov.24-25.

*Molybdenum is an important fission product formed in large quantity in the nuclear reactor. Reaction of molybdenum with other fission products changes the behaviour of the fuel. Sodium metal is used as a coolant in liquid metal fast breeder reactors (LMFBR). Uranium, thorium and plutonium are used as nuclear fuels. In accidental condition, sodium, actinides and Mo may interact among themselves and form different compounds.*

*This paper was adjudged the Second Best paper in the 12<sup>th</sup> National Symposium (THERMANS 2000) held at DDU Gorakhpur University, Gorakhpur, during March 26-27, 2000.*



After obtaining M.Sc. in Physical Chemistry from Poona University in 1979, Mr. N.D. Dahale joined BARC in 1981. His main area of research has been preparation of new compounds by solid state reactions and their characterisation by X-ray and thermal methods. He is also involved in development of X-ray fluorescence spectrometric methods of elemental analysis. He has published several papers in international journals and symposia.



After graduating in Physics from Bombay University in 1985, Mrs. Meera Keskar joined Fuel Chemistry Division in 1988. She obtained her M.Sc. degree in Physical Chemistry in January 2000. Her field of interest is preparation and characterisation of actinide compounds and elemental analysis by XRF.



Dr K.D. Singh Mudher joined BARC in 1971 after completing his post graduation from IIT Delhi in Chemistry and acquiring Ph.D. degree from IIT Mumbai. His main areas of research are X-ray diffraction, X-ray fluorescence and Thermochemical investigations of actinides. He has published more than 100 papers in international journals and conferences.



After obtaining M.Sc. in Chemistry from Allahabad University (1966), Mr Rajendra Prasad joined 10<sup>th</sup> batch of BARC Training School in 1967. His area of interest is thermodynamics of nuclear materials.



Dr. V. Venugopal is the Head of Fuel Chemistry Division, BARC. He is from 14<sup>th</sup> batch of Training School. He is a Ph.D. guide of Mumbai University. His main area of interest is thermodynamics of nuclear materials. He has more than 180 publications in reputed international journals.





# A STUDY OF SOLID STATE REACTION BETWEEN STRONTIUM CARBONATE AND RUTHENIUM DIOXIDE

R. K. Mishra, J. G. Shah and R. G. Yeotikar

Waste Management Facilities, Tarapur

and

S. R. Dharwadkar

Applied Chemistry Division

Bhabha Atomic Research Centre

## Abstract

*A solid state reaction between strontium carbonate and ruthenium oxide is studied employing thermogravimetry, effluent gas analysis and XRD techniques. In addition to temperature, other parameters such as ambient atmosphere and compaction of the reaction mixture influenced the reaction rate. The rate of reaction was much higher in oxygen compared to that in argon. The compaction of reaction mixture decreased the reaction rate.*

## Introduction

RUTHENIUM (Ru) AND ALKALINE earth elements such as strontium (Sr) and barium (Ba) are among the major fission products [1]. During reprocessing of spent fuel, these fission products form the major part of high level liquid radioactive waste (HLW). These fission products are highly radioactive and are immobilised in an inert matrix. The steps commonly employed for management of HLW, are immobilisation of HLW in the glass matrix, pouring in SS canisters, their interim storage and ultimate disposal in underground repositories [2].

In general, two methods are employed for immobilisation of HLW in glass [3]. In the first, the slurry containing glass forming additives and HLW are heated above the fusion temperature in a furnace. The processes involved in the vitrification are evaporation, calcination and

fusion. The molten glass so formed, is then poured into the SS canisters and transferred to the interim storage. In the alternate procedure, the waste is first calcined to get the calcined mass. The same and the preformed glass mixture is heated above the fusion temperature and poured into canisters. Some of the oxides such as those of Ru, Te and Cs have appreciable volatility and therefore can vaporise from the reaction mixture during vitrification and can get deposited on piping and other locations in the plant.

The present study is aimed at trapping the vapours of Ru from HLW during the stage of calcination / vitrification. It is observed that, by trapping the volatile Ru on alkaline earth carbonate can convert Ru to alkaline earth ruthenate, which is thermodynamically stable. In order to understand the formation of ruthenate, efforts were made to synthesize the same. In this paper, we present a case study of

the solid state reaction between alkaline earth carbonate  $\text{SrCO}_3$  and the ruthenium dioxide for the formation of  $\text{SrRuO}_3$ , and recommend the optimum conditions under which such compounds can be prepared in pure form.

## Experimental

All the chemicals used in this investigations were of analytical grade purity. The alkaline earth carbonates and ruthenium oxide were procured from S.D. Fine Chemicals, Mumbai and Arora - Mathey, Calcutta, respectively. The thermogravimetric analyses of 1:1 reaction mixture of  $\text{SrCO}_3$  and  $\text{RuO}_2$  in flowing oxygen and argon was carried on simultaneous TG/DTA unit (SETARAM, Model TG-DSC-92-16) employing the heating rate of 50C/min. A steady flow rate of 2.5 l/hr was maintained during the TG runs.

In addition to TG, separate experiments were performed for on-line monitoring of evolved  $\text{CO}_2$  in the reaction. In two separate experiments, purified argon and oxygen were passed over the reaction mixture placed in the uniform temperature zone of furnace. The  $\text{CO}_2$  gas evolved in the reaction was swept by these carrier gases into the electrolytic cell containing the standardised solution of  $\text{Ca(OH)}_2$ . The change in conductance of  $\text{Ca(OH)}_2$  solution as a function of time was monitored on X-T recorder. The experiments were performed at series of temperatures in the range 600 to 800°C. The samples in these experiments were employed both in the form of loose powder and pellet.

The reaction products obtained after the TG run and on heating the mixtures at different temperatures were characterised by Siemens X-ray diffractometer, Model D-500, employing the  $\text{Cu K}\alpha$  ( $\lambda = 0.154 \text{ nm}$ ) radiation. The progress of the reaction was followed by

monitoring the relative change in the intensity of most intense lines of the product and reactant phases in the recorded X-ray pattern.

## Results

Thermogravimetric curves for 1:1 powdered mixture of  $\text{SrCO}_3$  and  $\text{RuO}_2$  recorded in flowing oxygen and argon at 5°C/min are shown in Fig.1.

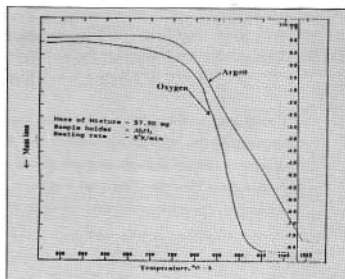
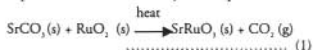


Fig.1 TG curves of 1:1 mixture of  $\text{SrCO}_3$  and  $\text{RuO}_2$  recorded in flowing argon and oxygen

From the mass loss in the TG, reaction between the components of the mixture could be expressed stoichiometrically as in equation-1.



Identification of the product of the TG by XRD and neutralisation of  $\text{Ca(OH)}_2$  solution in which  $\text{CO}_2$  was absorbed, further confirmed the stoichiometry of the reaction. It is interesting to note from Fig.1, that, the reaction in oxygen was initiated at much lower temperature and proceeded much more rapidly. Also, the temperature of the beginning of evolution of  $\text{CO}_2$  in both the cases was about 250°C lower compared to that for the thermal decomposition

of pure  $\text{SrCO}_3$  under identical conditions. One of the intriguing features of the TG curve for the mixture recorded in argon, is the intermediate step, in Fig.1 at around  $950^\circ\text{C}$ . This could probably be, in oxygen atmosphere, the reaction was completed before the initiation of the decomposition of pure  $\text{SrCO}_3$  ( $\sim 950^\circ\text{C}$ ), whereas, in argon, the reaction rate was slower and reaction was not completed prior to the decomposition of pure  $\text{SrCO}_3$ .

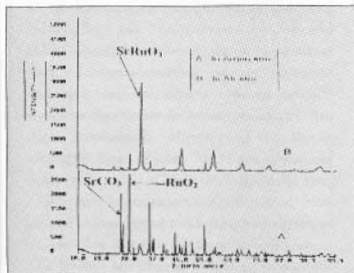


Fig.2 XRD patterns of  $\text{SrCO}_3 + \text{RuO}_2$  heated at  $600^\circ\text{C}$  in Ar and air atm.

The difference in the reactivity of the mixture observed in TG experiment carried out in oxygen/air and argon gas atmospheres was also evident in the isothermal experiments followed by X-ray diffraction. The XRD patterns of the powdered mixture heated in air and argon at  $600^\circ\text{C}$  for 5 hours (Fig. 2) was clearly different. While the reaction in air was virtually complete indicating the absence of peaks of  $\text{SrCO}_3$  and  $\text{RuO}_2$ , the mixture heated in argon showed presence of these reactants. The reaction of powdered mixture followed by the measurement of evolved  $\text{CO}_2$ , employing the conductometric apparatus described earlier, further confirmed the observations made by TG and XRD. The plots

of fraction transformed ( $\alpha$ ) versus time calculated from the conductivity data obtained at the reaction temperature of  $800^\circ\text{C}$  for the reaction mixtures heated in oxygen/air and argon are compared in Fig. 3.

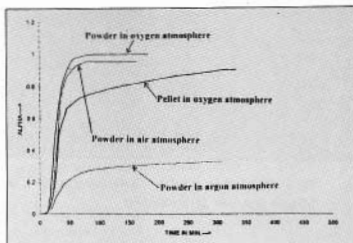


Fig. 3 Plot of  $\alpha$  vs time at  $800^\circ\text{C}$  in different environments

It can be seen that at  $800^\circ\text{C}$  the reaction in argon did not proceed beyond  $\sim 30\%$ , but was almost complete for the mixture heated in oxygen/air. An additional interesting part of this investigation is the influence of compaction on the reactivity of the mixture. The  $\alpha$  versus time plots obtained from the conductivity data on the powdered sample and the pellet (compacted at 8 tons/sq. inch) in oxygen atmosphere of identical weight at  $800^\circ\text{C}$  are compared in Fig. 3. It can be seen that, in the case of powdered sample, the reaction is complete in about 50 min., while in case of pellet, the same was completed only to the extent of 70%. The difference in the reactivity observed in the conductivity data was also obvious from the XRD pattern of the samples heat treated at  $700^\circ\text{C}$  for the same length of time (5 hours). It was observed that the ratio of the strongest peak intensity of  $\text{SrRuO}_3$  to  $\text{RuO}_2$  is much higher for the powder compared to that for the pelleted sample (Fig. 4).

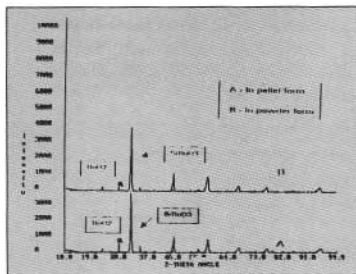
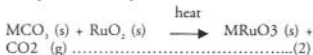


Fig. 4 XRD patterns of  $\text{SrCO}_3 + \text{RuO}_2$  heated at  $700^\circ\text{C}$  in (A) pellet form, and (B) powder form

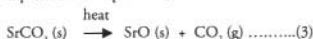
## Discussion

The results on the solid state synthesis of strontium ruthenate presented here are identical to those for other alkaline earth metal ruthenates, namely, those of barium and calcium [4]. In general, the solid state reaction for the formation of ruthenates from the reaction components can be expressed as in equation-2.



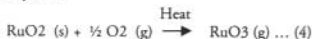
Thermogravimetric curves recorded both in oxygen as well as argon, show that the reaction in oxygen is quantitative and is completed before the decomposition temperature of  $\text{SrCO}_3$ . The reaction in argon is relatively slow, but nevertheless, occurred at temperature much lower than that of the decomposition of pure  $\text{SrCO}_3$ . It was however not complete below the decomposition temperature of pure  $\text{SrCO}_3$ . The lowering of temperature of evolution of  $\text{CO}_2$  in a mixture relative to that of  $\text{SrCO}_3$  decomposition could readily be understood on the basis of the formation of  $\text{SrRuO}_3$  in the reaction. This may be due to more negative

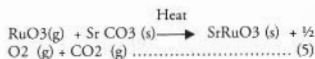
change in Gibbs energy for the reaction in equation-1, compared to that of the decomposition of  $\text{SrCO}_3$ , which could be expressed as in equation -3.



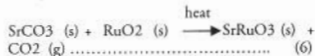
Since the formation of  $\text{SrRuO}_3$  from  $\text{SrCO}_3$  and  $\text{RuO}_2$  is a solid state reaction, compaction was expected to increase the rate of reaction. But, it was observed that, compaction decreases the rate. This observation of reduced reactivity of the mixture on compaction can be readily understood in terms of build up of  $\text{CO}_2$  pressure, in the pelleted sample. Such observations of compaction of sample on thermal decomposition of metal carbonates are common and well documented [5]. Decomposition of  $\text{SrCO}_3$  is suppressed considerably if evolved  $\text{CO}_2$  is not swept away from the sample. The stagnation of evolved  $\text{CO}_2$  in the reaction, in the compacted sample resulted in the suppression of the forward reaction. In the case of powdered sample, the evolved  $\text{CO}_2$  can diffuse readily and get mixed up in the ambient environment.

It is observed that the reaction rate leading to the formation of  $\text{SrRuO}_3$  is enhanced considerably in the oxidising environment at all temperatures. This leads to the speculation that, there must be a chemical reaction involving oxygen as one of the reactant species leading to the formation of ruthenate. It is known that,  $\text{RuO}_2 (\text{s})$  reacts with oxygen at high temperature to form  $\text{RuO}_3 (\text{g})$  [6], which is metastable and disproportionate at low temperatures. It is possible that the metastable  $\text{RuO}_3 (\text{g})$  formed in the presence of oxygen, reacts instantaneously with  $\text{SrCO}_3$  to form  $\text{SrRuO}_3$ . The reaction could be presented in a following sequence.





Thus, the overall reaction is,



### Conclusion

From the observations made in this investigation, it can be concluded that the reaction involving the synthesis of SrRuO<sub>3</sub> from SrCO<sub>3</sub> and RuO<sub>2</sub> should be carried out on powdered mixture in the presence of oxygen, since oxygen acts as a catalyst. The compound SrRuO<sub>3</sub> formed is highly stable. The study indicates that, there is possibility of trapping the Ru in volatilised form (RuO<sub>3</sub>, RuO<sub>4</sub> etc.) from the vessel off gas from the vitrification furnace, employing the heated column of SrCO<sub>3</sub> with the supply of air/oxygen. The volatilised species of

Ru will react with SrCO<sub>3</sub> and will get converted into a stable SrRuO<sub>3</sub> compound.

### References

1. G. Friedlander, J W Kennedy, E S Macias, J M Miller., Nuclear and Radiochemistry, Wiley - Inter science, New York, 1981.
2. J.G. Shah " Investigations of glass and Glass ceramics", Ph.D. Thesis, University of Mumbai 1996 and references therein.
3. International Atomic Energy Agency, "Techniques for solidification of HLW", Technical Report Series No. 176, IAEA, Vienna, 1977.
4. R.K. Mishra, M.Sc. Thesis, University of Mumbai 1998.
5. P.D. Garn., "Thermoanalytical methods of Investigations", Academic Press, New York (1963).
6. W.E. Bell and M. Tagami, J. Phys. Chem., 67 (1963)2432.

*The present study is aimed at trapping the vapours of Ru from HLW during the stage of calcination / vitrification. It is observed that, by trapping the volatile Ru on alkaline earth carbonate can convert Ru to alkaline earth ruthenate, which is thermodynamically stable. In order to understand the formation of ruthenate, efforts were made to synthesize the same. In this paper, we present a case study of the solid state reaction between alkaline earth carbonate SrCO<sub>3</sub> and the ruthenium dioxide for the formation of SrRuO<sub>3</sub> and recommend the optimum conditions under which such compounds can be prepared in pure form.*

*This paper was adjudged as the Second Best paper in Inorganic Chemistry Session in the symposium THERMANS-2000 held at DD University, Gorakhpur, during March 26-29, 2000.*



Mr R.K. Mishra, ( M.Sc., Chem.) joined Waste Management Facilities, BARC, Tarapur, in 1992. He has worked in Product Characterisation Laboratories, in the field of X-ray diffraction, Scanning Electron Microscope/Energy Dispersive X-ray studies of different matrices for immobilisation of high level radioactive liquid waste. His research interest includes study related to preparation and properties of some glasses of relevance in nuclear technology, suppression of volatilization of ruthenium, tellurium etc. during vitrification process of high level radioactive liquid waste. Presently, he is working in process control laboratories of Waste Management Facilities, Tarapur and is engaged in works related to management of high level radioactive liquid waste and low level radioactive liquid waste.



Dr J. G. Shah, (M.Sc., Chem., 1981; Ph.D., Chemistry, 1996 : University of Mumbai) joined Waste Management Facilities, BARC, Tarapur, after graduation from 25<sup>th</sup> batch of BARC Training School. He was deputed to INE Karlsruhe, Germany, in 1988 for advanced training in the application of sophisticated instruments like SEM/EDX, XRD under Indo-German bi-lateral programme. He has carried out pioneering work in the development of matrix for incorporation of high level nuclear waste in glass in Indian nuclear programme.



Mr R.G. Yeotikar, (M.Sc., Chem., M. Tech. Chemical Technology from Nagpur University) joined Waste Management Division, BARC, after graduation from 20<sup>th</sup> batch of BARC Training School. Presently, he is Superintendent, Laboratories, Waste Management Facilities, Tarapur, and is responsible for carrying out various research and development activities related to nuclear waste management and their possible adaptation on plant scale apart from normal analytical support to plant. His main field of works includes developments and detailed characterisation of matrices for immobilisation of high level radioactive liquid waste, intermediate level radioactive liquid waste and management of other types of radioactive wastes. He has contributed significantly in evaluation of chemical durability of waste products including development of methods, effect of various parameters and simulation with respect to interim and final disposal. He was a member of Co-ordinated Research Programme of International Atomic Energy Agency and participated in India and abroad.



Dr S.R.Dharwadkar retired as Head, High Temperature & Solid State Chemistry Section, Applied Chemistry Division, BARC, Mumbai, in Dec.1998 after a distinguished service of more than three decades. During his service, he worked extensively in the field of High Temperature and Solid State Chemistry and Chemical Thermodynamics. He has established a strong internationally recognized group in this area and has published more than 125 papers in reputed international journals. The main thrust of the work of his group had been in the field of Thermodynamics of Nuclear Materials.

After his retirement, Dr Dharwadkar, has taken up teaching assignment. Currently, he is an Honorary Professor of Physical Chemistry in the Institute of Science, Mumbai, where he is guiding the students for their masters and Ph.D. degrees in chemistry. He is currently engaged in research related to the control of pollution from industrial effluents employing photo chemical reactions in presence of catalysis. His other area of current interest is the development of methods for immobilisation and safe disposal of high level nuclear waste. Dr Dharwadkar is a recipient of the Netzsch-ITAS award for outstanding work in Thermal Analysis. He is an associate of IUPAC and is a life member of several national and international scientific societies. He was Hon. Secretary of Indian Thermal Analysis Society (1991-96) and its President (1997-98). He is at present the Vice President of the Indian Society for Solid State Chemists and Allied Sciences.

# MASS SPECTRAL STUDIES FOR THE DETERMINATION AND SPECIATION OF ARSENIC BY GAS CHROMATOGRAPHY-MASS SPECTROMETRY (GC-MS)

S. K. Aggarwal

Fuel Chemistry Division  
Bhabha Atomic Research Centre  
and

R. Fitzgerald and D.A. Herold

VA Medical Center-113, San Diego, CA 92161 and Department of Pathology  
University of California-San Diego, La Jolla, CA 92134, USA

## Introduction

**D**ETERMINATION OF ARSENIC (As) is important from the point of view of environmental and biological purposes. Some studies are reported in literature [1-9] using different derivatising agents for preparing volatile chelates of As(III), As(V) and organic arsenicals viz. monomethyl arsinic acid (MMAA) and dimethylarsinic acid (DMAA). In continuation of our work [10] the development of GC-MS methodology for trace elements determination in biological samples, we investigated two different derivatising agents viz. N-tert-butyl dimethyl silyl-N-methyl-trifluoroacetamide (MTBSTFA) with 1% tert-butyl dimethyl chlorosilane (TBDMSCl) and 4-fluorophenylmagnesium bromide (4-FPMB) for preparing the chelates of As(III), As(V) and organic arsenic viz. dimethyl arsenic acid (DMAA), also known as cacodylic acid. The sensitivities of three different modes of ionisation viz. electron ionisation (EI), positive chemical ionisation (PCI) and negative chemical ionisation (NCI) were evaluated and mass spectra obtained were compared to identify the

base peak of maximum intensity containing information on As for achieving a high sensitivity in quantitation.

## Experimental

The GC-MS system used was a Finnigan MAT 4500 mass spectrometer based on quadrupole mass analyser and a Finnigan A200S Autosampler. Perfluorotributylamine (PFTBA) was used to optimize tuning for EI, PCI and NCI. Methane was used as the reagent gas for PCI and NCI at an ionizer pressure of  $0.80 \pm 0.05$  torr and an analyser pressure of  $1.4 \times 10^{-5}$  torr. The EI, PCI and NCI tunings were optimized at  $m/z$  100 and 502; 219 and 414; and 414 and 613, respectively. After tuning, scans were obtained from  $m/z$  50 to 650 in 2 seconds. 70 eV electrons were used in the EI, PCI and NCI modes.

The As-chelates were prepared using MTBSTFA and 4-FPMB in independent experiments using aqueous solution of As(III) as  $As_2O_3$  in 10%  $HNO_3$ , methanolic solution of As(V) as  $As_2O_5$ , and methanolic solution of DMAA. First, the tert-butyl dimethyl silyl (t-BDMS) derivatives of

inorganic and organic arsenicals were prepared by treating  $As_2O_3$ ,  $As_2O_5$  and DMAA directly with MTBSTFA. Second, the t-BDMS derivatives were prepared by first synthesizing the pyrrolidine dithiocarbamates of As(III), As(V) and DMAA. The toluene solutions containing these derivatives were evaporated to complete dryness at 40°C under a steady stream of  $N_2$  gas. The dried residues were dissolved in 200  $\mu$ L of ethyl acetate and 50  $\mu$ L of MTBSTFA was added and used for preparing arsenic derivatives.

The fluorophenyl derivatives of As(III), As(V) and DMAA were synthesized by first preparing their respective pyrrolidine dithiocarbamates followed by treating with 8-10 drops of Grignard reagent (4-FPMB) [10].

One mL of the metal chelate, containing 200 to 400 ng of As, was injected into the GC in the splitless mode using autosampler. A 15 m x 0.32 mm i.d. cross-linked dimethylpolysiloxane (DB-1) capillary column with a 0.25  $\mu$ m film thickness was used in these studies. Ultra high purity helium (99.999%) was the carrier gas.

## Results and Discussion

A typical EI mass spectrum of  $As(FC_6H_4)_3$  is shown in Fig. 1. The fragmentation patterns observed with EI were interpreted through a combination of PCI and EI mass spectra. It was

observed that the t-BDMS derivatives of As eluted at lower temperature than the fluorophenyl derivatives and showed a simpler and cleaner EI mass spectra. From the mass spectra recorded on different arsenic chelates mentioned above, it was observed that the derivatives of As(III) or As(V) formed directly with MTBSTFA were  $(C_6H_{11}Si)AsO_4$  irrespective of As(III) or As(V) taken initially. With DMAA, the derivatisation resulted in the formation of  $(C_6H_{11}Si)_2AsO_4$  with small amounts of  $(C_6H_{11}Si)AsO_4$ , with each compound showing distinct elution peak in GC-MS. When derivatisation with MTBSTFA was performed by first preparing the pyrrolidine dithiocarbamates of As(III), As(V) or DMAA, the derivative formed was  $(C_6H_{11}Si)AsO_4$ . The 4-FPMB derivatised inorganic as well as organic arsenicals to  $As(FC_6H_4)_3$ , independent of the starting form of As.

Among the three different modes of ionisation used, EI was found to give the highest sensitivity for As quantitation whereas NCI was found to be the least sensitive for both the derivatives of As. For example, the relative sensitivity values for EI/PCI were found to be 6, 12 and 2, respectively, for direct derivatisation with MTBSTFA, derivatisation with MTBSTFA through pyrrolidine dithiocarbamates and derivatisation with 4-FPMB.

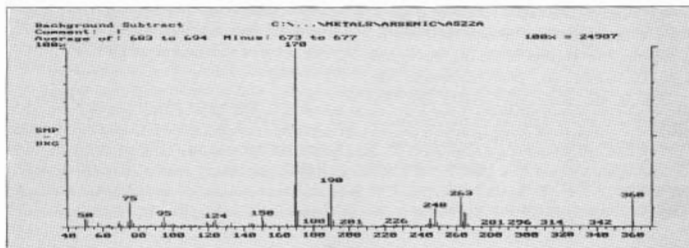


Fig. 1 A typical EI mass spectrum of  $As(FC_6H_4)_3$



## Conclusion

The results obtained clearly show that for the assay of As by GC-MS, derivatisation with MTBSTFA or with 4-FPMB through pyrrolidine dithiocarbamates can be employed. Direct derivatisation of As with MTBSTFA would not be useful in real-life samples because this would demand the quantitative dissolution of As(III) and As(V) in an organic solvent miscible with MTBSTFA. The t-BDMS derivatives of As formed with MTBSTFA do not require silation of the GC column. The final choice of the derivatising agent would, however, depend upon the quantitative and reproducible recovery of As when carried through the entire procedure. Since As is a mono-isotopic element, another element as a suitable internal standard or another external standard would be required for As quantitation by GC-MS.

## References

1. W.C. Butts, W.T. Rainey Jr., *Anal. Chem.* 43 (1971) 538.

2. F.T. Henry, T.M. Thorpe, *J. Chromatogr.* 166 (1978) 577.
3. E.H. Daughtrey Jr., A.W. Fitchett, P. Mushak, *Anal. Chim. Acta* 79 (1975) 199.
4. T.P. Mawhinney, *J. Chromatogr.* 257 (1983) 37.
5. H.D. Watts, D. Cameron, Proc. of 42nd ASMS Conference on Mass Spectrometry and Allied Topics, Chicago, IL, May 1994, p. 271 (1994).
6. D. Cameron, T. Brozovich-Ford, H. Watts, J. Wingham, Paper NO. WPF 163, presented at 43rd ASMA Conference on Mass Spectrometry and Allied Topics, Atlanta, GA, May 26-30, 1995.
7. B. Beckermann, *Anal. Chim. Acta* 135 (1982) 77.
8. S. Fukui, T. Hirayama, M. Nohara, Y. Sakagami, *Talanta* 30 (1983) 89.
9. J.-J. Yu, C.M. Wai, *Anal. Chem.* 63 (1991) 842.
10. S.K. Aggarwal, M. Kinter, R.L. Fitzgerald, D.A. Herold, *Crit. Rev. in Clin. Lab. Sci.* 31 (1994)

*This paper was awarded the Second Best Paper Prize in ISMAS Symposium on Mass Spectrometry, December 7-9, 1999 held at IICT, Hyderabad*

### About the author ....



Dr Suresh Kumar Aggarwal, born in 1953, is currently Head, Mass Spectrometry Section of the Fuel Chemistry Division, BARC, Trombay, Mumbai. He received his B.Sc. (Hons.) from Guru Nanak Dev University, Amritsar, in 1972 with two Gold Medals, he joined the 16<sup>th</sup> Batch of BARC Training School in 1972 and received the Homi Bhabha Award. He did his Ph.D. from Bombay University in 1980. He worked at the University of Antwerp, Belgium, on Spark Source Mass Spectrometry (SSMS) for 6 months during 1982-83. He had his Post-doctoral training (1987-89) in GC-MS for trace elements determination in biological samples at the University of Virginia Health Sciences Centre, USA. He is a coauthor of

300 scientific publications which include 100 articles published in reputed journals. Dr Aggarwal has participated in several international and national conferences and in different international intercomparison experiments on TIMS and alpha spectrometry of Pu and U. He is a specialist in the field of atomic mass spectrometry and alpha spectrometry and is interested in various atomic mass spectrometric techniques. His other areas of interest include electrochemistry and solvent extraction. He served ISMAS as a Secretary during 1992-1997 and is presently, Vice-President (HQ) of ISMAS. He represents India in the Executive Committee of International Mass Spectrometric Conference. He has visited several countries in America, Europe and Australia as an expert as well as for delivering lectures. He is one of the editors of three books and is a recognised Ph.D. Guide of the Mumbai University.

# ISOTOPE RATIO MEASUREMENTS FOR PLUTONIUM IN ISOTOPIC REFERENCE MATERIALS BY THERMAL IONISATION MASS SPECTROMETRY (TIMS) USING TOTAL EVAPORATION TECHNIQUE

**S.K. Aggarwal**

Fuel Chemistry Division  
Bhabha Atomic Research Centre  
and

**R. Fiedler and S. Deron**

Safeguards Analytical Laboratory  
Seibersdorf, Vienna, Austria

## Introduction

**T**OTAL EVAPORATION METHODOLOGY is expected to circumvent the ubiquitous problem of isotope fractionation during isotope ratio measurements by TIMS. Isotope fractionation has, in fact, been plaguing the overall accuracy achievable in the determination of Pu and U isotope ratios and concentration in dissolver solution of irradiated fuel and in other complex matrices. Hence, it was of interest to verify experimentally and determine, if any, the residual isotope fractionation factor commonly called as B-factor or K-factor. These studies were performed on MAT-1 (Pu) mass spectrometer using different isotopic reference materials of Pu available at SAL and obtained from IRMM, Belgium; NBL, USA and AEA, UK.

## Experimental

Different isotopic reference materials of Pu (IRMM-290 series, A1, B1, C1, F1 and G1) prepared at IRMM, Belgium by mixing highly

enriched  $^{239}\text{PuO}_2$  and  $^{242}\text{PuO}_2$ , and certified with overall uncertainty of 0.01% or better for  $^{242}\text{Pu}/^{239}\text{Pu}$  isotope ratios were used. In addition, the other isotopic reference materials of Pu available from IRMM, Belgium (CBNM-047A); NBL, USA (CRM-144, NBL-128, NBS-947) and from AEA, Harwell, UK (UKPu5) were also used.

Replicate mass spectrometric analyses (15 to 25 filament loadings) were performed on each of the isotopic reference material using the Measurement Protocol (MP 16) for total evaporation technique generally used at SAL. The protocol was based on heating the ionisation filament to a temperature corresponding to a signal of 275 mV for  $^{187}\text{Re}^+$  to ensure nearly same ionisation filament temperature in different mass spectrometric analyses. Then the sample filament was heated slowly at pre-defined rate (50 mA/step) to a temperature so as to get the sum of the ion current of all the isotopes of Pu corresponding to about 40 mV. After achieving this pre-set signal strength, the heating of the

sample filament was continued at one of the three defined heating rates (50 mA/step, 10 mA/step or 1 mA/step) depending upon the signal strength; and the ion current integration was performed. The integration of the ion current was continued until the Pu<sup>+</sup> signal strength fell below a pre-defined value (about 40 mV). This usually involved the heating of the sample filament to a current of about 6.2 A which was also pre-defined in the measurement

protocol and maintaining it at this value until the sample was practically exhausted.

## Results and Discussion

The results obtained from the replicate mass spectrometric analyses of different isotopic reference materials of Pu are given in Table 1. A number of interesting observations were made during the mass spectrometric analyses as well as during data evaluation.

**Table 1 : Comparison of the certified and experimentally determined isotope ratios in Pu reference materials**

Code (Atom Ratio)	Certified ±1σ	Observed <sup>a</sup> ±1σ	B factor/atom (%) (1σ)
IRMM-290-A1 (242/239)	0.97560 (0.0041%)	0.97545 (0.025%)	-0.0051 ± 0.0040 [25] <sup>b</sup>
IRMM-290-F1 (242/239)	0.099440 (0.0055%)	0.099483 (0.025%)	0.0144 ± 0.0043 [19]
IRMM-290-G1 (242/239)	9.86722 (0.0055%)	9.87088 (0.025%)	0.0124 ± 0.0042 [24]
IRMM-290-B1 (242/239)	0.432937 (0.0032%)	0.432996 (0.013%)	0.0046 ± 0.0037 [23]
IRMM-290-C1 (242/239)	2.14378 (0.0036%)	2.14423 (0.0058%)	0.0071 ± 0.0036 [20]
CBNM-047-A (244/239)	0.770461 (0.095%)	0.772611 (0.043%)	0.0560 ± 0.0190 [16]
NBL-CRM-144 (240/239)	15.11568 (0.023%)	15.11086 (0.016%)	-0.0320 ± 0.0250 [21]
NBL-CRM-144 (242/239)	21.01811 (0.019%)	21.00782 (0.015%)	-0.0160 ± 0.0072 [21]
NBL-CRM-144 (244/239)	7.986874 (0.027%)	7.986289 (0.021%)	-0.0015 ± 0.0058 [21]
NBL-128 (242/239)	1.000977 (0.013%)	1.000464 (0.030%)	-0.0170 ± 0.0059 [21]
NBS-947 (240/239)	0.241118 (0.060%)	0.241024 (0.0062%)	-0.0390 ± 0.0610 [14]
NBS-947 (242/239)	0.015599 (0.17%)	0.015560 (0.051%)	-0.0830 ± 0.0570 [14]
UKPu-5 (240/239)	0.965337 (0.055%)	0.964327 (0.014%)	-0.1050 ± 0.0560 [18]
UKPu-5 (242/239)	1.025620 (0.090%)	1.026322 (0.027%)	0.0230 ± 0.0300 [18]
UKPu-5 (244/239)	0.335914 (0.12%)	0.336570 (0.042%)	0.0390 ± 0.0240 [16]

<sup>a</sup>Measured in November 1997

<sup>b</sup>Replicate mass spectrometric analyses performed

In some cases, when the total number of scans collected during the measurement were low (say 50) compared to the usual number of scans ranging from 100 to 250, the experimentally measured isotope ratios (242/239, 244/239) were higher compared to the usually obtained ratio. The less number of scans are observed in a few cases, probably due to improper setting of the sample magazine/ extraction lenses focus during computer controlled automated mass spectrometric analysis. During the data acquisition for UKPu5 sample, it was observed that sufficient Pu<sup>+</sup> signal is obtained always without heating the sample filament. In other isotopic reference materials, data collection started only after heating the sample filament to appreciable temperature (filament current of 1.5-1.8A). This difference in the analytical conditions could lead to different B factor, if any, during the analyses. A comparison of the experimental data with the certified values indicates that the B factor determined can be related to the origin of the certified reference material. For example, the B-factors determined using the isotope ratios <sup>240</sup>Pu/<sup>239</sup>Pu are negative

while those determined using <sup>242</sup>Pu/<sup>239</sup>Pu and <sup>244</sup>Pu/<sup>239</sup>Pu isotope ratios are positive in case of UKPu3 and UKPu5 (i.e. prepared in UK). For the reference materials NBS-947, CRM-144 and NBL-128 (i.e. prepared in USA), the B-factors determined are always negative irrespective of the isotope ratio used. For the isotopic reference materials prepared in IRMM, Belgium from oxides, the B-factors are very small (less than 0.02% per mass unit) but these lie in both the directions.

From the experimental data on <sup>242</sup>Pu/<sup>239</sup>Pu and <sup>244</sup>Pu/<sup>239</sup>Pu isotope ratios of CRM-144, NBL-128 and IRMM-290 series reference materials, it can be stated that using total evaporation and the existing isotopic reference materials, the B-factor per mass unit is less than 0.02%. This is in contrast to the studies performed at SAL using the uranium isotopic reference materials when no B-factor was observed. This corroborates the studies published from the laboratory in Trombay showing that the B-factors for U and Pu are different and that the B-factor for Pu is higher than that for U.

Table 2 : Mean precision values (Pu isotope ratio measurements in reference materials)

Nuclides	Isotope ratio value	Precision (%)	Mean precision (%)
240/239	0.24	0.006	0.012
	0.96	0.014	
	15.12	0.016	
242/239	0.015	0.051	0.024
	0.099	0.025	
	0.43	0.013	
	0.97	0.025	
	1.00	0.030	
	1.03	0.027	
	2.14	0.006	
	9.86	0.025	
	21.02	0.015	
244/239	0.34	0.042	0.035
	0.77	0.043	
	7.99	0.021	

There is need to have some more new isotopic reference materials of Pu with certified  $^{244}\text{Pu}/^{239}\text{Pu}$  as well as  $^{242}\text{Pu}/^{239}\text{Pu}$  isotope ratios to confirm the existence of small but measurable mass discrimination effects even in total evaporation measurements and also to resolve the discrepancy of conventionally expected negative B-factor (as observed in case of CRM-144, NBL-128, IRMM-290/A1) versus positive B-factor (as observed from IRMM-290/B1, C1, F1, G1).

During the data evaluation from replicate mass spectrometric analyses, it was observed, as shown in Table 2, that the external reproducibility was dependent on the mass difference between the isotopes measured except for CRM-144. These values ranged from 0.010-0.020%, 0.020-0.030% and 0.040-0.045% for  $^{240}\text{Pu}/^{239}\text{Pu}$ ,  $^{242}\text{Pu}/^{239}\text{Pu}$  and  $^{244}\text{Pu}/^{239}\text{Pu}$  isotope ratios, respectively. This is another indication that inspite of using the total evaporation methodology, there is small residual B-factor present for Pu and this is affecting the reproducibility of the isotope ratios as a function

of the mass difference between the two isotopes measured.

It was also of interest to study the influence of starting ion current prior to integration, on the measurement of isotope ratios. For this purpose, the reference materials CRM 144 and IRMM 290/A1 were analysed using different ion intensities ( $20$  to  $200 \times 10^{-14}$  A) at the start of the measurement. Replicate mass spectrometric analyses were carried out for the two standards at four different values of the starting ion intensity. Measurements at SAL are normally performed with a starting current of  $40 \times 10^{-14}$  A. The Pu isotope ratios determined from the two reference materials are given in Table 3. There is no significant difference in the isotope ratios measured using varying values of the starting ion current and moreover, there is no clear trend observed for the dependence of isotope ratios on the starting ion current. This showed that there is no additional bias introduced in isotope ratio measurements by the total evaporation method.

**Table 3 : Effect of changing sum ion current parameter in data collection protocol of total evaporation for Pu isotope ratio determination**

Sum ion current	(Observed / Certified) Isotope Ratio		
	290/A1	CRM-144	
	242/239	242/239	244/239
	0.97560 <sup>a</sup>	21.01811 <sup>a</sup>	7.98687 <sup>a</sup>
20 mV	0.99981 [6] <sup>b</sup> (0.010%)	0.99967 [7] <sup>b</sup> (0.031%)	1.00004 [7] <sup>b</sup> (0.024%)
40 mV	0.99985 [25] (0.025%)	0.99951 [21] (0.015%)	0.99993 [21] (0.021%)
100 mV	0.99991 [10] (0.006%)	0.99956 [11] (0.019%)	1.00015 [11] (0.023%)
200 mV	0.99991 [6] (0.017%)	0.99970 [7] (0.020%)	1.00004 [7] (0.033%)
Mean	0.99987 (0.005%)	0.99961 (0.009%)	1.00004 (0.009%)

<sup>a</sup>Certified value

<sup>b</sup>Replicate mass spectrometric analyses

## Conclusion

The above studies emphasise the need of more isotopic reference materials for plutonium to confirm that the isotopic fractionation effects are completely eliminated using total evaporation and ion current integration methodology. Further, it is necessary to examine the percentage

contribution of different species produced during evaporation and ionisation in a surface ionisation source. These studies will further strengthen the data produced by TIMS and will be very useful in improving the precision (external) and accuracy values to better than 0.1% in the next millennium.

*This paper was awarded the Second Best Paper Prize in ISMAS Symposium on Mass Spectrometry, December 7-9, 1999 held at IICT, Hyderabad*

### *About the author ....*



*Dr Suresh Kumar Aggarwal, born in 1953, is currently Head, Mass Spectrometry Section of the Fuel Chemistry Division, BARC. He received his B.Sc. (Hons.) from Guru Nanak Dev University, Amritsar, in 1972 with two Gold Medals. He joined the 16<sup>th</sup> Batch of BARC Training School in 1972 and received the Homi Bhabha Award. He did his Ph.D. from Bombay University in 1980. He worked at the University of Antwerp, Belgium, on Spark Source Mass Spectrometry (SSMS) for 6 months during 1982-83. He had his Post-doctoral training (1987-89) in GC-MS for trace elements determination in biological samples at the University of Virginia Health Sciences Centre, USA. He is a coauthor of 300 scientific publications which include 100 articles published in reputed journals. Dr Aggarwal has*

*participated in several international and national conferences and in different international intercomparison experiments on TIMS and alpha spectrometry of Pu and U. He is a specialist in the field of atomic mass spectrometry and alpha spectrometry and is interested in various atomic mass spectrometric techniques. His other areas of interest include electrochemistry and solvent extraction. He served ISMAS as a Secretary during 1992-1997 and is presently, Vice-President (HQ) of ISMAS. He represents India in the Executive Committee of International Mass Spectrometric Conference. He has visited several countries in America, Europe and Australia as an expert as well as for delivering lectures. He is one of the editors of three books and is a recognised Ph.D. Guide of the Mumbai University.*



# VACUUM DECOMPOSITION PATTERN OF FERROUS AMMONIUM SULPHATE – A QUADRUPOLE MASS SPECTROMETRIC STUDY

Y. Sesha Sayi, P.S. Shankaran, C.S. Yadav, G.C. Chhapru and K.L.Ramakumar

Fuel Chemistry Division  
Bhabha Atomic Research Centre

## Introduction

**D**URING OUR ATTEMPTS TO develop an analytical technique for the determination of sulphur by vacuum combustion extraction-quadrupole mass spectrometry [1], preliminary experiments were carried out by taking ferrous ammonium sulphate as reference material. Measurement of composition of gases evolved by quadrupole mass spectrometry revealed that apart from  $\text{SO}_2$ , gases  $\text{N}_2\text{O}$ ,  $\text{NO}$  and  $\text{NO}_2$  were observed. But no peak due to ammonia  $\text{NH}_3$  could be detected. With a view to understanding the decomposition behaviour of ferrous ammonium sulphate, detailed investigations were carried out. Instead of adapting the conventional thermal analysis techniques, quadrupole mass spectrometry has been employed to monitor the product gases formed. The present paper gives a brief account of our observations on the decomposition of ferrous ammonium sulphate under vacuum at temperatures  $600^\circ\text{C}$  to  $1040^\circ\text{C}$ .

## Experimental

### Equipment

The hot vacuum extraction-quadrupole mass spectrometer employed for the present studies has been described in our paper [1]

### Chemicals

Analytical grade ferrous ammonium sulphate

### Methodology

Known amount of the sample was loaded into the quartz tube and the entire system was evacuated to  $10^{-3}$  mbar. The sample was then heated at the required temperature for 30 minutes under static vacuum conditions and the gases released were extracted into a known volume. The gas pressure and the composition were then determined by online differential oil manometer and quadrupole mass spectrometer respectively.

## Results and Discussion

The fragmentation patterns of  $\text{N}_2\text{O}$ ,  $\text{NO}$  and  $\text{NO}_2$  are taken from the mass spectrometer's library. Fractional abundances of the parent molecular peaks at  $m/z$ 's 30, 44 and 46 corresponding to  $\text{NO}$ ,  $\text{N}_2\text{O}$ , and  $\text{NO}_2$  respectively were calculated from the reference spectra. These were in turn used to measure the intensities of these mass peaks obtained in the sample analysis. A typical mass spectra obtained is given in Figure 1. A separate experiment was carried out to record the "blank" mass spectrum. The intensities at different  $m/z$  values were corrected for the blank. From the intensities of the

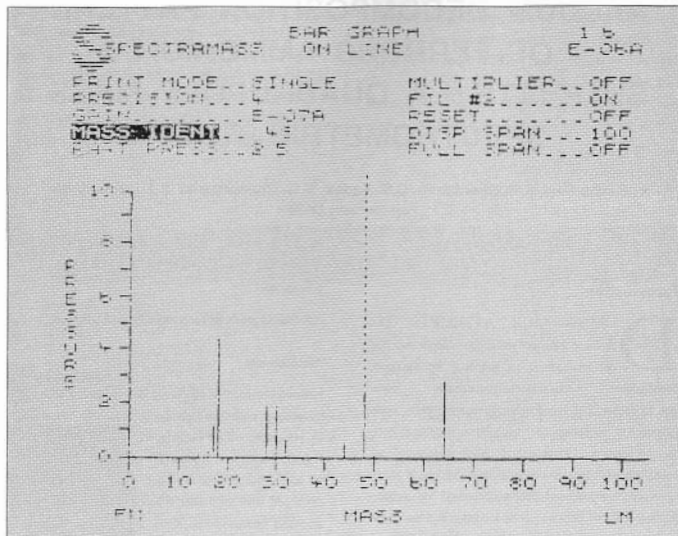


Fig. 1. Mass spectrum of gases released from the decomposition of Ferrous Ammonium Sulphate

various fragmentation peaks, total intensity of the respective parent molecular peak is computed. The relative intensities of various nitrogen oxides normalised with respect to  $N_2O$  were calculated and given in Table 1.

Table 1: Relative intensities of nitrogen oxides

TEMPERATURE (°C)	$N_2O : NO_2 : NO$
600	1 : 0 : 0.8
700	1 : 0 : 2.0
800	1 : 0 : 3.1
1040	1 : 0.01 : 0

From the Table, it can be seen that NO formation increases with temperature up to 800°C, and above this temperature it decomposes which is in agreement with the literature data [2]. But at all temperatures  $N_2O$  is the predominant species contrary to its reported behaviour [2]. On the other hand At 1040°C small quantity of  $NO_2$  is observed. However, both  $N_2O$  and  $NO_2$  are expected to decompose at these temperatures. No mass peak due to  $NH_3$  could be detected at all temperatures investigated. To substantiate the observations, it is desirable to carry out further work to study the decomposition of nitrates and



ammonium salts on these lines in vacuum, air and limited oxygen supply.

Nitrogen content in the sample was also computed from the concentration of  $N_2O$  and  $NO_2$  and it was found to be well within  $\pm 5\%$  of the expected value from its stoichiometry.

### Acknowledgement

The authors are thankful to Dr. V. Venugopal, Head, Fuel Chemistry Division, for his keen

interest and continuous encouragement in this work.

### References

1. Y. Sessa Sayi et al., Paper no. ICT-4, ISMAS Symposium (1999).
2. H.D. Gehani and S.M. Parekh, Modern Inorganic Chemistry, Educational Publishers, 1970.

*This paper was awarded the Second Best Paper Prize in ISMAS Symposium on Mass Spectrometry, December 7-9, 1999 held at IICT, Hyderabad*

*About the authors ....*



*Dr Yelkur Sessa Sayi joined BARC in 1978 after obtaining M.Sc. (Physical Chemistry in 1972) and Ph.D. (1977) from Sri Venkateswara University. He is mainly involved in chemical quality control of nuclear fuels. He has also carried out some thermodynamic studies on carbide fuels.*



*Mr P.S. Shankaran completed post graduation in Physical Chemistry from Bombay University in 1979. He is mainly involved in the chemical quality control and thermodynamic studies of nuclear fuels.*



*Mr C.S. Yadav obtained his M.Sc. in Inorganic Chemistry from Bombay University in 1979. He joined BARC in 1982. His is mainly involved in the chemical quality control and thermodynamic studies of nuclear fuels.*



*Mr G.C. Chhapru joined BARC after graduating in Chemistry from Bombay University (1973). He is mainly involved in the chemical quality control and thermodynamic studies of nuclear fuels.*



*Dr K.L. Ramakumar's field of interest include development of methodologies for trace analysis and separation procedures.*



# X-RAY AND THERMAL STUDIES ON Ti-Pu-Mo-O SYSTEM

N.D.Dahale, S.K. Sali, K.L.Chawla, R.Prasad and V.Venugopal

Fuel Chemistry Division  
Bhabha Atomic Research Centre

## Abstract

The quaternary Ti-Pu-Mo-O system was investigated for the first time and preparation and characterisation of new compound namely  $Ti_2Pu(MoO_4)_3$  was carried out. The compound was indexed on orthorhombic systems.  $PuO_2$  and  $MoO_3$  were mixed in 1:2 molar ratio and heated in platinum boat at  $600^\circ C$  to get  $Pu(MoO_4)_2$ .  $Ti_2MoO_4$  and  $Pu(MoO_4)_2$  were mixed in 1:1 molar ratio and heated at  $500^\circ C$ .



XRD pattern of  $Ti_2Pu(MoO_4)_3$  could be indexed on orthorhombic systems with cell parameters  $a = 10.056 \text{ \AA}$ ,  $b = 24.893 \text{ \AA}$ . Compound  $Ti_2Pu(MoO_4)_3$  was heated up to  $1200^\circ C$  in Mettler Thermal Analyser in air at the rate of  $10^\circ C/\text{min}$ . Simultaneous TG, DTA and DTG were recorded TG did not show any weight change up to  $700^\circ C$ . The DTA curve of this compound showed endothermic peak at  $565^\circ C$  due to melting of the compound. This was confirmed by physical verification of the sample. X-ray diffraction pattern before and melting were identical indicating  $Ti_2Pu(MoO_4)_3$  melts congruently. While on controlled cooling, sharp endothermic peak at  $460^\circ C$  was due crystallisation. Isothermal heating at  $1200^\circ C$  gave the product, which was identified by XRD as  $PuO_2$ .

*This paper was adjudged the Third Best paper at the National Symposium and Conference on Solid State Chemistry and Allied Areas (ISCAS 99), held at University of Jammu, during October 28 - 30, 1999.*



After obtaining M.Sc. in Physical Chemistry from Poona university in 1979, Mr N.D.Dahale joined BARC in 1981. His main area of research has been preparation of new compounds by solid state reactions and their characterisation by X-ray and thermal methods. He is also involved in development of X-ray fluorescence spectrometric methods of elemental analysis. He has published several papers in international journals and symposia.



Dr S.K.Sali completed his M.Sc. degree in Physical Chemistry from Poona University in 1981 and joined Fuel Chemistry Division in 1983. He obtained his Ph.D. degree from Bombay University in 1997. His field of research is thermochemical investigation of actinides.



Mr Rajendra Prasad, joined BARC after obtaining M.Sc. in Chemistry from Allahabad University (1966). He is from the 10<sup>th</sup> batch of BARC Training School. His area of interest is thermodynamics of nuclear materials.



Dr V.Venugopal is the Head of Fuel Chemistry Division, BARC. He is from 14<sup>th</sup> batch of BARC Training School. He is a Ph.D. guide of Mumbai University. His main area of interest is thermodynamics of nuclear materials. He has more than 180 publications in reputed international journals.



# NORMALIZED DZ/DT WAVEFORM FOR EASY ASSESSMENT OF PERIPHERAL BLOOD FLOW

Jagruti Chheda and Nagesh Chaugule

Final Year Students, B.E. (Biomedical Engineering)  
Thadomal Shahani Engineering College, Bandra (W), Mumbai  
and

T.S. Ananthkrishnan, J. Prakash Babu and G.D. Jindal

Guides from Electronics Division  
Bhabha Atomic Research Centre

## Abstract

*A new waveform called the normalized impedance plethysmographic waveform has been introduced for the easy assessment of peripheral blood flow. This waveform is obtained by taking the natural logarithm of the instantaneous impedance of the body segment and then differentiating with respect to time. The waveform thus obtained has its amplitude proportional to blood flow index in the body segment. This waveform gives an advantage to the clinician for easy and quick interpretation of the data in the manner similar to that of electrocardiography.*

## Introduction

Impedance Plethysmography was introduced by Jan Nyboer as far back as 1940 for the assessment of central and peripheral blood flow. He proposed parallel conductor theory for the estimation of peripheral blood flow in a given body segment and correlated the impedance plethysmographic estimates with the actual flow in in-vitro experiments and demonstrated high degree of correlation (6). According to this theory, the change in blood volume  $\Delta Z$  is given by the following relationship:

$$\Delta V = -\rho_b \times L^2 / Z_0^2 \times \Delta Z \quad \dots\dots\dots(1)$$

where  $\rho_b$  is the resistivity of the blood ( $\Omega\text{-cm}$ ),  $L$  is the length of the body segment (cm), and  $Z_0$  is the basal impedance of the body segment.

Equation 1 was further simplified for the estimation of peripheral blood flow by substituting  $V$  in place of  $\rho_b \times L^2 / Z_0$  (1,5).

$$\Delta V / V = -\Delta Z / Z_0 \quad \dots\dots\dots(2)$$

This equation was used to compute blood flow in the limb segment per 100 cm<sup>3</sup> of body tissue per minute by substituting  $V=100\text{cm}^3$  and measured values of  $Z_0$  and  $\Delta Z$ .

$\Delta Z$  could be measured by the Nyboer's back projection method (6), Kubicek's forward slope method (4) or the venous occlusion principle (5). The former two methods suffer from drawback of an error in front projection or the extension of forward slope. The venous occlusion principle had the advantage of giving enhanced signal as  $\Delta Z$  was integrated over a long interval of time in

contrast to the other two methods, (which measure  $\Delta Z$  for one cardiac cycle). However, venous occlusion principle method also suffered from the following drawbacks:

1. This method could be used to estimate the peripheral blood flow only in the distal segments of the extremities due to application of a tourniquet in the proximal part of the limb. Thus it was possible to detect the decreased arterial blood flow in the limb but it was not possible to specify approximate anatomical location of the arterial block.
2. Due to application of tourniquet, the method became off line and it was not possible to assess peripheral blood flow in real time and therefore rendered the method unsuitable for monitoring.

In patients with deep vein thrombosis or patients having oedema in the extremities due to other pathological conditions such as lymphangitis, renal failure, congestive cardiac failure, etc., the amplitude of the signal recorded was very low and could lead to a false diagnosis of peripheral arterial occlusive disease.

In view of the above, Parulkar et. al. (7) used  $dZ/dt$  waveform for the measurement of  $\Delta Z$  per cardiac cycle in the manner similar to that used by Kubicek et al. (1) to estimate the stroke output. Accordingly, they computed blood flow in ml per 1000  $\text{cm}^3$  of body tissue per cardiac cycle commonly known as Blood Flow Index (BFI) from the following relationship:

$$\text{BFI} = 1000 \times A_s \times T_s / Z_0 \dots\dots\dots (3)$$

where  $A_s$  is the amplitude and  $T_s$  is the duration of the systolic wave of the  $dZ/dt$  waveform.

The BFI thus obtained was found to decrease significantly at and below the sight of arterial occlusion in an extremity. Jindal et al. (2) employed Parulkar's method and investigated

211 patients with peripheral arterial occlusive diseases. In addition to Blood Flow Index, they introduced differential pulse arrival time to differentiate between the narrowing of an artery and an arterial block. Comparison of their data with angiographic observations revealed the sensitivity and specificity of this technique to be 97.5% and 98.1% respectively for the diagnosis of peripheral arterial occlusive diseases.

This method appeared to be of choice for the non-invasive diagnosis of peripheral arterial occlusive diseases. However the visual inspection of the waveform without taking cognizance of the value of basal impedance  $Z_0$  could mislead the clinician about the estimate of peripheral blood flow. The interpretation of data had therefore to wait till the BFI is calculated and therefore the method did not appear suitable for the long term monitoring of the patients. With this in view we undertook the development of normalizing the  $dZ/dt$  waveform with respect to the base impedance value so that the amplitude of this new waveform is representative of the Blood Flow Index in the body segment. The principle and method employed for obtaining this new waveform and the results obtained with this new waveform are presented in this paper.

## Materials and Methods

The normalization of the  $dZ/dt$  waveform has been obtained by using Impedance Cardiovasograph system developed at BARC. The simplified block diagram of impedance cardiovasograph is as shown in Fig.1. It comprises of a sine wave current source which passes user selectable sine wave current of constant amplitude with 50Hz frequency through the body segment under investigation. The voltage signal developed along the current path is sensed by sensing electrodes. This signal is amplified filtered and buffered to obtain a voltage signal  $Z$  that is proportional to the instantaneous

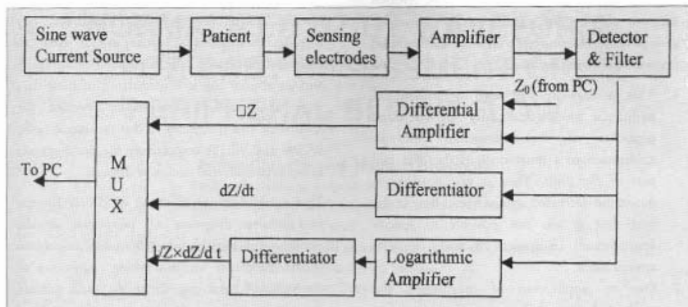


Fig. 1

electrical impedance of the body segment under investigation. This  $Z$  signal is used to obtain  $\Delta Z(t)$  by using a differential amplifier and  $Z_0$  signal obtained from PC.  $Z$  is also used to obtain  $dZ/dt$  signal by using an electronic differentiator.

The signal  $NdZ/dt$  ( $1/Z \times dZ/dt$ ) is obtained by using a logarithmic amplifier and a differentiator. The  $Z$  signal is fed to a logarithmic amplifier to obtain the natural logarithm of  $Z$  ( $\ln Z$ ). The output of log amplifier is fed to an electronic differentiator to obtain normalized  $dZ/dt$ .

Any one of the three outputs  $\Delta Z(t)$ ,  $dZ/dt$ , and  $NdZ/dt$  is selected by PC with the help of multiplexer. The output of the multiplexer is digitized and sent to PC for the processing and display of the output waveform.

## Results and Discussion

Fig.2 (a) shows the  $dZ/dt$  waveforms at different locations at the lower extremity of a normal subject. As can be seen from the figure the  $dZ/dt$  waveform varies significantly from location to location. This variation in principle can be due to:

1. Non-uniformity in the area of cross-section in an extremity.
2. Variation in tissue composition from location to location in an extremity.
3. Presence of an arterial occlusion in the proximal part of the body segment.

The variation in amplitude of  $dZ/dt$  waveform due to tissue composition variation or arterial occlusion is proportionally reflected in value of Blood Flow Index (BFI). Hence this variation is of importance to the clinician for the study of peripheral haemodynamics. But the variation in the amplitude of  $dZ/dt$  waveform due to non-uniformity in area of cross-section of the limb is always accompanied with proportional variation in the value of the basal impedance. Because of this it does not cause any significant change in the value of BFI. As seen from Fig.2 (a) the value of  $dZ/dt$  is comparatively greater in the calf region as the value of  $Z_0$  is more in the calf region while the value of  $dZ/dt$  is comparatively less at thigh, as the value of  $Z_0$  at thigh region is less. Thus the clinician will not be able to give the diagnosis just by looking at the graphs. Fig. 2(b) gives the recording of  $NdZ/dt$  waveform

INVESTIGATION : Aortic

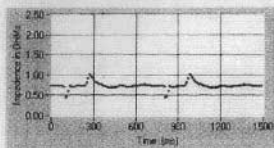
PATIENT: Iqbal

AGE: 60

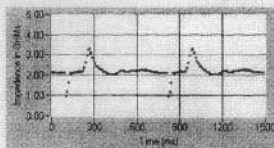
M/F: M

PAGE NO: 1

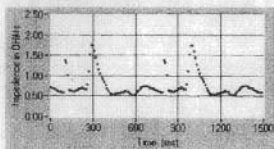
DATE: 03-16-1995



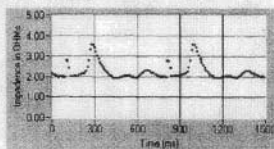
Upper Thigh  
 $Z_0$  19.33 PAT (ms) 170  
 $dZ/dt$  MAX 0.31 PTT (ms) 310



Upper Thigh  
 $Z_0$  21.33 PAT (ms) 170  
 $N dZ/dt$  MAX 1.26 PTT (ms) 310



Knee  
 $Z_0$  59.78 PAT (ms) 190  
 $dZ/dt$  MAX 1.23 PTT (ms) 400



Knee  
 $Z_0$  60.88 PAT (ms) 190  
 $N dZ/dt$  MAX 1.64 PTT (ms) 370

INVESTIGATION : Aortic

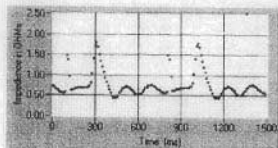
PATIENT: Iqbal

AGE: 60

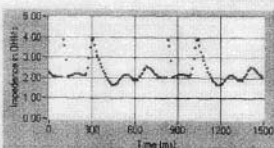
M/F: M

PAGE NO: 1

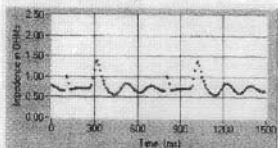
DATE: 03-16-1995



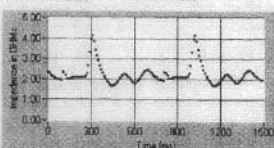
Calf  
 $Z_0$  63.85 PAT (ms) 210  
 $dZ/dt$  MAX 1.38 PTT (ms) 340



Calf  
 $Z_0$  83.33 PAT (ms) 210  
 $N dZ/dt$  MAX 2.24 PTT (ms) 350



Ankle  
 $Z_0$  43.89 PAT (ms) 220  
 $dZ/dt$  MAX 0.81 PTT (ms) 340



Ankle  
 $Z_0$  50.76 PAT (ms) 210  
 $N dZ/dt$  MAX 2.42 PTT (ms) 350

Fig 2

in same subject from corresponding locations. As can be seen from Fig.2 (b) the variation in the amplitude of  $NdZ/dt$  is nearly independent of the basal impedance value and therefore it is clear that the amplitude of  $NdZ/dt$  is proportional to BFI. Thus it directly reflects the haemodynamic variations. A clinician can therefore have just a look at the waveforms and interpret in a manner similar to that of ECG records.

To conclude, the amplitude of  $dZ/dt$  waveform depends on blood flow index in the body segment and also on the basal impedance value of the segment being diagnosed. Therefore the value of the basal impedance had to be taken into consideration while performing the diagnosis. In contrast to this the amplitude of  $NxdZ/dt$  waveform is independent of the basal impedance value and is directly related to the blood flow index in the limb segment. The clinician can thus give the diagnosis just by visual inspection of the waveforms.

## Acknowledgement

The authors express their gratitude to Dr. S.K. Kataria, Head, Electronics Division, BARC, for his continuous guidance and support for this work. The first two authors are thankful to Ms. Mita Bhowmick, Incharge Biomedical Engineering Department, Thadomal Shahani Engineering College for permitting to do implant training and project work at BARC.

## References

1. Hill, W. and Mohapatra, S.N. (1977): 'The current status of electrical impedance technique for monitoring of cardiac output

and limb blood flow', IEE Medical Electronics Monograph, 5, Peter Peregrinus Ltd., UK., pp. 58-105.

2. Jindal, G.D., Nerurkar, S.N., Pednekar, S.A., Babu, J.P., Kelkar, M.D., Deshpande, A.K. and Parulkar, G.B. (1990a): 'Diagnosis of peripheral arterial occlusive disease using impedance plethysmography', *J. Postgrad. Med.*, 36, pp. 147-153.
3. Jindal, G.D., Pednekar, S.A., Nerurkar, S.N., Babu, J.P., Masand, K.L., Gupta, D.K., Deshmukh, H.L., and Parulkar, G.B. (1990b): 'Diagnosis of venous disorders using impedance plethysmography', *J. Postgrad. Med.*, 36, pp. 158-163.
4. Kubicek, W.G., Karnegis, J.N., Patterson, R.P., Witsor, D.A., and Matison, R.H. (1966): 'development and evaluation of an impedance cardiac output system', *Aerosp. Med.*, 37, pp. 1208-1212.
5. Mohapatra, S.N. (1981): 'Non-invasive cardio-vascular monitoring by electrical impedance technique', Pitman Medicals, London, pp. 189-206.
6. Nyober, J. (1960): 'Regional pulse volume and perfusion flow measurements: Electrical impedance plethysmography', *Arch. Int. Med.*, 105, pp. 264-276.
7. Parulkar, G.B., Padmashree, Bapat, D., Ege, R.V., Bhagiani, K.C. and Jindal, G.D. (1981): 'A new electrical impedance plethysmograph: Observations in peripheral arterial occlusive disease', *J. Postgrad. Med.* pp. 66-72.

*This paper was awarded consolation (UG) prize in the Student Paper competition during the Symposium on Biomedical Engineering and Nuclear Medicine (SBME-NM 2000) held at BARC during January 27-29, 2000.*



*A new waveform called the normalized impedance plethysmographic waveform has been introduced for the easy assessment of peripheral blood flow. This waveform is obtained by taking the natural logarithm of the instantaneous impedance of the body segment and then differentiating with respect to time. The waveform thus obtained has its amplitude proportional to blood flow index in the body segment. This waveform gives an advantage to the clinician for easy and quick interpretation of the data in the manner similar to that of electrocardiography.*

*About the authors ...*

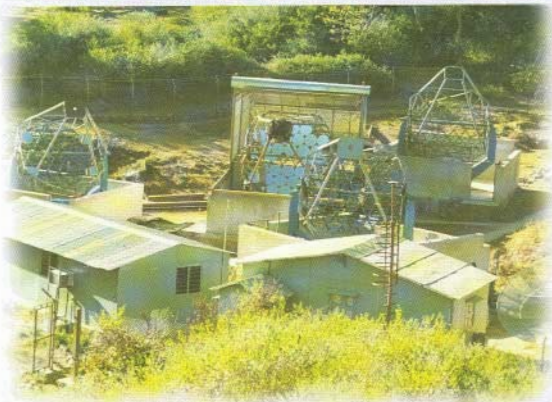


*Mr T.S. Ananthakrishnan is a Post Graduate in Physics from Calicut University (1975). He is from the 19th Batch of BARC Training School and has been working in Electronics Division, BARC, from 1976. For the last few years, he has been involved in software development for various instruments for Nuclear Accelerators, Reactor, Physics Experiments, Ultrasonic Imaging and Medical Instruments and in the review of Computer based systems for nuclear power plants.*



*Dr G.D. Jindal joined BARC Training School in 1973 after passing M.Sc. in Physics from Punjab University, Chandigarh. He joined Bio-Medical Instrumentation Group of Electronics Division in 1974 and since then has been working in the field of Bio-Medical Engineering. He has made noteworthy contribution in the field of Electromyography, Ultrasonography, Gamma Ray Scintigraphy and Impedance Plethysmography. He obtained Ph.D. in Applied Biology from University of Mumbai in 1989 for his work on Vector Impedance Cardiography. At present, he is leading a team of scientists working in the field of Biomedical Engineering at Electronics Division and working on Variability Analysis, Holter Monitoring, Topographic, Mapping of the Brain and Electrical Impedance Tomography.*





Top : Folded Tandem Ion Accelerator.  
Bottom : Tactic Telescopes.

Edited and published by Dr. Vijal Kumar, Head, Library & Information Services Division,  
Bhabha Atomic Research Centre, Trombay, Mumbai 400 085, INDIA.

Editorial Management : T.C. Balan. Computer graphics & layout : P.A.S. Warriyar. (For private circulation)